# UNIVERSIDAD AUTONOMA DEL ESTADO DE MÉXICO
# FACULTAD DE QUÍMICA



## *"Síntesis de materiales AIPO y zeolitas modificadas con aplicación en la reacción de metanol a aromáticos ligeros (MTA)"*

# TESIS

QUE PARA OBTENER EL GRADO DE:

## DOCTOR EN CIENCIA DE MATERIALES

P R E S E N T A:

## M.C. MISAEL GARCIA RUIZ

DIRIGIDA POR:

**Dra. Dora Alicia Solís Casados**
**Dra. Julia Aguilar Pliego**
**Dr. Enrique Sastre de Andrés**

**TOLUCA, MÉXICO, MARZO 2020**

**Listado de abreviaturas**

**MTH** Metanol a hidrocarburos

**MTA** Metanol a gasolinas

**MTO** Metanol a olefinas

**MTP** Metanol a propileno

**BTX** Benceno, Tolueno y Xilenos

**MFI** Mobil Five

**MSE** Mobil sixty-eight

**MWW** Mobil twenty-two

**TUN** Taejon University Taejon

**ATS** Aluminophosphate thirty-six

**AFI** Aluminophosphate five

**ADE** Agente director de estructura

**CHA** Chabacita

**AIPO** Aluminofosfato

**MR** Member Ring (anillos de n miembros)

**DRX** Difracción de Rayos X

**BET** Ecuación Brunauer, Emmett and Teller

**NMR** Resonancia magnética Nuclear

**TPD** Desorción a Temperatura Programada

**SEM** Microscopía Electrónica de Barrido

**TEM** Microscopía electrónica de transmisión

**XPS** Espectroscopía Fotoelectrónica de Rayos X

**Ea** Energía de activación

**SBU** Unidades secundarias de construcción

**PBU** Unidades primarias de construcción

# Índice

# Resumen

Primeramente, en el presente trabajo se estudió el efecto de la incorporación de zinc en diferentes zeolitas de canales de 10 miembros (ZSM-5, TNU-9 y MCM-22) y en la zeolita MCM-68 con canales de 12 miembros para la conversión de metanol a hidrocarburos (MTH) específicamente en la formación de aromáticos (MTA) y obtener una alta selectividad a la fracción BTX (benceno, tolueno y xilenos). Se estudió la correlación del método de incorporación de zinc y las propiedades ácidas de las zeolitas con la actividad catalítica. Las propiedades físico-químicas de las zeolitas se estudiaron mediante XRD, adsorción-desorción de $N_2$, desorción programada a temperatura de $NH_3$, NMR de $^{27}Al$, $^{29}Si$ y $^{31}P$, TGA, TEM y SEM. Se realizó la incorporación de Zn en zeolitas por dos métodos; intercambio iónico y zinc directamente en el gel de síntesis. En el primer método las zeolitas ácidas se intercambiaron usando una solución acuosa de sal de zinc, en el segundo método la sal precursora se coloca en el gel de síntesis antes del tratamiento hidrotérmico. La incorporación de Zn aumentó significativamente la selectividad a aromáticos totales en comparación con la zeolita puramente ácida. La forma de incorporación de zinc, la acidez y la temperatura de reacción tuvieron una gran influencia en la actividad catalítica en el proceso MTH. Además, se sintetizó la zeolita ZSM-5 nanocristalina para mejorar la difusión en los canales de la zeolita y mejorar la conversión y la selectividad a BTX. La síntesis de zeolita ZSM-5 de tamaño nanométrico resultó presentar una alta estabilidad y selectividad hacia los aromáticos. Estos resultados indican claramente que el tamaño del cristal influye significativamente en la vida útil del catalizador ZSM-5 y en la distribución de productos. Por otro lado, las zeolitas T9-15 0.5 Zn y T9-15 0.2 Zn (zeolitas TNU-9) presentaron una conversión de metanol completa hasta las 9 h de reacción. La zeolita T9-15 0.5 Zn presentó una selectividad a aromáticos totales del 32 % y una selectividad del 17 % a BTX a 450° C y 5 min de reacción. Las zeolitas TNU-9 (Si/Al 15) presentaron el siguiente orden creciente en términos de selectividad a aromáticos totales: T9-15 0.5 Zn > ZT9-15 > T9-15 > T9-15 0.2 Zn. Sin embargo, la zeolita MCM-22 presentó mejor selectividad a olefinas ligeras (etileno y propileno), debido a su estructura de canales y a su moderada acidez.

Finalmente se realizó la síntesis de materiales AlPO-5 y AlPO-36 doblemente sustituidos por Si y Zn como función ácida y función aromatizante, respectivamente (materiales MeAPSO). La incorporación de Zn y Si tuvo un efecto importante en las propiedades ácidas, texturales y en la morfología de las muestras. El tamaño de partícula tuvo un efecto significante en la actividad catalítica en la reacción de MTH en términos de conversión de metanol y selectividad a aromáticos totales. Se observó que conforme disminuye el tamaño de partícula, la conversión de metanol aumenta haciendo que el catalizador se desactive en un menor tiempo. La incorporación de Zn mejoró la selectividad a aromáticos totales por el efecto aromatizante del Zn. El material SAPO-5 (conformado por P, Al y Si) al tener un tamaño de partícula más pequeño (1.5 μm) presentó conversiones completas de metanol a tiempos cortos de reacción. Contrariamente, el material Z5 (conformado por P, Al y Zn) presentó bajas conversiones, pero una selectividad mayor a aromáticos totales (41 %). Por otro lado, el material S5-2 presentó una alta selectividad a aromáticos (58 %) debido a la alta cantidad de Zn y Si. Ambos metales proporcionaron cierto carácter ácido a los materiales.

## Abstract

First, in this work we studied the effect of zinc incorporation in different zeolites of 10-member channels (ZSM-5, TNU-9 and MCM-22) and in zeolite MCM-68 with 12-member channels for conversion of methanol to hydrocarbons (MTH) specifically in the formation of aromatics (MTA) and obtain a high selectivity to the BTX fraction (benzene, toluene and xylenes). The correlation of the zinc incorporation method and the acidic properties of the zeolites with the catalytic activity were studied. The physicochemical properties of the zeolites were studied by XRD, adsorption-desorption of $N_2$, temperature programmed desorption (TPD) of $NH_3$, $^{27}Al$, $^{29}Si$ and $^{31}P$ NMR MAS, TGA, TEM and SEM. Zn was incorporated into zeolites by two methods; ion exchange and zinc directly in the synthesis gel. In the first method the acidic zeolites were exchanged using an aqueous solution of zinc salt, in the second method the precursor salt is placed on the synthesis gel before the hydrothermal treatment. The incorporation of Zn significantly increased selectivity to total aromatics compared to purely acidic zeolite. The form of zinc incorporation, acidity and reaction temperature had a great influence on the catalytic activity in the MTH process. In addition, the ZSM-5 nanocrystalline zeolite was synthesized to improve diffusion in the zeolite channels and improve conversion and selectivity to BTX. The synthesis of ZSM-5 zeolite of nanometric size proved to have high stability and selectivity towards aromatics. These results clearly indicate that the crystal size significantly influences the useful life of the ZSM-5 catalyst and the distribution of products. On the other hand, zeolites T9-15 0.5 Zn and T9-15 0.2 Zn (zeolites TNU-9) showed a complete methanol conversion until 9 h of reaction. The zeolite T9-15 0.5 Zn showed a total aromatic selectivity of 32% and a 17% selectivity at BTX at 450 °C and 5 min reaction. The zeolites TNU-9 (Si / Al 15) presented the following increasing order in terms of selectivity to total aromatics: T9-15 0.5 Zn > ZT9-15 > T9-15 > T9-15 0.2 Zn. However, the MCM-22 zeolite showed better selectivity to light olefins (ethylene and propylene), due to its channel structure and its moderate acidity.

Finally, the synthesis of AlPO-5 and AlPO-36 materials doubled by Si and Zn was performed as acid function and flavoring function, respectively (MeAPSO materials). The incorporation of Zn and Si had an important effect on the acidic, textural and morphology properties of the samples. The particle size had a significant effect on the catalytic activity in the MTH reaction in terms of methanol conversion and selectivity to total aromatics. It was observed that as the particle size decreases, the methanol conversion increases causing the catalyst to deactivate in a shorter time. The incorporation of Zn improved the selectivity to total aromatics by the flavoring effect of Zn. The SAPO-5 material (consisting of P, Al and Si), having a smaller particle size (1.5 μm), showed complete conversions of methanol at short reaction times. On the contrary, the Z5 material (made up of P, Al and Zn) showed low conversions, but a selectivity greater than total aromatics (41%). On the other hand, the S5-2 material showed a high selectivity to aromatics (58%) due to the high amount of Zn and Si. Both metals gave a certain acidic character to the materials.

## 1. Introducción

La conversión de metanol a hidrocarburos (MTH) sobre zeolitas ácidas ha atraído considerable atención desde su descubrimiento en 1970 por Mobil Corporation. Dependiendo del producto de reacción, este proceso tiene varias designaciones MTG (metanol a gasolina), MTO (metanol a olefinas), MTP (metanol a propeno) y MTA (metanol a compuestos aromáticos). En este último proceso, los compuestos aromáticos ligeros (benceno, tolueno y xileno) o fracción BTX son materias primas esenciales en la industria química orgánica y petroleoquímica. Estos compuestos aromáticos son una de las materias primas básicas de productos químicos orgánicos y en la industria de polímeros. En la actualidad los compuestos BTX se obtienen a partir de distintas fracciones del petróleo, sin embargo, la escasez de reservas de petróleo implica un incremento en el costo de los compuestos aromáticos (Wang *et al.*, 2014). La conversión de metanol en hidrocarburos aromáticos (proceso MTA) es un método alternativo para satisfacer la demanda de estos compuestos aromáticos, especialmente el p-xileno, isómero más importante industrialmente. El proceso MTA resulta ser una alternativa benéfica para obtener compuestos BTX a partir de materias primas no fósiles (como el metanol), debido a que el metanol se obtiene a partir de biomasa residual, captura de $CO_2$, etc. En este contexto, las zeolitas son conocidas por convertir metanol en compuestos aromáticos ligeros BTX, debido sus propiedades ácidas y selectividad de forma. El rendimiento BTX se puede mejorar mediante la incorporación de especies metálicas en los materiales zeolíticos (como el Zn, Ag, Mg, etc) o mediante el control del tamaño de cristal y la concentración de sitios ácidos, parámetros importantes que afectan de forma determinante tanto a la actividad catalítica como a la resistencia a la desactivación. La presente tesis se basó en investigar materiales zeolíticos modificados y su aplicación en el proceso MTA. En el presento trabajo se sintetizaron zeolitas con sistemas de canales de 10 miembros, así como zeolitas con canales mixtos de 10 y 12 miembros. Dentro de las zeolitas de 10 miembros se estudió la zeolita ZSM-5 con estructura MFI (Mobil Five), la zeolita TNU-9 con estructura tipo TUN (Taejon National University-nine) y MCM-22 con estructura MWW (Mobil Composition of Matter-twenty-

two), y con canales mixtos de 10 y 12 miembros se estudió la zeolita MCM-68 con estructura tipo MSE (Mobil Composition of Matter-sixty-eight). Además, se sintetizó la zeolita ZSM-5 con estructura nanométrica y comprobar el efecto de los nanocristales en la actividad catalítica.

Por otro lado, se sintetizaron y se evaluaron materiales de tipo aluminofosfato (AlPO) específicamente el material AlPO-36 con estructura ATS (Aluminofosfato-Thirty six) y el material AlPO-5 con estructura AFI (Aluminofosfato-five), donde los átomos de P o Al de la red se pueden sustituir fácilmente por Si y Zn, respectivamente, generando acidez. El objetivo planteado en la presente tesis es la síntesis de $AlPO_4$ doblemente sustituidos, por Zn como función aromatizante y Si como función ácida, este tipo de materiales denominados MeAPSO presentan una potencial aplicación en la reacción MTH. En cada síntesis de estos materiales zeolíticos se emplearán estrategias encaminadas al control de la acidez y el tamaño de cristal ya que son puntos clave que definen el comportamiento de los catalizadores en el proceso MTH. Esto se realizó cambiando la proporción molar de Si y Zn en la red, y la relación Si/Al en el caso de las zeolitas, así como la forma de incorporación de Zn, ya sea por intercambio iónico o Zn directamente en el gel de síntesis.

## 2. Antecedentes

### 2.1. Procesos catalíticos en la conversión de metanol

El carbón, el petróleo y el gas natural, son los principales combustibles fósiles en la actualidad, sin embargo, el aumento en el precio del petróleo crudo, los problemas de seguridad energética y los problemas de emisiones de gases de efecto invernadero están motivando nuevos esfuerzos para encontrar procesos alternativos para la producción de combustibles y productos químicos con mejores eficiencias energéticas y ambientales (Bjørgen et al., 2007). Desde su descubrimiento por Chang y Silvestri (1977) en Mobil Central Research en la década de los 70 la conversión de metanol a hidrocarburos (MTH) usando zeolitas ácidas como catalizadores, ha recibido un considerable interés en la industria como una alternativa cada vez más importante para obtener diversos combustibles y productos químicos (Bleken et al., 2011).

La economía de metanol fomenta la utilización de metanol como materia prima para la síntesis de hidrocarburos y sus derivados para eliminar la dependencia de los recursos petroleros. El metanol, se puede obtener a partir de syn-gas (gas de síntesis) a base de combustibles fósiles, por conversión oxidativa directa de gas natural (metano), gasificación de carbón o de biomasa. Esto abre la posibilidad de utilizar el metanol para la generación de hidrocarburos y conducir a una "economía de metanol" factible (Olah, 2005).

Dependiendo de la topología del catalizador y las condiciones de proceso utilizadas, se puede obtener una amplia gama de productos a partir de la reacción de MTH. Procesos comerciales o casi comerciales, tales como metanol a olefinas (MTO) (Chen et al., 2005), metanol a gasolina (MTG) (Cobb, 1995) y metanol a propeno (MTP) (Koempel et al., 2007) y metanol a aromáticos (MTA) (Ono, 1988) se han desarrollado.

*El proceso de metanol a gasolina (MTG)* se cataliza utilizando zeolitas de poro medio, como la ZSM-5, con topología MFI (Mobil Five). En este proceso, el metanol se convierte principalmente en hidrocarburos de la gama de gasolina (hidrocarburos mayores de $C_5$). Mobil construyó y comercializó la primera planta de MTG en Nueva Zelanda en 1985, con

una producción de 14500 barriles por día (alrededor del 30% de la necesidad del país) de gasolina.

*La reacción de metanol a olefinas (MTO)* fue descubierto en los 80s por Union Carbide utilizando un material de zeotipo de poro pequeño, SAPO-34, con topología CHA. En este proceso, el metanol se convierte en alquenos ligeros, principalmente eteno y propeno. El tamaño de poro pequeño del SAPO-34 (alrededor de 4 Å) restringen la difusión de grandes hidrocarburos. La reacción MTO combina el proceso UOP e Hydro MTO implementado en Noruega. Este último convierte el metanol en etileno y propileno a una selectividad de carbono de aproximadamente 75 a 80%.

El proceso de *metanol a propeno (MTP)* se cataliza utilizando el catalizador ZSM-5 (MFI) fue desarrollado por Lurgi's Mega Methanol en Alemania. En este caso, el metanol se convierte en propeno con algunos subproductos de gasolina y combustibles de tipo Gas LP (Gas licuado del petróleo). La selectividad de la reacción se optimiza hacia el propeno por la alta temperatura y la baja presión empleadas durante la reacción, así como el reciclaje de los hidrocarburos más pesados.

Excepto por la reacción MTA, los procesos anteriores se han utilizado en aplicaciones comerciales, sin embargo, en todos los procesos se usan zeolitas ácidas como catalizadores.

## 2.2. Proceso de metanol a aromáticos (MTA)

Los compuestos aromáticos, como el benceno, el tolueno y los isómeros del xileno (fracción BTX), son productos químicos importantes en la industria petroquímica. Actualmente, más del 90% de estos compuestos aromáticos se obtienen por el reformado de distintas fracciones del petróleo y son necesarias etapas posteriores de tratamiento, purificación o modificación de la mezcla de aromáticos para obtener los compuestos más deseados, por ejemplo, el p-xileno es el compuesto más valioso entre los isómeros del xileno (p, m, o-xilenos) debido a que el p-xileno es una materia prima para el ácido tereftálico en la fabricación de poliésteres (Miyake et al., 2016). En este sentido, el

proceso MTA ha atraído una gran atención, ya que se considera una ruta efectiva para usar metanol y aumentar la producción de BTX, en vista del reciente aumento rápido en el precio del petróleo crudo, y la creciente demanda de hidrocarburos aromáticos.

## 2.3.    Zeolitas

Las zeolitas son aluminosilicatos cristalinos microporosos de estructura tridimensional ordenada conformados por canales y cavidades. Su estructura está constituida por una red tridimensional infinita formada por unidades primarias de tetraedros $TO_4$, donde T puede ser silicio (Si), o aluminio (Al), unidos entre sí a través de los átomos de oxígeno originando cavidades accesibles a través de poros de dimensiones moleculares (0.3 - 2 nm de diámetro) (Xu et al., 2007). Poseen una combinación única de propiedades tales como alta superficie, alta estabilidad térmica, abundantes sitios ácidos y selectividad de forma lo que explica su amplia aplicación como adsorbentes, intercambiadores iónicos o catalizadores (Groen et al., 2005). En la asociación de zeolitas internacional (IZA) se conocen a la fecha aproximadamente 200 topologías de marcos diferentes que tienen varios tamaños y conectividades de los canales (http://www.iza-online.org/). El alto número de estructuras de zeolita tiene un gran impacto en la investigación de las propiedades de zeolita y la utilización en aplicaciones apropiadas.
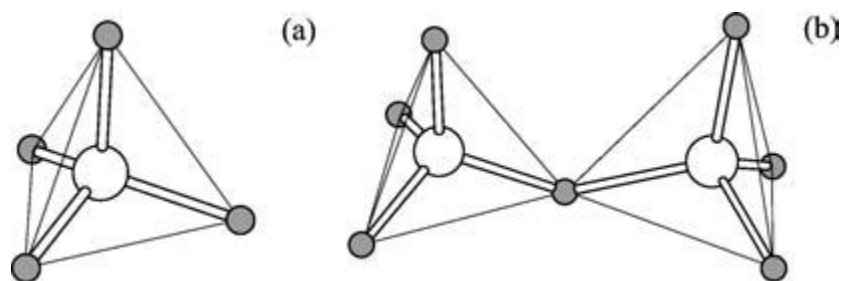


***Figura 2.1. a) tetraedro $TO_4$; (b) tetraedros $TO_4$ que comparten un vértice de oxígeno en común (Xu et al., 2007)***

Los tetraedros $TO_4$ ($SiO_4$ y $AlO_4$) unidas por átomos por oxigeno son las unidades más simples en el proceso de formación de un material zeolítico, denominadas unidades primarias de construcción (SPU). Durante el proceso, los tetraedros se ensamblan

formando unidades secundarias de construcción (SBU) que pueden ser desde anillos simples a poliedros. Estas unidades de construcción secundarias se pueden ensamblar de muchas maneras para dar un gran número de diferentes tipos de estructuras de zeolita. La red de tetraedros interconectados constituye el marco zeolita (Xu et al., 2009).



**Unidades primarias de construcción (PBU)**

**Unidades secundarias de construcción (SBU)**

**Unidades terciarias o poliedros de construcción**

**Estructuras zeolíticas**
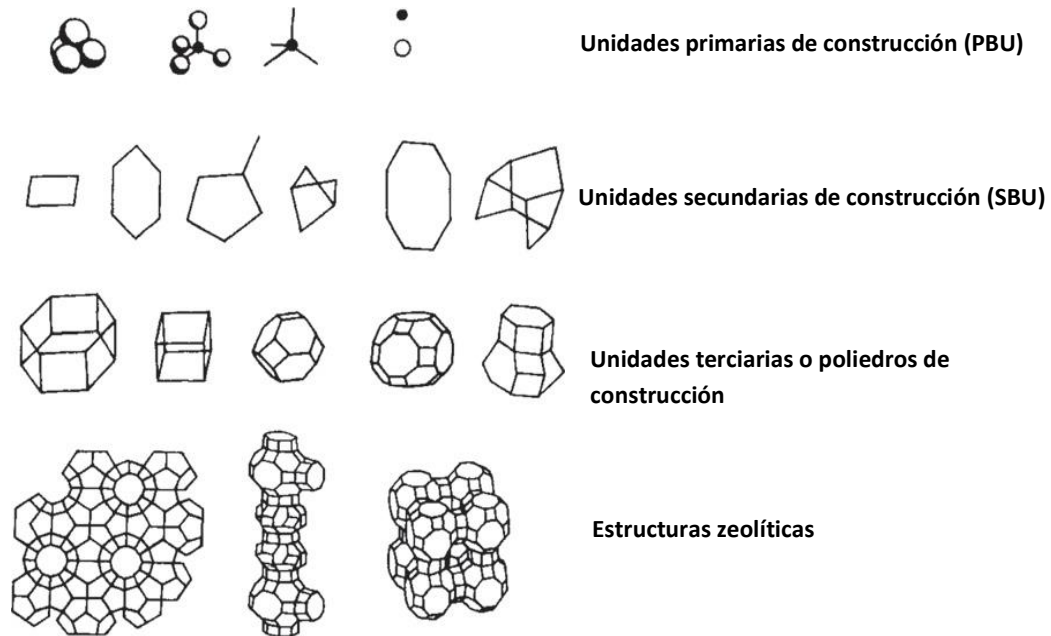
*Figura 2.2. Conformación de zeolitas mediante unidades primarias, secundarias y terciarias de construcción (Qinhua, 1990)*

La composición química de una zeolita puede por lo tanto representarse por una fórmula del tipo:

$$Al_2O_3 : x\ SiO_2 : M_{2/n}O : y\ H_2O$$

$$X \geq 2$$

$$M = Na^+, K^+, Ca^{2+}, \text{orgánicos....}$$
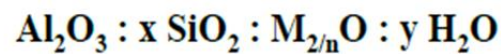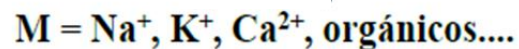
Donde "n" es la valencia del catión M, "x" es mayor o igual a 2 y "y" es la cantidad de agua contenida en los poros de la zeolita. Cuando la carga se compensa por protones, entonces se forman, en las zeolitas, centros ácidos de tipo Bronsted.

El acceso al espacio intercristalino de los microporos está limitado por la apertura que se encuentre en el camino de difusión, por lo que una clasificación de las zeolitas es en función del tamaño de los microporos, comúnmente valorado a partir del número de tetraedros que forman el menor anillo de un canal. Una primera clasificación de las zeolitas respecto al tamaño de poro se muestra en la Tabla 2.1.

**Tabla 2.1. Clasificación de las zeolitas en función del tamaño de poro**

| Tamaño de poro | Numero de tetraedros | Diámetro de poro (A) | Ejemplos |
|---|---|---|---|
| Pequeño | 8 | ~4.0 | Erionita, Zeolita A |
| Mediano | 10 | ~5.5 | ZSM-5, ZSM-11 |
| Grande | 12 | ~7.0 | Zeolita Y, β, Mordenita |
| Extragrande | >12 | > 7.0 | $AlPO_4$-8, VPI-5 |

## 2.4. Aplicaciones de las zeolitas

### 2.4.1. Catalizadores

Una de las más importantes aplicaciones de las zeolitas es como catalizadores en la industria química y petroquímica, debido a que son materiales que presentan una gran superficie específica, gran cantidad de sitios ácidos, contienen diámetros de poro uniformes en toda su estructura, buena estabilidad térmica y propiedades de tamiz molecular. Las zeolitas son empleadas como catalizadores principalmente en procesos petroquímicos como el craqueo catalítico, en la producción de aromáticos y derivados como: etilbenceno, cumeno, p-xileno; en la producción de olefinas (Sherman, 1999) y en procesos de química fina (Corma y Agustín, 1995). Tamiz molecular es un término genérico que comprende materiales sólidos microporosos cristalinos de diversas composiciones (Stöcker, 2005). La propiedad más importante de las zeolitas es actuar como un tamiz de dimensiones moleculares.

### 2.4.1.1. Selectividad de forma

Una de las aplicaciones más importantes de las zeolitas en el campo de la catálisis es la llamada selectividad de forma. El concepto de selectividad de forma en la catálisis de zeolita se introdujo en la década de 1960: la transformación química de las moléculas depende del espacio disponible dentro de los poros de la zeolita (Csicsery, 1971).

El tamaño y disposición de los canales y cavidades condiciona los reactivos, intermediarios de reacción y productos que se pueden encontrar en el interior de estos materiales y cuales pueden difundir al exterior y es clasificada en tres categorías (Csicsery, 1984).

(i)    Selectividad de la forma del reactivo (Figura 2.3). Si se dificulta la difusión de las moléculas reactivas más voluminosas dentro de los poros, las moléculas menos voluminosas reaccionarán preferentemente. El caso límite un reactivo con diámetros cinéticos más grandes que el diámetro de la zeolita no difunden o lo hacen más lentamente y por lo tanto no tiene acceso de los sitios activos, por lo tanto, no sufrirán transformación. Este tipo de selectividad también se llama *selectividad al tamaño molecular.*
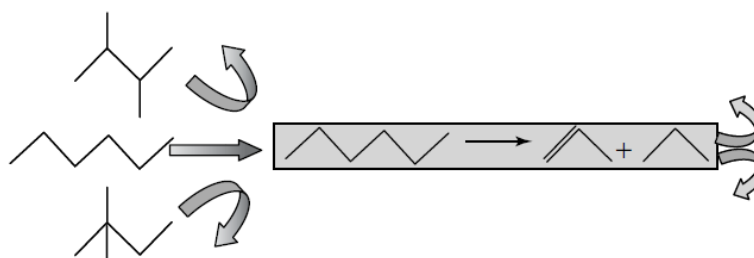


***Figura 2.3. Ejemplo de selectividad de forma del reactivo (Cejka et al., 2010)***

(ii)    Selectividad de la forma del producto (Figura 2.4). Los reactivos se adsorben dentro del marco de la zeolita y entre los diferentes productos formados dentro de los poros solo difunden hacia el exterior aquellos compatibles con las aberturas de los poros. Los otros experimentan una reacción adicional a las

especies menos impedidas, que se desorben, o moléculas más grandes permanecen atrapadas en los poros y contribuyen a la desactivación del catalizador (coquización).
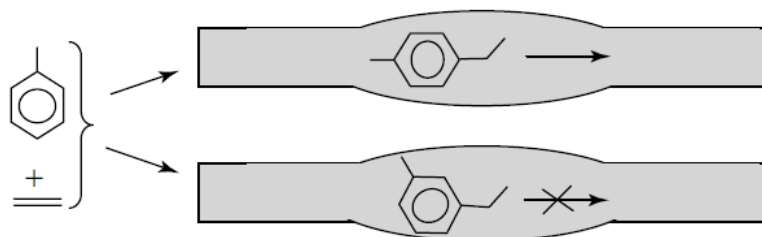


***Figura 2.4. Ejemplo de selectividad de forma del producto***

(iii)    Selectividad de forma de estado de transición restringida (Figura 2.5). En este caso, la selectividad está ligada a la dificultad o imposibilidad de formación de ciertos estados de transición voluminosos, debido a la falta de espacio existente en los centros activos de la zeolita. De esta manera, entre las diferentes vías de reacción posibles, solo se realizan aquellas o aquellas que involucran un estado de transición estéricamente compatible con las dimensiones del poro cercano al sitio activo, mientras que las otras están inhibidas. En este tipo de selectividad no depende del tamaño de cristal de la zeolita, solo depende del tamaño de los canales y cavidades del sólido.
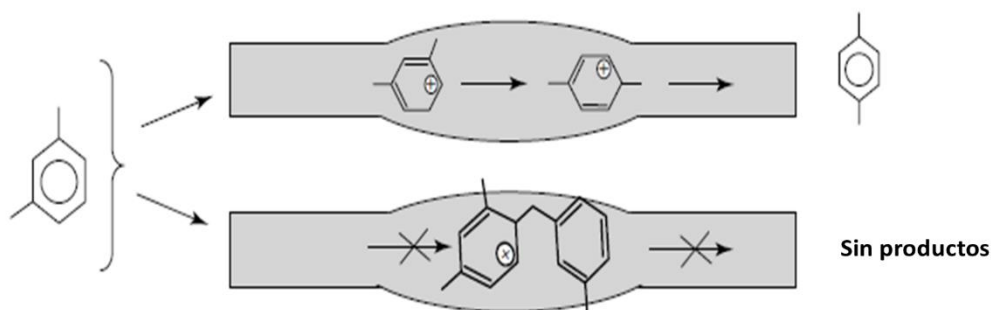


***Figura 2.5. Ejemplo de selectividad de estado de transición restringida***

## 2.5. Propiedades de las zeolitas

Las zeolitas presentan una gran diversidad y una amplia versatilidad en cuanto a sus propiedades derivadas de su diversidad estructural y de composición. Las propiedades características más relevantes de las zeolitas son:

### 2.5.1. Intercambio iónico

En las zeolitas, la sustitución isomórfica de $Si^{4+}$ por $Al^{3+}$ genera un exceso de carga negativa que es compensada por cationes situados fuera de la red. Estos cationes poseen generalmente una gran movilidad y es posible intercambiarlos por otros. Una ventaja de las zeolitas frente a otros intercambiadores iónicos es que estas presentan una red tridimensional y no sufren modificaciones estructurales después del intercambio (Townsend, 1991). La capacidad de intercambio depende de la carga negativa presente en la red y por lo tanto por la cantidad de aluminio sustituido en la estructura. El intercambio iónico es una herramienta muy útil en la modificación controlada de las propiedades de las zeolitas, especialmente en las propiedades ácidas y a su comportamiento como tamiz molecular lo que implica su uso como catalizador o soporte (Garcia Martínez y Pérez Pariente, 2002). Una característica común de las zeolitas es el reemplazo de iones de metales alcalinos (como el sodio) por protones ($H^+$). Este intercambio se lleva a cabo reemplazando los iones metálicos por iones $NH^{4+}$ mediante el intercambio de la zeolita sódica con una solución de $NH_4Cl$, comúnmente a 80 °C, seguido de una calcinación para eliminación de las sales de amonio resultantes a 550 °C en atmosfera de aire como se muestra en la figura 2.6.
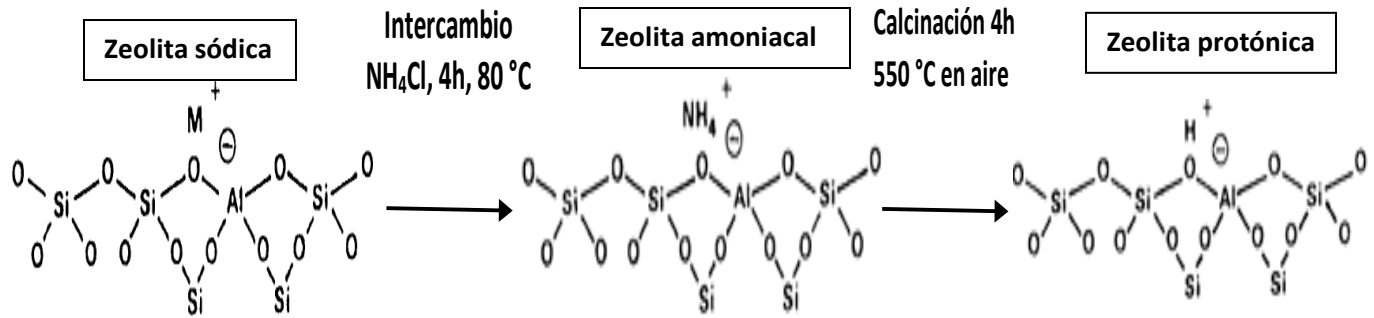
***Figura 2.6. Proceso de intercambio de una zeolita sódica con iones amonio (zeolita amoniacal) y posteriormente es calcinada para obtener una zeolita ácida (protonada)***

## 2.5.2. Adsorción

Debido a la presencia de canales y cavidades en el interior de la estructura y una red microporosa, las zeolitas presentan una elevada superficie específica y una alta capacidad de adsorción. Estos canales son de tamaño uniforme debido a la estructura cristalina, permitiendo el acceso únicamente a moléculas de tamaño inferior al del poro (correspondiente también a la propiedad de tamiz molecular). Lo que permite que las zeolitas sean utilizadas tanto en proceso de purificación como en procesos de separación.

## 2.5.3. Propiedades ácidas

Entre las propiedades más importantes de las zeolitas con respecto a su uso como catalizadores está su acidez superficial. Como se mencionó anteriormente, la presencia de elementos tetravalentes en la red, como el aluminio, generará una carga negativa en la red, la cual será compensada por especies catiónicas $K^+$, $Na^+$, $NH^{4+}$, etc. que se encuentra dentro de los poros de las zeolitas. Cuando los cationes que compensan la carga de la red aniónica son protones, se comportan como centros ácidos de tipo Brönsted, como se ilustra en la Figura 2.7. La incorporación del aluminio a la red sustituyendo al silicio en algunas posiciones T, genera una carga negativa, que si está

compensada por un protón, da lugar a un grupo hidroxilo puente Si-OH-Al capaz de ceder el protón. Por lo tanto, la acidez depende de la relación Si/Al en la zeolita. Se ha demostrado que la fuerza ácida de los puentes hidroxilos en especies de Si-OH-Al aumenta a medida que disminuye el contenido de Al, es decir, cuando aumenta la relación de Si/Al proporcionado sitios ácidos tipo Bronsted con mayor fortaleza (Barthomeuf, 1994). Así, en principio, el número de centros ácidos en una zeolita será igual al número de cationes trivalentes que contenga la red (Teketel et al., 2014). Por lo tanto, cuanto mayor sea la cantidad de $Al^{3+}$ que hay en la red, mayor será el número potencial de centros ácidos de las zeolitas. Estas propiedades ácidas, les confieren a su vez, propiedades catalíticas a las zeolitas. Además, dichos materiales aportan selectividad de tamaño y forma, dado que los centros ácidos se encuentran en una red de canales y cavidades.
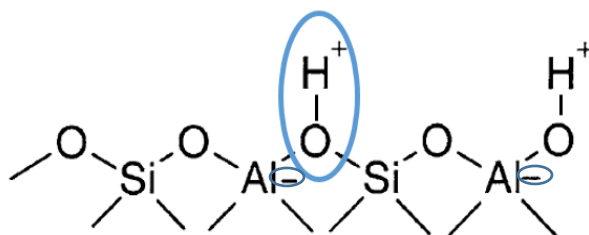


***Figura 2.7. Ilustración de sitios ácidos tipo Brønsted en una zeolita***

De esta manera, el número total de centros ácidos en una zeolita depende de la relación Si/Al en la red, o de forma más general, de la relación $M^{4+}/M^{3+}$ (Li et al., 2008). En general, la fuerza ácida de los sitios ácidos Brönsted depende de la fuerza del enlace OH. Dichos centros son capaces de donar protones. Por otra parte, las zeolitas también pueden poseer sitios de Lewis en la estructura, lo que inevitablemente afectará las propiedades catalíticas de la zeolita. Dichos sitios activos están asociados con especies de aluminio extrared y son capaces de aceptar electrones. Se forman en zonas de los materiales en las que existen especies aceptoras de electrones como el aluminio tricoordinado, esto se observa en la figura 2.8 (Pinilla, 2016). Razonablemente, los sitios de ácidos de Lewis son más prominentes en los materiales con alto contenido de Al o en las zeolitas sometidas a tratamientos térmicos o vapor de agua (Fang et al., 2017)
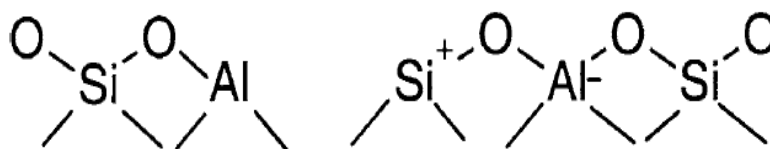
***Figura 2.8. Ilustración de sitios ácidos tipo Lewis en una zeolita***

Además de ser catalizadores con una acidez fuerte Brönsted, las zeolitas presentan una alta estabilidad por lo que tienen aplicación en procesos de craqueo, isomerización, alquilación y aromatización debido a su selectividad de forma. Por estas características las zeolitas se consideran catalizadores eficientes para la conversión de metanol a hidrocarburos (MTH).

## 2.6.    Zeolitas con aplicación en el proceso MTH

Entre los diversos tamices moleculares utilizados en el proceso MTH, la zeolita ZSM-5 es la más atractiva y las más reportada actualmente, ya que presenta una alta estabilidad y una gran densidad de sitios ácidos responsables de la generación de olefinas y aromáticos ligeros (Niu et al., 2014; Conte et al., 2012). Por otro lado, es otra estrategia para mejorar la selectividad de los productos deseados mediante la incorporación de especies metálicas. En particular, las especies de metales activas utilizadas para la aromatización (proceso MTA) del metanol incluyen principalmente Zn (Bi et al., 2014), Ga (Lopez-Sanchez et al., 2012), Ag (Inoue et al., 1995) y Sn (Xin et al., 2013). Sin embargo, en este proceso existen dos retos fundamentales por resolver. Por una parte, de entre los tres isómeros de xileno, la selectividad hacia el compuesto más deseado, el para-xileno, es insuficiente para evitar procesos de isomerización posteriores. Por otra parte, en esta reacción, al contrario de lo que ocurre en el caso del proceso MTG (methanol to gasoline), que también emplea ZSM-5 como catalizador, el catalizador se desactiva en tiempos de reacción relativamente cortos. Se ha demostrado ampliamente que Zn especies y especies de Ga podrían aumentar considerablemente la selectividad de BTX en la reacción de MTA en comparación con otras especies de metales. El papel

esencial de las especies Ga y Zn puede estar asociado en gran medida con su capacidad de deshidrogenación (Jia et al., 2017).

Las especies de zinc pueden introducirse en diversas zeolitas mediante diversos métodos: por impregnación húmeda incipiente, intercambio iónico y directamente en el gel de síntesis (Gabrienko et al.,2017). El método de preparación tiene una influencia importante en el estado de existencia de las especies de zinc, la interacción entre los iones de zinc y los sitios ácidos, y el rendimiento catalítico en MTA (Jia et al.,2017).

Por otra parte, se estudian estructuras con potencial interés por presentar sistemas de canales combinados de 10 y 12 miembros, por ejemplo, las zeolitas MCM-68 (MSE), TNU-9 (TUN) y MCM-22 (MWW).

## 2.6.1. Zeolita ZSM-5

La zeolita ZSM-5 es un catalizador ácido altamente estudiado en proceso de petroquímica y por lo tanto en reacciones de aromatización de metanol debido a su estabilidad hidrotérmica, a su excelente selectividad de forma y a una estructura cristalina adecuada para una alta actividad catalítica (Su et al., 2016 y Wang et al., 2016). Gran parte del éxito de la zeolita ZSM-5 se atribuye a la presencia de sitios de ácidos fuertes, que son responsables de la actividad catalítica en el proceso MTH, y de los microporos del anillo de 10 miembros (MR) que se intersectan (5.5 x 5.1; 5.3 x 5.6 Å), que tienen en cuenta la selectividad de la forma y la resistencia a la deposición de coque exhibidas sobre este catalizador (Kokotailo et al., 1978). En general, se considera que los sitios ácidos fuertes en la zeolita ZSM-5 son los sitios activos para la aromatización con metanol.

Las zeolitas ZSM-5 modificadas con metales como Zn son catalizadores bifuncionales altamente eficientes para convertir olefinas en compuestos aromáticos a partir del metanol. En los últimos años se han conseguido algunos logros importantes, como la

estabilidad catalítica de la reacción de MTH se puede mejorar mediante la generación de mesoporos (Kim et al., 2016) o la síntesis de zeolitas nanométricas (Konno et al., 2013).

### 2.6.2. Zeolita TNU-9

TNU-9 (estructura TUN) es una zeolita de poro medio con un complejo sistema de canales tridimensional. Su estructura es análoga a la de la zeolita ZSM-5 (MFI) con respecto a su proyección hacia abajo del eje b. Sin embargo, la conectividad y distribución de los canales en la estructura TUN son más complejas que las de la topología de MFI. La zeolita TNU-9, es una nueva zeolita con sistema de canales 3D de 10 anillos rectos distintos (5.2 x 6.0 y 5.1 x 5.5 Å), fue sintetizada previamente por Suk Bong Hong et al., en 2007. La forma ácida TNU-9 exhibe una alta estabilidad hidrotérmica, acidez fuerte y selectividades de forma únicas para las reacciones catalizadas por ácido de hidrocarburos monoaromáticos, como la desproporción de tolueno y la isomerización y desproporción de m-xileno (Kubu et al., 2010).

### 2.6.3. Zeolita MCM-22

La zeolita MCM-22 (código MWW), sintetizada por primera por vez por Mobil en 1990 (Rubin y Chen, 1990) es un tamiz molecular que se cristaliza como láminas o placas delgadas y tiene una estructura de cristal única e inusual. Puede verse como un apilamiento de capas dobles unidas por puentes de oxígeno individuales. La zeolita MCM-22 posee tres sistemas de poros independientes, el primero está formado por grandes supercajas cilíndricas (7.1 x 7.1 x 18.2 Å) entre las capas, el segundo está formado por 10 canales sinusoidales (4.1 x 5.1 Å) y el último está ubicado en la superficie externa, cubierto con bolsillos de 12 miembros (7.1 x 7.1 x 7 Å) (Leonowicz et al., 1994). Debido a la peculiar estructura de los poros, la zeolita MCM-22 se ha aplicado en muchos procesos catalíticos y se considera un catalizador potencial en la reacción de MTO.

Los tres sistemas de poros contienen grupos OH de puente, es decir, sitios ácidos. Por lo tanto, en cada uno de ellos pueden ocurrir transformaciones catalizadas ácidas de varios reactivos, con grandes diferencias en velocidad, selectividad y estabilidad. Las propiedades selectivas de forma de los tres sistemas de poros MCM-22 (incluida su actividad y estabilidad) se establecieron previamente para la transformación catalizada de varios reactivos: los tres isómeros de xileno (Laforge et al., 2003) la mezcla de tolueno-propeno (Rigoreau et al., 2005) y el metilciclohexano (Matias et al., 2008).

### 2.6.4. Zeolita MCM-68

La zeolita MCM-68 (código MSE) es un tipo de aluminosilicato creado por los investigadores de Mobil en 1997 y se publicó por primera vez como patente en 2000 utilizando diyoduro de dipirrolidinio (TEBOP(I)$_2$) como agente director de estructura (ADE) (Calabro et al., 2000). Es una zeolita con un sistema tridimensional de 12 × 10 × 10 canales, que incluye un canal recto de 12 anillos (6.4 × 6.8 Å) que se cruza con dos canales de 10 anillos independientes (5.2 × 5.8 y 5.2 × 5.2 Å) que se cruzan entre sí (Douglas et al., 2006; Shibata et al., 2008). La zeolita MCM-68 tiene una super jaula cilíndrica (anillos de 18 x12 miembros), a la que solo se puede acceder a través de canales de 10 anillos, que puede difundir especies de estados de transición de tamaños cinéticos gran (Baerlocher, 2007). Las características de la zeolita MCM-68 están atrayendo la atención porque solo hay unas cuantas zeolitas que contienen sistemas de canales tridimensionales con poros grandes.

Las zeolitas MCM-68 se han utilizado como catalizadores en diferentes reacciones, como oxidación con fenol (Sasaki et al, 2014), alquilación de compuestos aromáticos (Shibata et al., 2009), desproporción de etilbenceno (Ernst et al., 2005) o tolueno (Zilková et al.,2009), craqueo con hexano (Inagaki et al., 2013) y reacción de dimetil éter a olefinas (Inagaki et al., 2013).

## 2.7. Zeolitas de tamaño nanométrico

Como se mencionó anteriormente, en reacción de MTH la estabilidad y actividad catalítica de las zeolitas ácidas se puede mejorar mediante la generación de mesoporos (Koohsaryan y Anbia, 2016) o la síntesis de zeolitas nanométricas (Wan et al., 2016) esto debido a una baja eficiencia de difusión en microporos en zeolitas ácidas convencionales. En recientes trabajos, se ha trabajado mucho para diseñar zeolitas con estructura jerárquica para mejorar la difusión de reactivos y facilidad de acceso a los sitios activos. Los nanocristales de zeolita con un tamaño de cristalito más pequeño y mayor área de superficie externa exhiben longitudes de difusión más cortas, mejorando así la difusión molecular y por lo tanto la optimización de las propiedades ácidas de la zeolita para mejorar la actividad catalítica (Miar, 2016).

Al disminuir el tamaño del cristal, las rutas de difusión del reactivo y las moléculas del producto dentro de los poros se vuelven más cortas, y esto puede resultar en una reducción o eliminación de difusión no deseadas (Ji et al. 2017). Recientemente, los investigadores han confirmado que el ZSM-5 nanocristalino muestra una buena resistencia a la deposición de coque y un excelente rendimiento catalítico en la reacción de MTG (Gabrienko et al., 2017).

## 2.8. Zeotipos: Aluminofosfatos

Inicialmente las zeolitas tienen composición exclusivamente de aluminosilicato, sin embargo, en las redes zeolíticas, tanto el aluminio como el silicio pueden ser sustituidos por otros elementos susceptibles de formar redes tetraédricas de óxido, originándose así un nuevo tipo de materiales llamados zeotipos. Dentro de este grupo se pueden destacar los materiales microporosos aluminofosfatos ($AlPO_4$), sintetizados por primera vez por Wilson *et al.*, en 1982. Este tipo de materiales consisten en una red microporosa que está formada por unidades tetraédricas de $AlO_4$ y $PO_4$ que están unidas de manera alterna (Bennett et al., 1986) (Figura 2.9). Este tipo de materiales poseen estructuras análogas

a la de las zeolitas. Lok et al., en 1984 descubrieron los denominados silicoaluminofosfatos (SAPO), mediante la incorporación de silicio en la red $AlPO_4$ por sustitución isomórfica. Messina et al., en 1985 obtuvieron una serie de metaloaluminofosfatos que denominaron MeAPO, y contenían en su estructura fósforo, aluminio y un tercer catión metálico (V, Co, Mg, Ga, Fe, Zn, etc.). Por otro lado, hay otros materiales denominados MeAPSO, donde se incorpora Zn y Si, reemplazando al Al y P, respectivamente. Estos materiales se estudiaron en el presente trabajo, donde se intuye que el Zn actúa como un agente aromatizante y el Si como un agente ácido para catalizar la reacción MTH. Los materiales de tipo SAPO, MeAPO y MeAPSO poseen estructuras similares a la de las zeolitas pero con distinta composición (estructura análoga). De esta manera poseen la misma topología que las zeolitas, pero los centros Brönsted generados presentan una acidez moderada comparados con los que se generan en la red de la zeolita. Por lo que presentan nuevas propiedades fisicoquímicas que están vinculadas a su composición única y tienen aplicaciones potenciales en catálisis, adsorción e intercambio iónico (Xu et al., 2008).
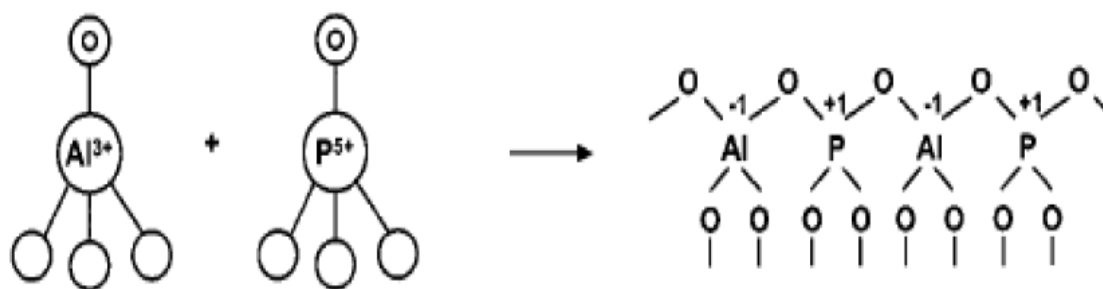


**Figura 2.9. Estructura de un $AlPO_4$ (Weckhuysen et al., 1999)**

Los materiales MeAPSO pueden considerarse catalizadores potenciales para la reacción de MTH, debido a la presencia de Zn y Si en la estructura. En este estudio, se compara la actividad catalítica de dos tipos de estructuras llamadas MeAPSO-5 (AFI) y MeAPSO-36 (ATS). Cabe mencionar que estos zeotipos propuestos no se han utilizado previamente en la reacción MTH, específicamente para el proceso MTA.

### 2.8.1. Sustitución isomórfica

La sustitución isomórfica puede definirse como el reemplazo de un elemento en una red cristalina, por un heteroátomo con radio catiónico y requisitos de coordinación similares, de tal manera que pueda acomodarse en la misma posición del elemento de la red al que sustituye (Martens et al., 1990).

Los materiales $AlPO_4$, como ya se ha mencionado, están formados por la unión de tetraedros alternados de $AlO_4$ y $PO_4$, y son eléctricamente neutros por lo que no presentan centros ácidos Brönsted. La sustitución isomórfica es un proceso que tiene lugar en los materiales zeolíticos y que permite la obtención de zeotipos de composiciones variadas. Además, puede dar lugar a la generación de acidez en este tipo de materiales. El elemento al que un heteroátomo sustituye en una red aluminofosfato dependerá principalmente del estado de oxidación de dicho heteroátomo.

En los materiales silicoaluminofosfatos (SAPO) pueden considerarse como el $AlPO_4$ correspondiente al que se introduce silicio en la red. En los SAPO, la sustitución de Al(III) o P(V) por Si(IV) va a generar una carga negativa en la estructura que puede ser contrarrestada por protones y por lo tanto introduce acidez en el material. Por lo tanto, en los materiales SAPO, el número de centros ácidos está relacionado con el mecanismo de incorporación de átomos de silicio en el material. El número y la fuerza de los centros Brönsted en los materiales $AlPO_4$ dependerán de los mecanismos de incorporación de silicio en la red (Martens et al., 1990).

Martens y sus colaboradores propusieron tres mecanismos de sustitución (SM) que pueden tener lugar en una red $AlPO_4$ garantizando que no se formen redes con carga positiva o con una carga negativa demasiado elevada.

En primer lugar, cuando los átomos de Si se incorporan en el marco de un hipotético $AlPO_4$ en los sitios de fósforo (mecanismo SM2), se generará un sitio ácido tipo Bronsted por cada átomo de Si. Otra posibilidad es la sustitución simultánea de un par de átomos de Al y P por dos átomos de Si (mecanismo SM3). En este caso no se genera ninguna

carga. La combinación del modelo de sustitución 3 y 2 (SM3 + SM2) propuesto por Makarova et al., en 1992, genera la formación de "islas de silicio" donde los átomos de silicio están unidos entre si a través de los oxígenos donde estos silicios están ocupando los sitios del Al y P en la estructura del $AlPO_4$. Por otro lado, un metal divalente como el Zn, puede sustituirse por átomos de $Al^{+3}$ por el mecanismo SM1.

Por lo tanto, las propiedades ácidas de los materiales SAPO depende en gran medida del contenido de Si ordenado en la red, gracias a esta propiedad se pueden obtener catalizadores con un número variable de centro activos con diferente fuerza ácida que pueden llevar a cabo ciertas reacciones de catálisis ácida (Marchese et al., 1993). Por eso es importante controlar la síntesis de estos materiales y poder obtener catalizadores con contenido controlado de silicio en la red.

La formación de las denominadas "islas de silicio" (Figura 2.10) se debe a la combinación de SM2+SM3 generando cargas negativas en la red que, cuando se compensa con un protón, da lugar a la formación de un sitio ácido Si-OH-Al. Cuando el silicio incorporado rodeado de al menos por un átomo de Al en la primera esfera de coordinación tetraédrica proporciona un sitio ácido, es decir, que cuanto menor sea el número de átomos de Al vecinos al átomo de Si el sitio tendrá una mayor fortaleza ácida (del Val et al., 1995). Por lo que según el entorno de cada átomo de Si, en la isla de silicio tiene influencia en su acidez y por lo tanto en su actividad catalítica. La acidez de estos sitios aumenta en el orden: $Si(OSi)_3(OAl)$ > $Si(OSi)_2(OAl)_2$ > $Si(OSi)(OAl)_3$ > $Si(OA)_4$ (Barthomeuf, 1994). Por el contrario, los átomos de $Si^{4+}$ en ambientes de solamente silíceos $(Si(OSi)_4)$ dentro de islas de $SiO_2$ similares a las zeolitas no tienen propiedades ácidas en absoluto, entonces, la acidez total de los catalizadores de SAPO (número y fuerza de sus sitios) con un contenido de Si dado, está controlada por el tamaño de las islas de $SiO_2$.
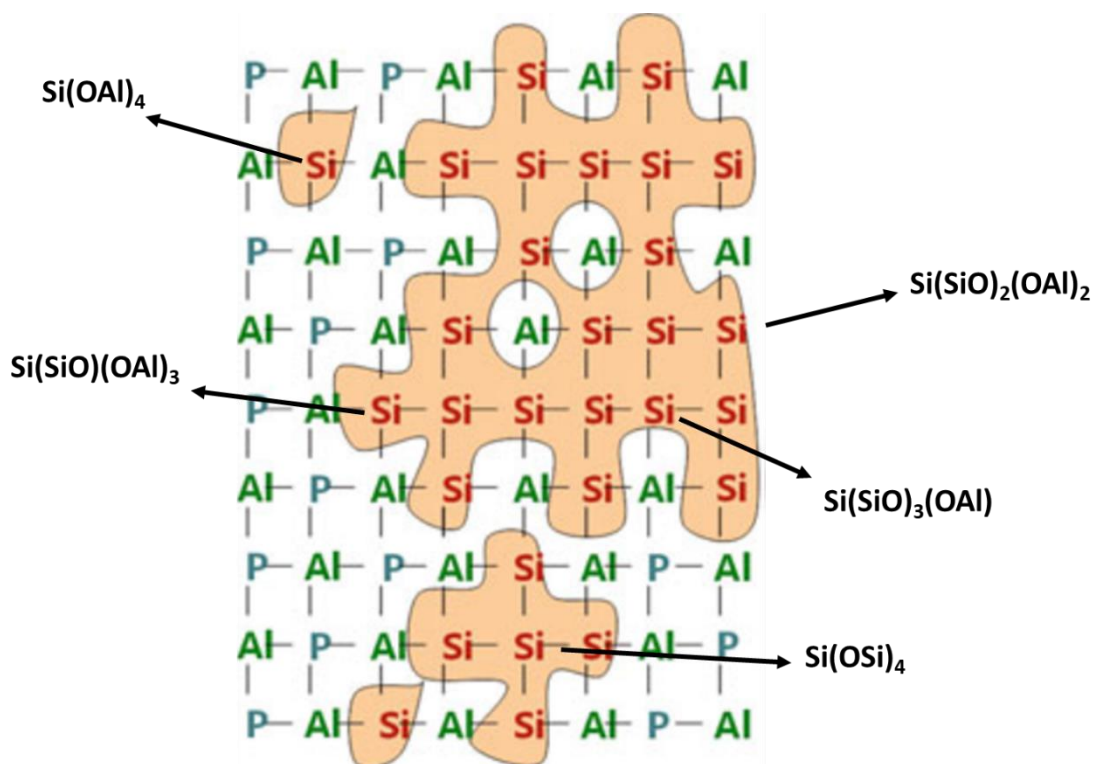
***Figura 2.10. Átomos de aluminio sustituyendo a silicios en las regiones de "islas de silicio" (Pinilla, 2016)***

Si se requiere una mayor acidez, será necesario optimizar la formación de estas islas de silicio en la estructura, puesto que los centros ácidos en el borde de las islas presentan una fuerza ácida mayor (Briend et al., 1993). El número y la fuerza de los centros ácidos en los SAPO van a determinar sus aplicaciones como catalizadores. Sus aplicaciones principales son procesos de refino y procesos de conversión, en petroquímica.

### 2.8.2. Aluminofosfato AlPO$_4$-5

AlPO$_4$-5, reportado por primera vez por Wilson et al., en 1982 tiene una estructura tridimensional con simetría hexagonal (Figura 2.11), que contiene canales unidimensionales orientados en paralelo al eje c y delimitados por anillos de 12 miembros que comprenden AlO$_4$ alternante y tetraedros PO$_4$ (0.73 x 0.73 nm) (Finger et al.; Hartmann et al., 1999). AlPO-5 es una estructura estable y eléctricamente neutra capaz de soportar temperaturas por encima de 600 °C, que solo muestra cambios menores en

el eje cristalográfico después de la calcinación y la deshidratación (Choudhary et al., 1988).
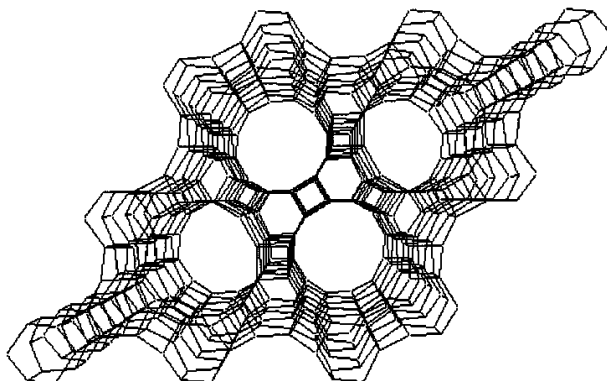


***Figura 2.11. Representación de la estructura de AlPO-5 (Weckhuysen et al., 1999)***

Debido a la similitud estructural con las zeolitas y la acidez moderada, SAPO-5 se ha probado como catalizador en varias aplicaciones, por ejemplo, en la conversión de metanol a olefinas (Terasaka et al., 2015), la alquilación de tolueno y la isomerización de xilenos (Wang et al., 2003). El material SAPO-5 también ha sido utilizado como adsorbente para la eliminación de diferentes gases de diversos tamaños moleculares, incluyendo $N_2$, $CO_2$, $CH_4$ y $H_2O$ (Martin et al., 1998).

En este trabajo, se sintetizaron materiales MeAPSO-5 formados en presencia de N-metildiciclohexilamina (MCHA) usado como agente director de estructura (ADS), con heteroátomos de Si y Zn para la reacción MTA. El compuesto MCHA, es propuesto como ADS para materiales AFI y evitar fases de tridimita (TRI) y chabazita (CHA). La fase principal de AFI, presenta dificultades en la preparación de la fase de AFI puro, como lo demuestra Sanchez-Sanchez et al., en 2003 donde usa este agente de dirección de estructura, N-metildiciclohexilamina (MCHA), para la producción de AlPO-5 microporoso y sus variantes sustituidas con heteroátomos.

### 2.8.3. Aluminofosfato AlPO₄-36

AlPO-36 con la topología estructural ATS se caracteriza por canales elípticos unidireccionales (6.5 x 7.5 Å) con aberturas de 12 anillos. La incorporación por sustitución isomorfica de cobalto, magnesio, manganeso, silicio, titanio, vanadio y zinc en el marco de AlPO$_4$ puede generar centros catalíticamente activos y producir catalizadores heterogéneos creando sitios ácidos Bronsted (Akolekar et al., 1998). Estas características proporcionan un potencial de AlPO-36 dopado con heteroátomos (MeAPO-36) como catalizador en áreas como el craqueo de n-butano y la formación de aromáticos (Kumar-Saha et al., 2005). Hasta el momento, no se ha preparado un material en forma de aluminofosfato puro (SAPO-36), debido a que se necesita la presencia de un metal divalente utilizando una plantilla de tripropilamina (TPA).

En el presente trabajo se plantea la aplicación catalítica de AlPO$_4$ doblemente modificados, primeramente, sustituir Al$^{3+}$ por Zn$^{2+}$ como función aromatizante, seguido de P$^{5+}$ por Si$^{4+}$ para la generación la acidez de Bronsted (Roldan et al., 2007). El Zn puede acomodarse en cantidades relativamente grandes en las redes tipo aluminofosfato (AlPO$_4$), mientras que Si proporciona carácter ácido dependiendo de su mecanismo de incorporación por sustitución isomórfica.

## 3. Justificación

Los compuestos aromáticos ligeros BTX son sustancias químicas muy importantes en la industria de la medicina, perfumería, colorantes, etc. Actualmente, más del 90% de estos compuestos aromáticos se obtienen por distintos métodos que emplean petróleo crudo, como la reformación, craqueo y alquilación (Fahim et al., 2010). Una de las principales desventajas de este tipo de procesos es la amplia cantidad de productos que generan, lo que hace que sean necesarias etapas de separación o modificación de la mezcla de aromáticos para obtener los compuestos más deseados, como por ejemplo el para-xileno, lo que, evidentemente, encarece aún más el proceso.

En los últimos años, la conversión de metanol en aromáticos ligeros (proceso MTA) ha generado un gran interés debido a que ofrece una alternativa en principio eficaz para obtener este tipo de compuestos químicos a partir de una materia prima más sostenible y renovable como el metanol (Quan et al., 2014). Y al mismo modo permita eliminar la dependencia que existe del petróleo en vista de que este recurso será más escaso y de menor calidad, contribuyendo así a la producción sostenible de productos químicos básicos.

El proceso MTA es una vía alternativa para la obtención de altas fracciones de aromáticos ligeros. Esta proporciona una elevada selectividad a dichos productos, especialmente el p-xileno, el isómero más importante debido a su gran aplicación industrial. Una de las principales ventajas de este proceso es que el metanol es producido de diferentes fuentes; principalmente del gas de síntesis que parte de múltiples recursos tales como, el carbono, gas natural y biomasa (Niu et al., 2014).

## 4. Estado del arte de catalizadores empleados en el proceso MTH y MTA

La aromatización del metanol también ha despertado un gran interés. Ono et al., en 1992 investigan el efecto de la carga de Zn en el rendimiento catalítico de Zn/ZSM-5 en la reacción de aromatización del metanol, y se verificó el papel esencial de las especies de Zn en la mejora de la selectividad a los compuestos aromáticos. En comparación con la matriz ZSM-5, la introducción de Ag, Cu y Ni incrementó la selectividad de productos de compuestos aromáticos de C6 a C11 en un factor de dos o más.

Existen diversos factores propios de los materiales zeolíticos que influyen en la actividad catalítica del proceso MTA, entre los que destacan la acidez y el tamaño de cristal. El tamaño de cristal se refiere a la dimensión de una sustancia sólida con un ordenamiento periódico de átomos, iones o moléculas que presenta un diagrama de difracción. La variación del tamaño cristalino es una vía para el control de los caminos difusionales de estos materiales. La reducción del tamaño cristalino, en general, provoca una mejor accesibilidad del reactivo a los centros activos y una mejor difusión de los productos formados, esperándose que esto mejore el rendimiento hacía aromáticos ligeros BTX,

así como la resistencia a la deposición de coque (Quan et al., 2014). Pinilla et al., 2015 demuestran previamente que existe una relación entre el tamaño cristalino y el tiempo de vida media de los catalizadores. Por una parte, la elección del agente director de estructura (ADE) puede implicar cambios de tamaño (Álvaro, 2012), así mismo, también se han observado variaciones en el tamaño por el empleo de diferentes fuentes de los elementos que forman la red (Álvaro et al., 2014), o por la selección de determinadas condiciones de síntesis, tales como el empleo de un tiempo de síntesis menor (Pinilla, 2016). De esta manera se pueden obtener materiales con un tamaño de cristal ligeramente menor, pero sobre todo, con mayor volumen de poro intercristalino y mayor superficie externa. Esto facilita la accesibilidad de las moléculas de metanol a los centros ácidos, causando que los catalizadores se desactiven más lentamente (Álvaro, 2012).

Sin embargo, sólo se han descrito unas pocas investigaciones en relación con la mejora de la selectividad para los hidrocarburos aromáticos. Para la transformación de metanol en aromáticos ligeros (BTX), es necesaria la presencia de un catalizador sólido ácido de tipo zeolítico.  Dentro de estos materiales, la zeolita HZSM-5 se ha utilizado ampliamente como un catalizador para las reacciones de aromatización debido a su selectividad de forma, alta actividad, y buena estabilidad en reacciones de aromatización (Cejka et al., 2005). En los últimos años, la conversión de MTA sobre materiales zeolíticos modificados con metales está atrayendo cada vez más atención.

Choudhary et al., en 1996 y Song et al., en 2004 consideran que los sitios ácidos fuertes de la zeolita HZSM-5 funcionan como sitios activos para la producción de compuestos aromáticos ligeros, sin embargo, dichos sitios provocan la formación de coque que da origen a la desactivación del catalizador. Por lo tanto, sitios ácidos con fuerza media son idóneos para evitar la formación de coque, pero también da lugar a la pérdida de actividad de aromatización de metanol. Por lo que la estabilidad del catalizador está estrechamente relacionada con la distribución de sitios ácidos en el catalizador.

Catalizadores zeolíticos, como el de tipo MFI, con especies de Zn muestran un mayor rendimiento de aromatización. Específicamente, Bi et al., 2014 estudian la zeolita HZSM-

5 modificada con varias sales precursoras de Zn: sulfato de zinc, acetato de zinc, nitrato de zinc y cloruro de zinc. Las zeolitas modificadas se prepararon por el método de impregnación húmeda con 5 % en peso de Zn. En dicho trabajo se muestra que el tipo de sal de Zn afecta directamente la fuerza y la distribución de sitios ácidos tipo Brönsted en la superficie del catalizador. Los resultados muestran que los catalizadores preparados con sulfato de zinc ($ZnSO_4$) presentan la mejor actividad catalítica en BTX, con un rendimiento de 77.9 %, sin embargo, este rendimiento baja a 60 % a las 2 h de reacción.

De manera similar, Quan *et al.*, 2014, evalúan la zeolita nano-HZSM-5 con una relación Si/Al de 50 modificada con Zn, logrando un rendimiento BTX de 67.7 %, con 0.5 % en peso de Zn. Ellos demuestran que la eficiencia de este catalizador se relaciona con la concentración y distribución de sitios ácidos y un tamaño de cristal pequeño, que mejora la difusión de aromáticos ligeros. Por otro lado, Inoue *et al.*, 1995 informan que un catalizador de Ag/ZSM-5 muestra un rendimiento a aromático del 80 %, pero sólo el 40 % pertenece a la fracción BTX. Así mismo el catalizador presenta una baja estabilidad, desactivándose a las pocas horas. En otro estudio, Ni *et al.*, 2011 evalúan una zeolita ZSM-5 con Zn preparada mediante síntesis directa. Este catalizador presenta un largo tiempo de vida de 160 h y una tasa media de formación de coque de 0.2 %/h, sin embargo, el rendimiento BTX es menor al 50 % y baja a 32 % después de 160 h. En el mismo año, Youming *et al.*, 2011 realizan un estudio similar, en donde incorporaron de La y Zn a la zeolita HZSM-5 por el método de co-impregnación. Demuestran que el Lantano resulta ser un buen promotor que aumenta la selectividad a la fracción BTX y prolonga la vida del catalizador, inhibiendo la formación de coque. El mejor catalizador resulta ser el preparado con la composición de 0.6% La 0.8% Zn/HZSM-5 logrando una selectividad BTX del 56.6 % a 437 °C tras 4 h de reacción. Todos estos trabajos concuerdan con lo reportado por López Sánchez *et al.*, 2012, en donde mencionan que la impregnación de una zeolita conduce a la formación de nanoparticulas de metal (Zn, Ag o Ga) u óxido de metal, ya sea dentro o fuera de los canales de la zeolita y maximiza la selectividad a productos aromáticos ligeros.

Los catalizadores con diferentes especies de Zn en zeolitas HZSM-5 pueden ser preparados por diferentes métodos que incluyen impregnación, intercambio iónico, mezcla física con ZnO, y síntesis directa. Dependiendo del método de preparación las propiedades de texturales y ácidas pueden variar de gran manera. Niu *et al*., 2014 encuentran que la distribución de los sitios ácidos y la naturaleza de las especies de zinc, así como el rendimiento catalítico en MTA están influenciados de manera significativa por el método de preparación para la introducción de zinc en la zeolita. Por ejemplo, catalizadores de Zn/ZSM-5 preparados por síntesis directa (con Zn en el gel de síntesis), debido a su tamaño de partícula pequeño presentan tiempos de vida más largos en la reacción MTA, casi el doble que la zeolita HZSM-5 ácida. Como se ha mencionado claramente se comprueba que la adición de Zn favorece la formación de compuestos aromáticos ligeros con altos rendimientos a los productos BTX.

Con base a la información anterior, se comprueba que la zeolita ZSM-5 es un catalizador prometedor en la aromatización debido a su estabilidad hidrotérmica, estructural y su fuerte acidez, sin embargo, en comparación con las zeolitas ZSM-5 convencionales, se ha comprobado las zeolitas nanocristalinas presentan ventajas como una mejor difusión, así como una gran superficie externa, lo que mejora la actividad catalítica y la vida útil del catalizador (Taufiqurrahmi et al., 2010).

Existen pocos reportes publicados sobre zeolitas nanocristalinas para la conversion catalítica de metanol. Por ejemplo, Rownaghi y Hedlund en 2011 demuestran que nanocristales ZSM-5 uniformes conducen a una mayor capacidad de conversión y selectividad hacía aromáticos en comparación con los cristales mesoporosos de ZSM-5. De manera similar Wan et al., en 2016 comprobaron la actividad catalizadores nanocristalinos de ZSM-5 donde obtuvieron 100 % de conversión de metanol en el proceso MTG. Ellos demuestran que la formación de nanocristales promovieron la reacción de aromatización y disminuyeron la formación de coque, lo que aumentó la vida útil del catalizador.

A pesar de estos trabajos realizados, en cuestión a la reactividad y estabilidad del catalizador HZSM-5 modificado para la reacción de MTA, el rendimiento BTX es generalmente bajo, con una rápida desactivación del catalizador. En este contexto, Ni *et al.*, 2011 mencionan los parámetros claves a estudiar en la actividad catalítica de zeolitas en la reacción MTA; primero tratar de evitar la desactivación del catalizador por la deposición de residuos carbonosos y segundo estudiar el efecto de la localización de las especies metálicas en la superficie externa o bien en el interior de los canales de las zeolitas.

Debido a la rápida desactivación que sufren los catalizadores estudiados, se establece como objetivo el estudio de la influencia del empleo de distintas estrategias de síntesis y relacionar sus propiedades fisicoquímicas de los materiales con el fin de obtener a materiales con propiedades tales que los hagan más resistentes a la desactivación. Se implementan estrategias, tal control de la acidez, tamaño de cristal, variar el método de incorporación de Zn y tipo de topología con el fin de obtener zeolitas activas en el proceso MTH. Este tipo de estudio, no se ha reportado anteriormente en la literatura por lo que resulta ser un tema sobresaliente en el estudio de la conversión catalítica de metanol.

Como se mencionó anteriormente los materiales MeAPO y MeAPSO no han sido estudiados en este tipo de reacciones, a excepción de silicoaluminofosfatos (SAPO) como es el SAPO-5 y SAPO-34. Específicamente, el SAPO-5 ha sido previamente reportado por Terasaka et al., 2005 en el proceso MTO. En su estudio obtuvieron predominantemente propeno seguido de butenos con la conversión completa de metanol usando materiales SAPO-5 con diferentes materiales de morfología. Por el otro lado el SAPO-34 ha sido ampliamente estudiado en el proceso MTO por Álvaro en 2012 y Pinilla en 2016. Ellos demuestran que el SAPO-34 es altamente activo y selectivo en el proceso MTO mostrando una selectividad excepcionalmente alta, con selectividades reportadas para olefinas C2-C4 superiores al 80%.

Con base en estos antecedentes, en este trabajo se plantea el estudio de catalizadores zeolíticos, con un diseño controlado de sus propiedades químicas y estructurales para

mejorar la selectividad, estabilidad y resistencia a la desactivación de los catalizadores en el proceso MTH.

## 5. Objetivos

### 5.1. Objetivo general

Relacionar la actividad catalítica de la reacción de metanol a aromáticos (MTA) con zeolitas y AlPOs doblemente modificados con el método de incorporación de Zn, así como con el tamaño de cristal y la acidez de los materiales.

### 5.2. Objetivos específicos

➢ Conocer la variación de la selectividad a diferentes productos (olefinas, aromáticos entre otros) así como con la conversión de metanol de zeolitas de canales de 10 y 12 miembros modificadas con Zn (ZSM-5, TNU-9, MCM-68 y MCM-22).

➢ Relacionar las variaciones de acidez y de las diferentes formas de incorporación de Zn en las zeolitas con la actividad catalítica.

➢ Sintetizar zeolitas ZSM-5 con estructura nanocristalina y evaluar su actividad catalítica en la producción de aromáticos BTX y comparar su actividad con una zeolita ZSM-5 convencional.

➢ Determinar la influencia de la cantidad molar de Zn y Si en materiales AlPO-36 y AlPO-5 en la producción de productos de compuestos aromáticos, olefinas y otros productos.

➢ Caracterizar las zeolitas y zeotipos obtenidas por diferentes técnicas como XRD, Fisisorción de $N_2$, TGA, NMR de $^{29}Si$, $^{27}Al$ y $^{31}P$, Desorción a temperatura programada (TPD-$NH_3$), TEM, SEM y XPS.

# 6. Metodología

## 6.1. Reactivos utilizados

En esta primera sección se indican los reactivos químicos que han sido empleados en el desarrollo cada parte del trabajo de investigación.

- Tetraetil ortosilicato (TEOS, 98%, Sigma Aldrich),
- Hidróxido de aluminio hidratado ($Al(OH)_3$, Sigma-Aldrich),
- Acetato de zinc dihidrato ($Zn(CH_3COO)_2$-$2H_2O$, 99% Sigma Aldrich),
- Tripropilamina (TPA, 99%, Sigma Aldrich),
- N-metildiciclohexilamina (MCHA, 99%, Sigma Aldrich)
- Ácido fosfórico ($H_3PO_4$, 85 wt. % en $H_2O$, Aldrich).
- Hidróxido de sodio (98 %NaOH, Sigma Aldrich)
- Aluminato de sodio (41 %$Al_2O_3$, 37 wt.% $Na_2O$),
- Hidróxido de tetrapropil amonio (1 M TPAOH, Acros Organics, 8 mL),
- Bromuro de tetrapropil amonio (TPABr 98 wt.%, Sigma Aldrich)
- Etanol absoluto (99.8%, Sigma-Aldrich)
- Nitrato de zinc hexahidrato ($Zn(NO_3)_2$•$6H_2O$ grado reactivo, 98%, Sigma-Aldrich).
- Sílice fumante (Aerosil 200, Degussa)
- Biciclo [2.2.2]oct-7-ene-2,3,5,6-tetracarboxilic dihadride (> 95.0%, Sigma-Aldrich)
- Hexametilenimina (HMI, 99 %, Sigma Aldrich)
- Sílice coloidal (40% de suspensión en H2O, LUDOX HS-40, Aldrich)
- Nitrato de aluminio nonahidratado ($Al(NO_3)_3$$9H_2O$ reactivo ACS, 98%, Sigma-Aldrich),
- 1,4-dibromobutano (99%, Aldrich)
- 1-metilpirrolidona (97%, Aldrich)
- Metanol, HPLC 99,9% (Sigma-Aldrich)

## 6.2. Síntesis de zeolitas (aluminosilicatos)

En este apartado se describen los procedimientos generales que se han seguido para la preparación de los materiales zeolíticos (ZSM-5, MCM-22, TNU-9 y MCM-68) obtenidos durante la tesis.

### 6.2.1. Zeolita ZSM-5

#### 6.2.1.1. Síntesis de zeolita ZSM-5 por síntesis hidrotérmica

La zeolita sódica ZSM-5 se sintetizó a partir de una composición molar de $xSiO_2$-$yAl_2O_3$-$0.2TPABr$-$0.09Na_2O$-$zZnO$-$35H_2O$. Donde x/y representa la relación molar Si/Al y z representa la cantidad de zinc (0 y 0.01 moles). En una síntesis convencional, se disolvió aluminato de sodio, hidróxido de sodio (y $Zn(NO_3)_2 \cdot 6H_2O$ como fuente de zinc en su caso) en agua desionizada y, una vez disuelto, se añadió bromuro de tetrapropil amonio (TPABr) como agente de dirección de la estructura (ADE). Finalmente, se añadió sílice fumante como fuente de sílice, el gel se agitó durante una hora temperatura ambiente. El gel de síntesis se colocó en una autoclave de acero inoxidable con funda de teflón, a 160 °C en condiciones estáticas durante 72 h. El sólido se recuperó por filtración, se secó a 70 °C, se molió y se calcinó a 550 °C durante 8 h en una atmósfera de aire. Las muestras de Na-ZSM-5 calcinadas se intercambiaron con una solución de $NH_4NO_3$ 1 M a 80 °C durante 4 h, seguido de calcinación a 550 °C durante 6 h para intercambiar iones $Na^+$ por protones. El esquema de síntesis se representa en la Figura 6.1.

durante 2 horas a temperatura ambiente, posteriormente el gel fue colocado en una autoclave de acero inoxidable revestidos con teflón y se calentó a 160 °C durante 11 días, tanto en condiciones de agitación a 60 rpm (A) y en condiciones estáticas (S). Después de este período de tiempo, la autoclave se retiró del horno, se enfriaron en hielo y el sólido se filtró y se lavó con agua desionizada. El producto se secó a 110 °C durante la noche y se calcinó a 550 ° C durante 20 h en atmósfera de aire. El esquema de síntesis es el mismo que la figura 6.1.

### 6.2.4.    Síntesis de la zeolita TNU-9

La zeolita TNU-9 se sintetizó en condiciones hidrotérmicas siguiendo el procedimiento de Hong et al., 2007 usando 4-bis (metilpirodinio) pentano (1,4-MPP) en forma de bromuro como agente de dirección de estructura (ADE) el cual fue preparado, purificado y caracterizado según lo reportado por Hu et al., en 2014. Esta sal de amonio cuaternaria se almacenó en un desecador para su uso como ADE.

En una síntesis típica, $Al(NO_3)_3$-$9H_2O$ y NaOH se disolvieron en agua desionizada en un recipiente de teflón, y la mezcla se agitó vigorosamente durante 2 h. El ADE (1,4-MPP) se añadió y una vez disuelto, se añadió sílice fumante como fuente de sílice, el gel se mezcló vigorosamente durante 2 h más a temperatura ambiente. El gel se colocó en autoclave a 160 °C con agitación continua a 60 rpm durante 10 días. El gel de síntesis final tenía la siguiente composición molar: $xSiO_2$: $11Na_2O$: $yAl_2O_3$: 4.5 (1,4-MPP): $1200H_2O$, donde x/y representa la relación molar Si/Al. El sólido se recuperó por filtración, se secó a 70 °C y se calcinó con corriente de aire a 550 °C durante 10 h para eliminar el ADE orgánico ocluido.

Por otro lado, la síntesis de zeolitas TNU-9 sustituidas con zinc se realizó utilizando el procedimiento anterior, sin embargo, la composición final del gel fue 30 $SiO_2$: 11 $Na_2O$: $xZnO$: $yAl_2O_3$: 4.5 (1,4-MPP): $1200H_2O$, donde x es la cantidad en moles de óxido de zinc colocado en el gel de síntesis usando acetato de zinc dihidrato $(Zn(CH_3COO)_2 \cdot 2H_2O$

como sal precursora de Zn. Para estos geles, la cantidad de ZnO se varió para una relación x/x+y de 0.33 y 0.16, que corresponde a 0.5 y 0.2 moles de ZnO, respectivamente.

### 6.2.5. Síntesis de la zeolita MCM-68

MCM-68 zeolita se sintetizó de acuerdo con lo reportado por Hao et al., en 2018. El ADE (TEBOP$^{2+}$(I$^-$)$_2$) se sintetizó exactamente siguiendo el procedimiento informado [16] a partir de biciclo [2.2.2] oct-7-eno-2,3:5,6-tetracarboxílico anhídrido disponible por Aldrich. La composición de gel fue de xSiO$_2$:0.1TEBOP$^{2+}$(I$^-$)$_2$:0.375KOH: yAl(OH)$_3$: 30H$_2$O, donde x/y representa la relación molar Si/Al. En una síntesis típica, sílice coloidal, agua destilada y Al(OH)$_3$ se mezclaron y se agitaron a temperatura ambiente durante 10 min, luego se añadió KOH a la solución y se agitó durante otros 15 min. Posteriormente, se añadió TEBOP$^{2+}$(I$^-$)$_2$ y la mezcla se agitó durante 2 h. Luego, el gel se transfirió a una autoclave revestida con teflón de 50 ml y se colocó en un horno a 160 °C durante 14 días en condiciones estáticas. El producto sólido obtenido se separó por filtración, se lavó varias veces con agua destilada y se secó durante la noche. El MCM-68 como se sintetizó se calcinó en un horno de mufla a 650 ° C durante 6 h para eliminar el ADE.

### 6.2.6. Preparación de zeolitas modificas por intercambio iónico de Zn

Las zeolitas sódicas se convirtieron en zeolitas ácidas (protónicas) por reflujo con solución de NH$_4$NO$_3$ 1 M a 80 °C durante 4 h (el intercambio de realizó dos veces), seguido de filtración y secado a 70 °C durante una noche. Finalmente la muestra se calcino a 550 °C durante 4 h con flujo de aire. Las zeolitas ácidas sintetizadas previamente se intercambiaron con una solución 0.025 M de Zn(NO$_3$)$_2$•6H$_2$O a 80 °C durante 4 h. La zeolita se filtró, se lavó y se secó a 70 °C, finalmente el polvo resultante se calcinó a 550 ° C durante 4 h con flujo de aire. En la Tabla 6.1 se enumeran los resultados de las síntesis realizadas y sus condiciones e igualmente la síntesis se esquematiza en la Figura 6.1

**Tabla 6.1. Condiciones experimentales para la síntesis los materiales zeolíticos ZSM-5, TNU-9, MCM-68 y MCM-22**

| Zeolita | Relación Si/Al | Condiciones de síntesis | Método de incorporación de Zn | Clave |
|---|---|---|---|---|
| ZSM-5 | 25 | Agitación | Intercambio iónico | nano HZnZ25-i |
| | 25 | Agitación | Intercambio iónico | nano HZ25 |
| | 25 | Estático | Intercambio iónico | HZnZ25-i |
| | 25 | Estático | N/A | HZ25 |
| | 50 | Estático | Gel de síntesis | HZ50 0.01 Zn-G |
| MCM-22 | 30 | Agitación | Gel de síntesis | M22-30A-G |
| | 30 | Estático | Gel de síntesis | M22-30S-G |
| | 30 | Estático | Gel de síntesis | ZM22-30S |
| | 30 | Estático | Gel de síntesis | ZM22-30S-G |
| | 30 | Agitación | Intercambio iónico | ZM22-30A |
| | 50 | Agitación | N/A | M22-50A |
| | 50 | Estático | N/A | M22-50S |
| MCM-68 | 11 | Estático | Intercambio iónico | ZM68-11 |
| TNU-9 | 15 | Agitación | N/A | T9-15 |
| | 15 | Agitación | Intercambio iónico | ZT9-15 |
| | 15 | Agitación | Gel de síntesis | T9 0.5 Zn |
| | 15 | Agitación | Gel de síntesis | T9 0.2 Zn |
| | 30 | Agitación | N/A | T9-30 |
| | 30 | Agitación | Intercambio iónico | ZT9-30 |
| | 50 | Agitación | N/A | T9-50 |
| | 50 | Agitación | Intercambio iónico | ZT9-50 |

*A= Condiciones de síntesis en agitación*

*S= Condiciones de síntesis en estático*

*G= Zn incorporado como gel de síntesis*

### 6.3. Síntesis de materiales AlPO doblemente sustituidos por Zn y Si (MeAPSO)

#### 6.3.1. Síntesis de materiales MeAPSO-36

MeAPSO-36 se sintetizó de acuerdo con el procedimiento reportado por O'Brien et al., en 2007. Los geles se prepararon usando ácido fosfórico, hidróxido de aluminio hidratado y tripropilamina como ADE. La relación molar fue igual a 1.0 P: y Zn: 1-y Al: x Si: 0.8 TPA :10 $H_2O$.

En una síntesis típica, $H_3PO_4$ y $Al(OH)_3$-x$H_2O$ se disolvieron en agua desionizada con agitación continua durante 15 min. Tras disolverse, se añadió lentamente acetato de zinc dihidratado ($Zn(CH_3$-$COO)_2$-2$H_2O$) a la solución con agitación vigorosa hasta que se consiguió un gel homogéneo. Finalmente, el ADE se añadió al gel gota a gota con agitación vigorosa durante 1 h. El gel de síntesis se colocó en una autoclave inoxidable revestido con Teflón (PTFE) y se calentaron durante 18 h a 160 °C. Posteriormente, el sólido resultante, se lavó con agua destilada y se secó a 100 °C durante una noche. Las muestras preparadas se calcinaron a 550 °C durante 6 h bajo un flujo de aire. Anteriormente, la muestra se calentó a una velocidad de 1 °C/min bajo un flujo de $N_2$ y se mantuvo durante 1 hora a 550 °C bajo esa atmósfera. El esquema de síntesis de muestra en la Figura 6.2.

Primero, la relación molar de zinc (y) se modificó entre 0 y 0.15 moles, manteniendo constante la cantidad de silicio en los geles (x). Complementariamente en una segunda etapa, la cantidad de zinc que se incorporó en los geles de síntesis (y = 0.1) se mantuvo constante el contenido de silicio (x) agregando entre 0 y 0.25 moles. La composición del gel y las condiciones de síntesis se presentan en la Tabla 6.2.

6.3. Las muestras se sintetizaron en las condiciones similares que los MeAPSO-5, sin embargo, la temperatura de síntesis fue de 175 °C por 4 h (Figura 6.3)

**Tabla 6.3. Materiales MeAPSO-5 sintetizados**

| Muestra | Denotación | Moles de Zn (y) | Moles de Si (x) |
|---|---|---|---|
| A5-0.02 Zn-0.15 Si | S5-1 | 0.02 | 0.15 |
| A5-0.15 Zn-0.15 Si | S5-2 | 0.15 | 0.15 |
| A5-0.05 Zn-0.02 Si | S5-3 | 0.05 | 0.02 |
| A5-0.05 Zn-0.05 Si | S5-4 | 0.05 | 0.05 |
| A5-0.15 Si (SAPO-5) | S5 | - | 0.15 |
| A5-0.04 Zn (ZnAPO-5) | Z5 | 0.04 | - |

## 6.4. Caracterización de las zeolitas y zeotipos

Los sólidos microporosos obtenidos fueron caracterizados empleando diversas técnicas para conocer sus propiedades fisicoquímicas. El estudio completo de las propiedades de los materiales será clave a la hora de comprender su comportamiento catalítico en el proceso MTH.

Los patrones de difracción de rayos X de las muestras preparadas se registraron en un difractómetro PANalytical X'Pert Pro, empleando la radiación Kα del cobre (λ=1.54Å) en el intervalo de ángulos entre 4 y 80º. Para los análisis se usó un tamaño de paso de 0.2º/min y un tiempo de acumulación de 50 segundos por paso. Se usó un detector X'Celerator de Tecnología de tiras múltiples en tiempo real (RTMS).

Los experimentos termogravimétricos (TGA en inglés) se han llevado a cabo en una termobalanza Perkin Elmer TGA 7. Las muestras (5-15 mg) se calentaron en el rango de temperaturas entre 30 y 900 ºC con una rampa de calentamiento de 20 ºC/min bajo un flujo de aire de 40 ml/min. Para llevar a cabo los análisis de TGA las muestras deben ser homogéneas, de manera que se tenga una información representativa, y estar apropiadamente molidas.

Para los análisis de microscopia electrónica de barrido (SEM en inglés) empleado un microscopio Hitachi TM-1000 operando a 15 kV y un microscopio marca Carl Zeiss,

modelo Supra 55VP. La muestra se adhiere sobre un soporte metálico empleando una cinta adhesiva conductora de doble cara. Las imágenes se obtuvieron utilizando un detector de electrones retrodispersados.

Para los análisis químicos, se ha empleado la técnica de ICP-OES para determinar la composición química de los materiales zeolíticos después de su calcinación. Las muestras se analizaron en un espectrómetro de emisión atómica Perkin-Elmer Optima 3300DV. Antes de realizar el análisis las muestras se colocan en una estufa a 110 °C por 24 h. Una vez eliminada el agua adsorbida, las muestras se disgregan por un tratamiento de fusión alcalina para lo cual se emplea una mezcla fundente de metaborato de litio y tetraborato de litio (relación de peso 1:1). El fundido se recoge en una disolución de ácido nítrico al 10%. La disolución se introduce al espectrómetro en forma de aerosol mediante un sistema de nebulización. La disgregación de las muestras se llevó a cabo en un equipo de fusión automático Claisse, modelo Fluxy-30.

Las medidas de adsorción-desorción de nitrógeno de este trabajo se han llevado a cabo a la temperatura del nitrógeno líquido (-196ºC) en un equipo Micrometrics ASAP 2010. Antes de los análisis las muestras fueron pretratadas por desgasificación a vacío durante 24 h a 350ºC para eliminar cualquier molécula adsorbida en el material.

Los espectros de $^{29}Si$, $^{27}Al$ y $^{31}P$ CP/MAS NMR se registraron en un espectrómetro Brucker AV 400WB, empleando una sonda de 4mm y operando a 79.5 MHz. El tiempo de contacto fue de 1s para el $^{27}Al$ y 60 s para el $^{27}Al$ y $^{31}P$, el tiempo de reciclo fue de 5s para los tres análisis. Las muestras se giraron en el ángulo mágico a 10kHz.

Los experimentos de desorción térmica programada (TPD-NH$_3$) se llevaron a cabo en un equipo de Quimisorción Micromeritics Autochem II 2920 para análisis de quimisorción de gases a temperatura programada. El equipo cuenta con un detector de conductividad térmica (TCD). Típicamente, la muestra calcinada y tamizada en partículas de 400-840 mm se somete a un pretratamiento a 500 ºC durante una hora bajo flujo de helio (25ml/min), tras el cual se enfría hasta la temperatura de adsorción (177 ºC). Entonces se pasa durante 4 horas con un flujo de mezcla de amoniaco y helio de 15 ml/ml (5%vol.

de NH$_3$ en He). Posteriormente, manteniendo la temperatura a 177 ºC, se pasa un flujo de helio (25ml/min) para eliminar el amoniaco débilmente adsorbido. Posteriormente se mide la desorción de amoniaco subiendo la temperatura hasta 550ºC a 10ºC/min.

## 6.5. Evaluación catalítica

Para el ensayo catalítico de las muestras se ha empleado un equipo microactivity PID acoplado a un cromatógrafo de gases los cuales se describen a continuación

### 6.5.1. Equipo *Microactivity Reference PID*

Para la prueba catalítica de las zeolitas y zeotipos, se empleó un equipo de laboratorio de tipo Microactivity Reference (PID Eng&Tech), totalmente automático y programado desde un software de control controlado con un equipo de cómputo (Figura 6.4).

El sistema consta de un reactor de lecho fijo de vidrio de 15 mm de diámetro interno en el que el catalizador se aloja sobre una placa porosa, que opera a presión atmosférica con flujo descendente, de manera que el metanol se alimenta por una bomba peristáltica en la parte superior del reactor, y los productos de reacción se obtienen en la parte inferior del mismo. El reactor se encuentra alojado en el interior de una caja caliente que se mantiene durante los experimentos a 180 ºC, para mantener el metanol siempre en fase gas. La salida del reactor se conecta on-line a un cromatógrafo de gases para la identificación y cuantificación de los productos de reacción. De modo similar, la tubería que transfiere la mezcla de productos desde la salida del reactor hasta la entrada del cromatógrafo de gases se mantiene calefactada (180-200 ºC) para evitar la condensación de productos. Los productos condensados sin analizar se recolectan en un matraz recolector en donde se observa el burbujeo como producto del gas de arrastre.

### 6.5.2. Cromatógrafo de gases Varían CP3800

El cromatógrafo de gases empleado para el análisis de los productos de reacción que se obtienen en los ensayos llevados a cabo en el equipo de reacción Microactivity Reference es un equipo Varian CP3800 provisto de dos detectores que analizan los productos que les llegan a través de dos columnas distintas conectadas en paralelo. Primeramente, hay un detector de ionización de llama (FID) conectado a una columna capilar Petrocol DH50.2. La columna (de 50 m de largo x 0.20 mm de diámetro externo) está recubierta con una película de fase activa de 0.5 mm de metilsilicona no enlazada. La combinación Petrocol-FID se emplea para la separación y análisis de hidrocarburos. Por otra parte, se conecta un detector de conductividad térmica (TCD) a una columna empaquetada Hayesep Q (2 m de largo, 1/8 de pulgada de diámetro externo y 2 mm de diámetro interno) para la separación de los compuestos orgánicos oxigenados. La inyección de la muestra se lleva a cabo mediante una válvula automática con dos muestreadores de 0.25 ml, lo que permite la separación del flujo que llega al cromatógrafo y la inyección de cada una de las partes en las dos columnas descritas.

El programa de análisis que se usa se optimizó para lograr una buena separación de los productos de reacción. Primeramente, se mantiene el horno del cromatógrafo a 40 ºC durante 5 min. Posteriormente se aumenta la temperatura de 40 a 150 ºC con una rampa de 5 ºC/min. A continuación, se aumenta la temperatura hasta 270 ºC a una velocidad de 10 ºC/min, y finalmente se mantiene el horno a 270 ºC durante 10 min más. De ese modo, cada análisis dura 49 min, tras los cuales se deja pasar 10 min más para el enfriamiento del horno del cromatógrafo para la siguiente inyección automática. La presión de helio a la entrada de la columna capilar es de 40psi, y su relación de split, 150:1. El caudal de helio tanto en la columna Hayesep Q como en el detector TCD es de 30 ml/min. Ambos detectores (FID y TCD) se mantienen a 270 ºC.

### 6.5.3. Cálculos de conversión y selectividad

Para cada ensayo catalítico se calculó la conversión de metanol y la selectividad a los distintos productos de reacción dependiendo del tiempo de retención en la columna del cromatógrafo. En esta reacción el dimetiléter (DME) se forma como intermediario por lo que no considera estrictamente un producto de reacción, por lo que los moles de DME se consideran como moles de reactivo tal y como se muestra en la ecuación:

$$Conversion\ de\ oxigenados\ (\%\ molar)$$
$$= \frac{\sum Moles\ totales\ obtenidos - Moles\ de\ DME - Moles\ de\ metanol\ (\sin reaccionar)}{\sum moles\ de\ metanol\ alimentados}\ x\ 100$$

Para el cálculo de la selectividad a los distintos productos de reacción en ambos detectores del cromatógrafo se dividen los moles de cada producto entre la suma de los moles de todos los productos obtenidos (sin incluir el DME).

$$\boldsymbol{Selectividad\ a\ producto\ i}\ (\%\ \boldsymbol{molar}) = \frac{moles\ de\ producto\ formado\ i}{\sum moles\ productos\ totales}\ x\ 100$$

### 6.5.4. Productos de reacción analizados en el cromatógrafo

Tanto en el FID y TCD se detectan alrededor de 30 productos que salen en la corriente gaseosa del reactor. Cada producto fue inyectado con un estándar para conocer su tiempo de retención en las columnas del cromatógrafo. En la tabla 6.4 y 6.5 se enlistan los productos analizados en el TCD y en el FID, respectivamente.

**Tabla 6.4. Productos de reacción analizados por el detector TCD**

| Producto | Tiempo de retención RT [min] |
|----------|------------------------------|
| Metano | 1.8 |
| $CO_2$ | 2.53 |
| Etileno | 4.2 |
| Etano | 5.5 |
| Agua | 9.8 |
| Propileno | 15 |
| Propano | 15.9 |
| MeOH + DME | 18.04 |
| Trans+Cis-C4= | 22.8 |
| 1+i-C4= | 23.4 |
| i+n C4 | 24.4 |
| C4+ | 38 |

**Tabla 6.5. Productos de reacción analizados por el detector FID**

| Producto | Tiempo de retención RT [min] |
|---|---|
| Metano | 4.12 |
| TC2 | 4.15 |
| TC3 | 4.23 |
| DME | 4.32 |
| Iso Butano | 4.37 |
| Metanol | 4.4 |
| 1+I Buteno | 4.45 |
| N-Butano | 4.48 |
| Trans-Buteno | 4.52 |
| Cis Buteno | 4.58 |
| TC5 a | 4.9 |
| TC5 b | 5.3 |
| TC6 (no aromáticos) | 6.75 |
| Benceno | 8.35 |
| TC7 (no aromáticos) | 9.8 |
| Tolueno | 12.55 |
| TC8 (no aromáticos) | 14.6 |
| Etilbenceno | 16.71 |
| m-/p-xilenos | 17 |
| o-xileno | 17.97 |
| Ar C9 | 21 |
| Ar C10 | 26.48 |
| Ar C11-C12 | 33 |

### 6.5.5. Reacciones químicas en el proceso MTH

Como se muestra en la Figura 6.5, el proceso MTH tiene lugar en una serie de pasos donde la primera etapa es la deshidratación de metanol para formar DME. A partir de esta mezcla intermedia de compuestos oxigenados, se dice que se producen alquenos o productos olefínicos producidos en la etapa secundaria, los cuales su formación es importante en el proceso MTO, mientras que en la etapa terciaria se obtienen productos de grado de gasolina, aromáticos ligeros y pesados. Los productos del proceso MTG consisten en una mezcla de parafinas, aromáticos y olefinas, y para el sistema termodinámico, se tratan como productos de equilibrio en este análisis.
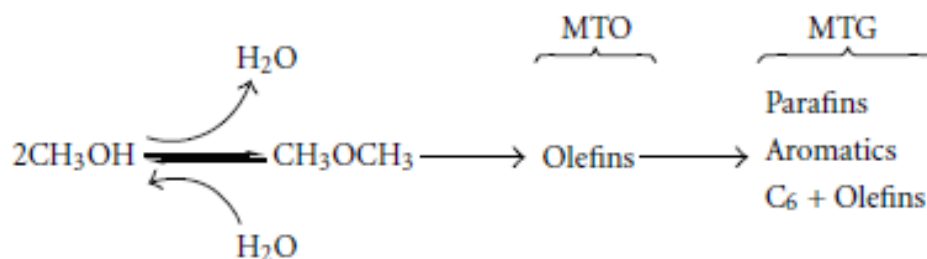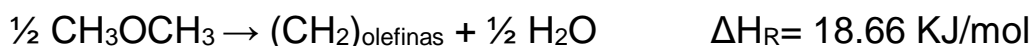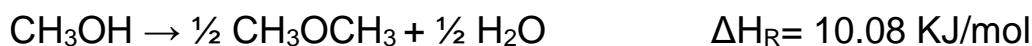


***Figura 6.5. Vía de reacción propuesta inicialmente para la conversión de metanol en hidrocarburos (Gunawardena y Fernando, 2011)***

Para la formación de metano, la reacción es la siguiente

$$4CH_3OH \rightarrow 3CH_4 + 2H_2O + CO_2$$

Esta reacción tiene una entalpia de reacción ($\Delta H_R$) igual a -281.79 KJ/mol.

Para la formación de olefinas C2-C5, como DME como intermedario, la reacción es la siguiente.

$$CH_3OH \rightarrow \tfrac{1}{2} CH_3OCH_3 + \tfrac{1}{2} H_2O \qquad \Delta H_R = 10.08 \text{ KJ/mol}$$

$$\tfrac{1}{2} CH_3OCH_3 \rightarrow (CH_2)_{olefinas} + \tfrac{1}{2} H_2O \qquad \Delta H_R = 18.66 \text{ KJ/mol}$$

(Para olefinas C2-C5)

Para la formación de aromáticos BTX y etilbenceno, la reacción es la siguiente

$$29 \; CH_3OH \rightarrow C_6H_6 + C_7H_8 + C_8H_{10} + C_8H_{10} + 29 \; H_2O + 11 \; H_2$$

(Benceno)  (Tolueno)  (xyleno)  (Etilbenceno)

Esta reacción es altamente exotérmica con una entalpia de reacción igual a -868.27 KJ/mol.

### 6.5.6. Cálculo de energía de activación de catalizadores seleccionados

La energía de activación Ea representa la energía necesaria para que los reactivos puedan transformarse en productos, dicho de otra forma, es la barrera energética que los reactivos deben vencer para poder modificar sus estructuras y convertirse en productos.

Svante Arrhenius propuso una ecuación para establecer la influencia de la temperatura sobre la constante de velocidad, la cual es válida para un rango de temperaturas

$$k = A \; e^{-Ea/RT}$$

Donde k0 y A son el factor de frecuencia o factor pre-exponencial, Ea es la energía de activación de la reacción. T es la temperatura absoluta a cuál la k es evaluada. R es la constante universal de los gases.

De manera general la velocidad de la reacción aumenta cuando, T aumenta debido al crecimiento de la constante de velocidad, según la ley de Arrhenius en su forma logarítmica es:

$$ln \; k = lnA - Ea/RT$$

Esta ecuación tiene la forma de una ecuación lineal donde al graficar ln k vs 1/T da como resultado una pendiente y una ordenada al origen igual a

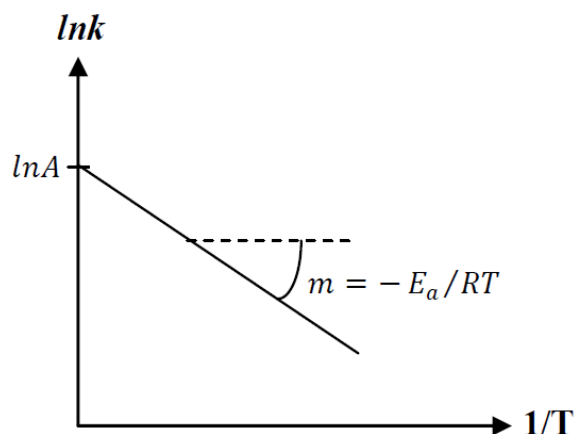$$m = -Ea/RT \; \text{y} \; b = lnA$$
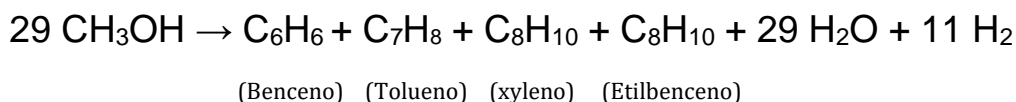
***Figura 6.6. Grafica de Ln A vs 1/T para el calculo de Ea para una reacción a diferentes temperaturas***

De acuerdo con la gráfica anterior se calculó la Ea de algunos catalizadores para la producción de la fracción BTX a tres temperaturas (400, 425 y 450 °C). La figura 6.7 el cálculo de la energía de activación de zeolitas seleccionadas, la cual varía dependiendo de la estructura y de la presencia de zinc. La zeolita ZSM-5 con estructura nanocristalina y la zeolita T9-15 0.5 Zn presentaron los valores de Ea mas pequeños, lo cual indica que son las zeolitas para activas para el proceso MTA, u otra manera de explicarlo es que, la barrera de activación es menor para que los reactivos se transformen en productos. Del mismo modo, la Ea para la zeolita sin estructura nanocristalina es mayor, indicando que se requiere mayor energía para la generación de productos BTX.

## 7. Referencias

Akolekar BD (1998) Multimetal-substituted aluminophosphate molecular sieves. Applied Catalysis A: General 171: 261-272

Alipour SM (2016) Recent advances in naphtha catalytic cracking by nano ZSM-5: A review. Chinese J Catal 37: 671–680

Álvaro Muñoz T., Síntesis de catalizadores sólidos ácidos para el proceso MTO de conversión de metanol en olefinas. Tesis doctoral, Madrid 2012. Instituto de catálisis y petroleoquímica (ICP), consejo superior de investigaciones científicas (CSIC)

Álvaro T, Márquez-Álvarez C, Sastre E (2012) Use of different templates on SAPO-34 synthesis: Effect on the acidity and catalytic activity in the MTO reaction. Catal Today 179: 27-34

Álvaro T., Márquez-Álvarez C, Sastre E (2014) Aluminium chloride: a new aluminium source to prepare SAPO-34 catalysts with enhanced stability in the MTO process. Appl Catal A-Gen 472: 72-79

Baerlocher Ch, McCusker LB, Olson DH, Atlas of Zeolite Framework Types, 6th ed., Elsevier, Amsterdam,2007, see also: http://www.iza-structure.org/ databases

Barthomeuf D (1994) Topological model for the compared acidity of SAPOs and SiAl zeolites Zeolites 14: 394–401

Bennett JM, Dytrych WJ, Pluth JJ, Richardson Jr. JW, Smith JV (1986) Structural features of aluminophosphate materials with aluminium/phosphorus= 1. Zeolites 6: 349-360

Bi Y, Wang Y, Chen X, Yu Z, Xu L (2014) Methanol aromatization over HZSM-5 catalysts modified with different zinc salts. Chinese J Catal. 35: 1740–1751

Bjørgen M, Svelle S, Joensen F, Nerlov J, Kolboe S, Bonino F, Palumbo L, Bordiga S, Olsbye U (2007) Conversion of methanol to hydrocarbons over zeolite H-ZSM-5: On the origin of the olefinic species. J Catal. 249: 195–207

Bleken F, Skistad W, Barbera K, Kustova M, Bordiga S, Beato P, Lillerud KP, Svellea S, Olsbye U (2011) Conversion of methanol over 10-ring zeolites with differing volumes at channel intersections: comparison of TNU-9, IM-5, ZSM-11 and ZSM-5. Phys. Chem. Chem. Phys. 13: 2539–2549

Briend M, Derewinski M, Lamy A, Barthomeuf D (1993) In New Frontiers in Catalysis; 10th Internat. Congr. Catal., L. Guczi, F. Solymosi, P. Tenteyi, Eds., Akademiai Kiado, Budapest, Hungary, 409

Calabro DC, Cheng JC, Crane Jr RA., Kresge CT, Dhingra SS, Steckel MA, Stern DL, Weston SC, U. S. Patent. 6049018, 2000

Cejka J, Corma A, Zones S (2010) Zeolites and Catalysis: Synthesis, Reactions and Applications. Ed WILEY-VCH

Cejka J, Van Bekkum H (2005) Zeolites and Ordered Mesoporous Materials: Progress and Prospects. Amsterdam: Elsevier 380

Chang CD, Silvestri AJ (1997) The conversion of methanol and other O-compounds to hydrocarbons over zeolite catalysts. J. Catal 47: 249-259

Chen JQ, Bozzano A, Glover B, Fuglerud T, Kvisle S (2005) Recent advancements in ethylene and propylene production using the UOP/Hydro MTO process. Catal. Today 106: 103–107

Choudhary TV, Kinage A, Banerjee S, Choudhary VR (2006) Influence of Si/Ga and Si/Al ratios on propane aromatization over highly active H-GaAlMFI. Catal. Commun. 7: 166

Choudhary V (1988) Influence of thermal, hydrothermal, and acid-base treatments on structural stability and surface and catalytic properties of AlPO4-5. J. Catal 111: 254-263

Cobb J (1995) in New Zealand Synfuel, ed. G. Connell, Cobb/Horwood. Publications, Auckland, New Zealand, p. 1.

Conte M, Lopez-Sanchez JA, He Q, Morgan DJ, Ryabenkova Y, Bartley JK, Carley AF,Taylor SH, Kiely CJ, Khalid K, Hutchings GJ (2012) Modified zeolite ZSM-5 for the methanol to aromatics reaction. Catal. Sci. Technol., 2: 105–112

Corma A, Agustín A (1995) Zeolites and Zeotypes as catalysts. Adv. Mater. 7(2): 137-144

Csicsery SM (1971) The cause of shape selectivity of transalkylation in mordenite, Journal of Catalysis 23: 124-130

Csicsery SM (1984) Shape-selective catalysis in zeolites. Zeolites 4: 203-213

Del Val S, Blasco T, Sastre E, Perez-Pariente J (1995) Synthesis of SiVPI-5 with Enhanced Activity in Acid Catalyst Reactions. J. Chem. Soc., Chem. Commun. (7): 731–732

Dorset DL, Weston SC, Dhingra SS (2006) Crystal Structure of Zeolite MCM-68: A New Three-Dimensional Framework with Large Pores. J. Phys. Chem. B. 110: 2045-2050

Ernst S, Elangovan SP, Gerstner M, Hartmann M, Hecht T, Sauerbeck S (2004) Characterization and catalytic evaluation of zeolite MCM-68. Stud Surf Sci Catal. 154: 2861-2868

Fahim MA, Alsahhaf TA, Elkilani A (2010) Fundamentals of Petroleum Refining, Elsevier, Amsterdam, 95-152

Fang Y, Su X, Bai X, Wu W, Wang G, Xiao L, Yu A (2017) Aromatization over nanosized Ga-containing ZSM-5 zeolites prepared by different methods: Effect of acidity of active Ga species on the catalytic performance. J. Energy Chem. 26: 768–775

Finger G, Kornatowski J, Jancke K, Matschat R, Baur WH (1999) AlPO4-31 derivatives doped with various metals: effects on crystal symmetry and thermal stability, Micropor Mesopor Mater 33: 127-136

Flanigen EM, Lok BH, Patton RL, Wilson ST (1986) Aluminophosphate Molecular Sieves and the Periodic Table. Pure Appl. Chem. 58: 1351-1358

Gabrienko AA, Arzumanov SS, Toktarev AV, Danilova IG, Prosvirin IP, Kriventsov VV, Zaikovskii VI, Freude D, Stepanov AG (2017) Different Efficiency of Zn2+ and ZnO Species for Methane Activation on Zn-Modified Zeolite. ACS Catal 1-45

García-Martínez J, Pérez Pariente J (2003) Materiales Zeolíticos: Síntesis, Propiedades y Aplicaciones. Publicaciones de la Universidad de Alicante, ISBN: 84-7908- 722-6

Gunawardena DA, Fernando SD (2011) Deoxygenation of Methanol over ZSM-5 in a High-Pressure Catalytic Pyroprobe. Chem. Eng. Technol. 34 (2): 173–178.

Groen JC, Peffer LA, Moulijn JA, Perez-Ramirez J (2005) Mechanism of Hierarchical Porosity Development in MFI Zeolites by Desilication: The Role of Aluminium as a Pore-Directing Agent. Chem. Eur. J. 11: 4983 – 4994

Hao H, Chang Y, Yu W, Lou LL, Liu S (2018) Hierarchical porous MCM-68 zeolites: Synthesis, characterization and catalytic performance in m-xylene isomerization. Micropor Mesopor Mater 263: 135–141

Hartmann M, Kevan L (1999) Transition-metal ions in aluminophosphate and silicoaluminophosphate molecular sieves: location, interaction with adsorbates and catalytic properties. Chemical reviews 99: 635-664

Hong SB, Min HK, Shin CH, Cox PA, Warrender SJ, Wright PA (2007) Synthesis, Crystal Structure, Characterization, and Catalytic Properties of TNU-9. J. Am. Chem. Soc. 129: 10870-10885

Hong SB, Nam IS, Min HK, Shin CH, Warrender SJ, Wright PA, Cox PA, Gramm F, Baerlocher Ch, McCusker LB, Liu Z, Ohsuna T, Terasaki O (2007) TNU-9: a novel medium-pore zeolite with 24 topologically distinct tetrahedral sites. Zeolites to Porous MOF Materials – the 40th Anniversary of International Zeolite Conference

Hu J, Wu S, Liu H, Ding H, Li Z, Guan J, Kan Q (2014) Effect of mesopore structure of TNU-9 on methane dehydroaromatization. RSC Adv. 4: 26577–26584

Inagaki S, Tsuboi Y, Nishita Y, Syahylah T, Wakihara T, Kubota Y (2013) Rapid Synthesis of an Aluminum-Rich MSE-Type Zeolite by the Hydrothermal Conversion of an FAU-Type Zeolite. Chem Eur J. 19: 7780–7786

Inoue Y, Nakashiro K, Ono Y (1995) Selective conversion of methanol into aromatic hydrocarbons over silver-exchanged ZSM-5 zeolites. Micropor Mater 4: 379 383

Ji Y, Yang H, Yan W (2017) Strategies to Enhance the Catalytic Performance of ZSM-5 Zeolite in Hydrocarbon Cracking: A Review. Catalysts 7: 367

Jia Y, Wang J, Zhang K, Liu S, Chen G, Yang Y, Ding C, Liu P (2017) Catalytic Conversion of Methanol to Aromatics over Nanosized HZSM-5 Zeolite Modified by $ZnSiF_6 \cdot 6H_2O$. Catal. Sci. Technol. 7(8): 1-18

Kim J, Choi M, Ryoo R (2010) Effect of mesoporosity against the deactivation of MFI zeolite catalyst during the methanol-to-hydrocarbon conversion process. J. Catal. 269: 219–228

Koempel H, Liebner W (2007) Lurgi's Methanol To Propylene (MTP®) Report on a successful commercialization. Natural Gas Conversion VIII

Kokotailo GT, Lawton SL, Olson DH, Meier WM (1978) Structure of synthetic zeolite ZSM-5, Nature, 272: 437

Konno H, Tago T, Nakasaka Y, Ohnaka R, Nishimura J, Masuda T (2013) Effectiveness of nano-scale ZSM-5 zeolite and its deactivation mechanism on catalytic cracking of representative hydrocarbons of naphtha. Micropor Mesopor Mater. 175: 25–33

Koohsaryan E, Anbia M (2016) Nanosized and hierarchical zeolites: A short review. Chinese J Catal. 37: 447–467

Kubu M, Zones SI, Cejka J (2010) TUN, IMF and -SVR Zeolites; Synthesis, Properties and Acidity. Top Catal. 53:1330–1339

Laforge S, Martin D, Paillaud JL, Guisnet M (2003) m-Xylene transformation over H-MCM-22 zeolite 1. Mechanisms and location of the reactions. J. Catal 220: 92–103

Leonowicz ME, Lawton SL, Partridge RD, Chen P, Rubin MK (1994) MCM-22: A Molecular Sieve with Two Independent Multidimensional Channel Systems. Science 264(5167): 1910-1913

Li Y, Liu S, Zhang Z, Xie S, Zhu X, Xu L (2008) Aromatization and isomerization of 1-hexene over alkali-treated HZSM-5 zeolites: Improved reaction stability. Applied Catalysis A: General 338: 100–113

Lok BM, Messina CA, Patton RL, Gajek RT, Cannan TR, Flanigen EM (1984) The role of organic molecules in molecular sieve synthesis. JACS 106: 6092-6093

Lopez-Sanchez JA, Conte M, Landon P, Zhou W, Bartley KJ,Taylor SH, Carley AF, Kiely CJ, Khalid K, Hutchings GJ (2012) Reactivity of Ga2O3 Clusters on Zeolite ZSM-5 for the Conversion of Methanol to Aromatics. Catal Lett 142:1049–1056

Makarova M, Ojo A, Al-Ghefaili K, Dwyer J (1992) in: Proceedings of the IX International Zeolite Conference, Montreal, Canada, 2: 259

Marchese L, Chen J, Wright PA,Thomas JM (1993) Formation of H3O+ at the Bronsted Site in SAPO-34 Catalysts. J. Phys. Chem. 97 (31): 1-4

Martens JA, Grobet PJ, Jacobs PA (1990) Catalytic activity and Si, Al, P ordering in microporous silicoaluminophosphates of the SAPO-5, SAPO-11, and SAPO-37 type. J. Catal 126(1): 299-305

Martin C, Tosi-Pellenq N, Patarin J, Coulomb JP (1998) Sorption properties of AlPO4-5 and SAPO-5 zeolite-like Materials. Langmuir 14: 1774-1778

Matias P, Lopes JM, Laforge S, Magnoux P, Russo PA, Ribeiro-Carrott MML, Guisnet M, Ribeiro FR (2008) Methylcyclohexane transformation over HMCM22 zeolite: Mechanism and location of the reactions. J. Catal 259: 190–202

Messina CA, Lok BH, Flanigen EM, U. S. Patent 4,544,143 (1985)

Miyake K, Hirota Y, Ono K, Uchida Y, Nishiyama N (2016) Selective Production of Benzene, Toluene and p-Xylene (BTpX) from Various C1-3 Feedstocks over ZSM-5/Silicalite-1 Core-Shell Zeolite Catalyst. ChemistrySelect, 5: 967 –969

Ni Y, Sun A, Wu X, Hai G, Hu J, Li T, Li G (2011) The preparation of nano-sized H[Zn, Al]ZSM-5 zeolite and its application in the aromatization of methanol. Micropor Mesopor Mater.143: 435

Niu X, Gao J, Miao Q, Dong M, Wang G, Fan W, Qin Z, Wang J (2014) Influence of preparation method on the performance of Zn-containing HZSM-5 catalysts in methanol-to-aromatics. Micropor Mesopor Mater 197: 252–261

O'Brien MG, Sanchez-Sanchez M, Beale AM, Lewis DW, Sankar G, Catlow CR (2007) Effect of Organic Templates on the Kinetics and Crystallization of Microporous Metal-Substituted Aluminophosphates. J. Phys. Chem. C 111: 16951-16961

Olah GA (2005) Beyond Oil and Gas: The Methanol Economy. Angew. Chem. Int. Ed. 44: 2636 –2639

Ono Y (1992) Transformation of lower Alkanes into Aromatic Hydrocarbons over ZSM-5 Zeolites. Catal. Rev.-Sci. Eng. 34(3): 179-226

Ono Y, Adachi H, Senoda Y (1988) Selective conversion of methanol into aromatic hydrocarbons over zinc-exchanged ZSM-5 zeolites. J. Chern. Soc., Faraday Trans. 1, 84(4): 1091-1099

Park S, Inagaki S, Kubota Y (2016) Selective formation of light olefins from dimethyl ether over MCM-68 modified with phosphate species. Catal Today, 265: 218-224

Petushkov A, Yoon S, Larsen SC (2011) Synthesis of hierarchical nanocrystalline ZSM-5 with controlled particle size and mesoporosity. Micropor Mesopor Mater 137: 92–100

Pinilla Herrero I. Diseño de materiales SAPO de poro pequeño para su ensayo como catalizadores en el proceso MTO. Tesis doctoral, Madrid 2016. Instituto de Catálisis y Petroleoquímica (ICP), Consejo superior de investigaciones científicas (CSIC)

Qinhua X, Aizhen Y (1991) Hydrothermal synthesis and crystallization of zeolites. Prog Cryst Growth Ch, 21 (1–4): 29-70

Quan G, Bai T, Fei TC, Tao WF, Zhang X (2014) Conversion of Methanol to Light Aromatics on Zn-Modified Nano-HZSM-5 Zeolite Catalysts. Ind. Eng. Chem. Res. 53: 14932−14940

Rigoreau J, Laforge S, Gnep NS, Guisnet M (2005) Alkylation of toluene with propene over H-MCM-22 zeolite. Location of the main and secondary reactions. J. Catal 236: 5–54

Roldan R, Sanchez-Sanchez M, Sankar G, Romero-Salguero FJ, Jimenez-Sanchidrian C (2007) Influence of pH and Si content on Si incorporation in SAPO-5 and their catalytic activity for isomerisation of n-heptane over Pt loaded catalysts. Micropor Mesopor Mater 99: 288–298

Rownaghi AA, Hedlund J (2011) Methanol to Gasoline-Range Hydrocarbons: Influence of Nanocrystal Size and Mesoporosity on Catalytic Performance and Product Distribution of ZSM-5. Ind. Eng. Chem. Res. 50: 11872–11878

Rubin MK, Chen P, US patent 4,954,325, 1990

Sanchez-Sanchez M, Sankar G, Simperler A, Bell RG, Catlow CR, Thomas JM (2003) The extremely high specificity of N-methyldicyclohexylamine for the production of the large-pore microporous AFI material. Catal Lett. 88 (3–4): 163-167

Sasaki M, Sato Y, Tsuboi Y, Inagaki S, Kubota Y (2014) Ti-YNU-2: A Microporous Titanosilicate with Enhanced Catalytic Performance for Phenol Oxidation. ACS Catal. 4(8): 2653-2657

Sherman JD (1999) Synthetic Zeolites and Other Microporous Oxide Molecular Sieves. Proc. Natl. Acad. Sci. 96: 3471-3478.

Shibata T, Kawagoe H, Naiki H, Komura K, Kubota Y, Sugi Y (2009) The alkylation of naphthalene over MCM-68 with MSE topology. Journal of Molecular Catalysis A: Chemical 297: 80–85

Shibata T, Suzuki S, Kawagoe H, Komura K, Kubota Y, Sugi Y, Kim JH, Seo G (2008) Synthetic investigation on MCM-68 zeolite with MSE topology and its application for shape-selective alkylation of biphenyl. Micropor Mesopor Mater. 116: 216–226

Song Y, Zhu X, Xie S, Wang Q, Xu L (2004) The effect of acidity on olefin aromatization over potassium modified ZSM-5 catalysts. Catal. Lett. 97: 31

Stöcker M (2005) Gas phase catalysis by zeolites. Micropor. Mesopor. Mater. 82: 257-292

Su X, Wang G, Bai X, Wu W, Xiao L, Fang Y, Zhang J (2016) Synthesis of nanosized HZSM-5 zeolites isomorphously substituted by gallium and their catalytic performance in the aromatization. Chem Eng J. 293: 365–375

Taufiqurrahmi N, Mohamed AR, Bhatia S (2010) Deactivation and coke combustion studies of nanocrystalline zeolite beta in catalytic cracking of used palm oil. Chem. Eng. J. 163: 413–421

Teketel S, Erichsen MW, Bleken FL, Svelle S, Lillerud PK, Olsbye U (2014) Shape selectivity in zeolite catalysis. The Methanol to Hydrocarbons (MTH) reaction. Catalysis 26: 179–217

Terasaka K, Imai H, Li X (2015) Control of Morphology and Acidity of SAPO-5 for the methanol-to- olefins (MTO) reaction. J. Adv. Chem. Eng. 5(4): 1000138

Townsend RP (1991) Chapter 10 Ion Exchange in Zeolites, Stud Surf Sci Catal. 58: 359-390

Wan Z, Wu W, Li GK, Wang C, Yang H, Zhang D (2016) Effect of SiO2/Al2O3 Ratio on the Performance of Nanocrystal ZSM-5 Zeolite Catalysts in Methanol to Gasoline Conversion. Appl. Catal. A-Gen. 523: 312-320

Wang L, Guo C, Yan S, Huang X, Li Q (2003) High-silica SAPO-5 with preferred orientation: synthesis, characterization and catalytic applications. Micropor Mesopor Mater. 64: 63-68

Wang N, Qian W, Shen K, Su C, Wei F (2016) Bayberry-like ZnO/MFI zeolite as high performance methanol-to-aromatics catalyst. Chem. Commun. 52: 2011—2014

Weckhuysen BM, Rao RR, Martens JA, Schoonheydt RA (1999) Transition metal ions in microporous crystalline aluminophosphates: Isomorphous substitution. Eur. J. Inorg. Chem., 25: 565-577

Wilson ST, Lok BM, Messina CA, Cannan TR, Flanigen EM (1982) Aluminophosphate molecular sieves: a new class of microporous crystalline inorganic solids. JACS 104: 1146-1147

Wu Y, Ren X, Lu Y, Wang J (2008) Crystallization and morphology of zeolite MCM-22 influenced by various conditions in the static hydrothermal synthesis. Micropor Mesopor Mater 112: 138–146

Xin Y, Qi P, Duan X, Lin H, Yuan Y (2013) Enhanced Performance of Zn–Sn/HZSM-5 Catalyst for the Conversion of Methanol to Aromatics. Catal. Lett. 143: 798–806

Xu J, Zhou D, Song X, Chen L, Yu J, Ye C, Deng F (2008) Crystallization of magnesium substituted aluminophosphate of type-36 as studied by solid-state NMR spectroscopy. Microporous and Mesoporous Materials 115: 576–584

Xu R, Pang W, Yu J, Huo Q, Chen J (2007) Chemistry of Zeolites and Related Porous Materials: Synthesis and Structure. Ed John Wiley & Sons

Zilková N, Bejblová M, Gil B, Zones SI, Burton AW, Chen CY, Musilová-Pavlacková Z, Košová G, Cejka J (2009) The role of the zeolite channel architecture and acidity on the activity and selectivity in aromatic transformations: The effect of zeolite cages in SSZ-35 zeolite. J. Catal 266: 79–91

# Resultados

## 8.1. Primer artículo: publicado

### Springer

| Online First: your article is published | 2020-01-03 |
|---|---|

# Congratulations

Dear Misael Garcia Ruiz,

We are pleased to inform you that your article has just been published:
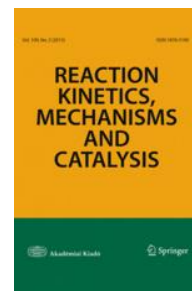
**Title**
ZSM-5 zeolites modified with Zn and their effect on the crystal size in the conversion of methanol to light aromatics (MTA)

**Journal**
Reaction Kinetics, Mechanisms and Catalysis, (), 1-20

**DOI**
10.1007/s11144-019-01716-4

Your article is available as 'Online First':
http://link.springer.com/article/10.1007/s11144-019-01716-4

It is fully accessible to all users at libraries and institutions that have purchased a SpringerLink license. If your article is published under one of our Open Access programs, it will be freely accessible to any user.

**Announce Your Publication**
We encourage you to forward this email to your co-authors. Additionally we recommend you mention your article's publication and its DOI on your website or your social media profiles. The article's SpringerLink page features easy-to-use "share" buttons for popular social media channels as well as the real-time display of your article's citations and social shares.

# ZSM-5 zeolites modified with Zn and their effect on the crystal size in the conversion of methanol to light aromatics (MTA)

**Misael García Ruiz, et al.** *[full author details at the end of the article]*

## Abstract

ZSM-5 zeolite catalysts modified with zinc were prepared by two forms of Zn incorporation the synthesis gel, and ion exchange techniques. The physico-chemical properties of zeolites were studied by XRD, $N_2$-adsorption, $NH_3$ temperature-programmed desorption, $^{27}Al$ and $^{29}Si$ MAS NMR, SEM, TEM and TGA. ZSM-5 zeolite in its acid form was exchanged using an aqueous zinc salt solution and demonstrated a significantly higher selectivity for the aromatic products in comparison with the purely acidic catalysts. The samples with distribution of $ZnOH^+$ species are more active than the samples with ZnO sites in the zeolites. The synthesis of zeolite ZSM-5 of nanometric size resulted to present high stability and selectivity towards light aromatics. The influence of the form of zinc incorporation, the acidity and the reaction temperature had a great influence on the catalytic activity. The MTA catalyst lifetime is increased by several times due to the enhanced mesoporosity and decreased acidity. In the present work the zeolite HZSM-5 exchanged with Zn with Si/Al 25 ratio presented conversions close to 100% methanol with 32% selectivity to the BTX fraction, however, this catalyst was deactivated after 8 h of reaction with a weight hourly space velocity of 4.74 $h^{-1}$ at 450 °C. On the other hand, a HZSM-5 zeolite with nanoscale crystals was found to be more stable in the MTA reaction. The nanometric catalyst showed conversions around 100% methanol after 8 h of reaction and 32.5% selectivity to the BTX fraction to 450 °C. These results clearly indicate that crystal size significantly influence the ZSM-5 lifetime and product distribution.

**Keywords** ZSM-5 zeolite · MTA process · BTX fraction · Modified zeolites · Nanocrystalline zeolite

Published online: 02 January 2020

Springer

# ZSM-5 zeolites modified with Zn and their effect on the crystal size in the conversion of methanol to light aromatics (MTA)

Misael García Ruiz*[a], Dora A. Solís Casados[b], Julia Aguilar Pliego[c], Carlos Márquez Álvarez[d], Enrique Sastre de Andrés[d], Diana Sanjurjo Tartalo[d], Raquel Sáinz Vaque[d], Marisol Grande Casas[d]

[a] Doctorado en Ciencia de Materiales de la Facultad de Química, Universidad Autónoma del Estado de México, Paseo Colón Esquina Paseo Tollocan S/N, Toluca Estado de México, México, C.P. 50000.

[b] Universidad Autónoma del Estado de México, Centro Conjunto de Investigación en Química Sustentable UAEM-UNAM. Personal Académico Adscrito a la Facultad de Química, UAEMex.

[c] Área de Química Aplicada, Departamento de Ciencias Básicas, UAM-A, San pablo 180, C.P. 02200, Cd de México.

[d] Instituto de Catálisis y Petroleoquímica, CSIC, C/Marie Curie 2, Campus Cantoblanco, 28049 Madrid, España

**Abstract.** ZSM-5 zeolite catalysts modified with zinc were prepared by two forms of Zn incorporation the synthesis gel, and ion exchange techniques. The physico-chemical properties of zeolites were studied by XRD, $N_2$-adsorption, $NH_3$ temperature-programmed desorption, $^{27}Al$ and $^{29}Si$ MAS NMR, SEM, TEM and TGA. ZSM-5 zeolite in its acid form was exchanged using an aqueous zinc salt solution and demonstrated a significantly higher selectivity for the aromatic products in comparison with the purely acidic catalysts. The samples with distribution of $ZnOH^+$ species are more active than the samples with ZnO sites in the zeolites. The synthesis of zeolite ZSM-5 of nanometric size resulted to present high stability and selectivity towards light aromatics. The influence of the form of zinc incorporation, the acidity and the reaction temperature had a great influence on the catalytic activity. The MTA catalyst lifetime is increased by several times due to the enhanced mesoporosity and decreased acidity. In the present work the zeolite HZSM-5 exchanged with Zn with Si/Al 25 ratio presented conversions close to 100% methanol with 32% selectivity to the BTX fraction, however, this catalyst was deactivated after 8 h of reaction with a weight hourly space velocity (WHSV) of 4.74 $h^{-1}$ at 450 °C. On the other hand, a HZSM-5 zeolite with nanoscale crystals was found to be more stable in the MTA reaction. The nanometric catalyst showed conversions around 100% methanol after 8 h of reaction and 32.5% selectivity to the BTX fraction to 450 °C. These results clearly indicate that crystal size significantly influence the ZSM-5 lifetime and product distribution.

Keywords: ZSM-5 zeolite, MTA Process, BTX Fraction, modified zeolites, nanocrystalline zeolite

## 1. Introduction

Aromatic compounds, especially benzene, toluene and xylenes (BTX) are important chemical compounds conventionally obtained from raw materials based on crude oil. Currently, more than 90% of these aromatic compounds are obtained by reforming different petroleum fractions and subsequent stages of treatment, purification or modification of the aromatic mixture are necessary to obtain the most desired compounds, such as the para-xylene, which, obviously, makes the process even more expensive [1]. In the last decade, the route of methanol conversion to aromatics (MTA) has received great attention considering that methanol is readily available from general resources such as coal, natural gas or biomass [2].

Zeolites are crystalline metallosilicates containing ordered micropores that enable shape-selective transformation. Given the high thermal stability and strong Brønsted acidity of zeolite catalysts, they are widely used in cracking, disproportionation, isomerization, alkylation, and aromatization [3-6]. The aromatization reaction has been observed with a range the active metal species in zeolites include Zn, La, Ga, Ag, Cu, Sn, Ni, Mo and Cr, however, the selectivity to a specific product versus time is different in each case. Furthermore, it has been widely accepted that Zn species could greatly increase the selectivity of BTX in MTA reaction compared with other metal species. Inoue and coworkers [7] reported that an Ag/ZSM-5 catalyst the products contain too much heavy aromatics and the stability is poor. The aromatization performance of methanol over $Mo_2C$/ZSM-5 was also investigated for Barthos and coworkers [8], and it was found that the loading of $Mo_2C$ enhanced the formation of aromatics enormously. Nevertheless, in this process there exist difficulties for controlling the exothermicity of the reaction and for decreasing the rapid rate of catalyst deactivation. Therefore, the main challenge of our work is to improve the lifetime of the catalyst, because in previous reports the ZMS-5 zeolite is deactivated in relatively short reaction times. In this context, nanosized zeolites with a considerable amount of fully accessible acid sites located on the external surface may be potentially interesting catalysts for methanol reactions.

ZSM-5 zeolite has proved to be the most promising component of aromatization catalyst because of its hydrothermal stability, shape-selective behavior, and proper crystal structure for high activity. [9-11]. As demonstrated in previous studies [12], certain medium pore zeolites (with 10-membered channels) such as ZSM-5, doped with Zn is capable of transforming methanol into aromatic compounds, presenting high selectivities to the BTX fraction. In this case, Zn-containing zeolites are usually synthesized by traditional techniques such as ion exchange (i) or in the synthesis gel (G) [13]. Pan and coworkers [14] demonstrated that the Zn introduction method had obvious influences on texture properties, acidic properties and subsequent influences on catalytic activity. The BTX selectivity was effectively improved by introduction of Zn species in ion exchange, owing to the enhancement of Zn-based acid sites with increased density to aromatization of intermediates in MTA reaction. On the contrary, zinc in synthesis gel produce ZnO clusters at the pore entrances might restrict large molecule products diffusion and deteriorated the catalyst deactivation.

The zeolite ZSM-5 of nanometric size has a long catalytic life, due to the fact that the reduction of the size of crystal shortens the length of diffusion of molecules, making the zeolite more stable and increasing the selectivity to the BTX fraction [15]. The catalysts were prepared by the ion exchange of ZSM- 5 zeolite (acid-form) with aqueous solution of zinc salts and demonstrated significantly higher selectivity for aromatics compared to the catalysts on pure acid-form ZSM-5 zeolite [13]. Although some significant achievements have been made in recent years, it is necessary to further improve the activity and stability of the catalyst in the MTA reaction [3-6]. For this, the relationship between the properties of the catalyst and its behaviour in the reaction has been studied in order to be able to develop a more efficient catalyst. Therefore, in the present work the study of zeolitic catalysts with different forms of Zn incorporation is proposed, realizing a comparison between the catalytic behaviour of nanocrystalline and microcrystalline ZSM-5 samples for MTA reaction, improving the resistance to the deactivation of the catalysts.

## 2. Experimental

### 2.1. Materials

The reagents used for the preparation of ZSM-5 zeolites are tetraethyl orthosilicate (TEOS, 98%, Aldrich), fumed silica, sodium hydroxide (NaOH), sodium aluminate (41 wt %$Al_2O_3$, 37 wt.% $Na_2O$), the cationic template (1 M TPAOH, Acros Organics, 8 mL), tetrapropyl ammonium bromide (TPABr 98 wt.%), ethanol absolute, for HPLC, ≥99.8% (Sigma-Aldrich) and zinc nitrate hexahydrate ($Zn(NO_3)_2$•$6H_2O$ reagent grade, 98%, Sigma-Aldrich).

### 2.2. ZSM-5 by hydrothermal synthesis

HZSM-5 zeolites were synthesized for hydrothermal method with a molar ratio of $xSiO_2$-$yAl_2O_3$-0.2TPABr-0.09$Na_2O$-35$H_2O$, where x/y represents the Si/Al molar ratio of 25. In a conventional synthesis, sodium aluminate and sodium hydroxide were dissolved in deionized water, and once dissolved, tetrapropyl ammonium bromide (TPABr) was added as structure directing agent (SDA). Finally, fumed silica was added as the silica source and the gel was stirred for one hour. The synthesis gel was placed in stainless steel autoclaves with Teflon sheath, at 160 ° C under static conditions for 72 h. The solid was recovered by filtration, dried at 70 °C, ground and calcined at 550 °C for 8 h in an air atmosphere. The H-type ZSM-5 (H-ZSM-5) samples were obtained as follows. The calcined Na-ZSM-5 samples It was exchanged with a solution 1 M $NH_4NO_3$ at 80 °C for 4 h followed by calcination at 550 °C for 6 h to exchange $Na^+$ ions for proton. The acid zeolites with a Si/Al molar ratio of 25 was denoted as HZ25. Zeolite modified with Zn in synthesis gel (G) was synthetized under similar conditions as the previous zeolite, except, in the first step sodium aluminate and sodium hydroxide were dissolved and $Zn(NO_3)_2$•$6H_2O$ as a source of zinc was added. The molar relation was $xSiO_2$-$yAl_2O_3$-0.2TPABr-0.09$Na_2O$-zZnO-35$H_2O$, where x/y represents the molar ratio Si/Al (50) and z represents the amount of zinc. Similar in conventional synthesis. The material was denoted as HZ50 0.01 Zn-G.

## 2.3. Synthesis of nanocrystalline ZSM-5 zeolite

Nano-ZSM-5 zeolites with an average crystal size of 60 nm [16] and ratio Si/Al 25 and 50 were synthesized from a gel mixture with a final molar composition: $xTEOS-NaAlO_2-5TPAOH-4TPABr-1000H_2O$. First, the sodium aluminate was dissolved in deionized water, the TPABr was added and stirred until was completely dissolved. Then the TPAOH was added to the synthesis gel. TEOS was added dropwise to the reaction mixture which was stirred overnight at room temperature. The reaction mixture was evaporated at 60 °C until 20% of the total volume amount of the mixture evaporated.

The reaction solution was placed in a stainless-steel autoclave. The synthesis was carried out with constant agitation at 250 rpm at 160 °C for 72 h. After the synthesis, the zeolite crystals were separated by centrifugation at 14,000 rpm for 20 min. 100 ml ethanol was added to the solid and the resulting suspension was subjected to a sonication process for 1 h, the crystals were again separated by centrifugation at 14,000 rpm for 20 min. The solid was redispersed by sonication in water for 1 h, the solid was separated by centrifugation, dried at 70 ° C and calcined at 550 ° C for 6 h with air flow. The Na-ZSM-5 zeolite is exchanged with a 1 M solution at 80 ° C for 4 h, the solid is filtered, dried and calcined at 550 ° C for 4 h in air. This acid catalyst was denoted as nano HZ25.

## 2.4. Synthesis of HZSM-5 zeolites exchanged with Zn

The acid zeolites previously synthesized (H-ZSM-5) was exchanged with a 0.025 M solution of $Zn(NO_3)_2•6H_2O$ at 80 °C for one night. The zeolite was filtered, washed and dried at 70 ° C, finally the resulting powder was calcined at 550 °C for 4 h with air flow. The zeolites synthesized by hydrotreatment with ratio Si/Al 25 was denoted as HZnZ25-i. The nanocrystalline zeolite with zinc was denoted as nano HZnZ25- i.

## 2.5. Catalyst characterization

X-ray diffraction of powders (XRD) was collected with an XPert Pro PANalytical diffractometer (CuKα1 radiation = 0.15406 nm). Scanning electron microscopy (SEM) images were recorded on a Hitachi S-3000N microscope. Transmission electron microscopy (TEM) study was carried on a JEOL 2100F microscope opering to 200KV. Nitrogen adsorption/desorption isotherms were measured at −196 °C in a Micromeritics ASAP 2020 device. Before the measurement, calcined samples were degassed out at 350 °C under high vacuum for at least 10 h. Surface areas were measured by using the Brunauer-Emmet-Teller (BET) equation, whereas microporous and external surface areas were estimated by applying the t-plot method.

Solid-state magic-angle spinning (MAS) NMR experiments were conducted on a Brucker AV 400WB spectrometer operated with frequency at 79.5 MHz and spinning rate at 10 KHz. The $^{27}$Al NMR spectra were recorded using a pulse width of 0.5 μs (π/12 flip angle), 2400 scans and a recycle delay of 1 s.

The Al and Si concentrations of samples were obtained by inductively coupled plasma-optical emission spectroscopy (ICP-OES) with a Optima 3300 DV Perkin Elmer. Ammonia Temperature programmed desorption (NH$_3$-TPD) was acquiered using a Micrometrics Autochem II chemisorption analysis equipment. Typically, 100 mg of sample pellets (30–40 mesh) were pretreated at 550 °C for 1 h in helium flow (25 mL/min) and then cooled to the adsorption temperature (177 °C). A gas mixture of 5.0 vol.% NH$_3$ in He was then allowed to flow over the sample for 4 h at a rate of 15 mL/min. Afterwards, samples were flushed with a 25 mL/min helium flow for 30 min while maintaining the temperature at 177 °C to remove weakly adsorbed NH$_3$, and finally the temperature was increased to 550 °C at a rate of 10 °C/min. The thermal gravimetric analyses (TGA) were carried out at a heating of 30 °C to 900 °C with a rate of 20 °C/min under air flow and registered in a PerkinElmer TGA7 instrument. X-ray Photoelectron spectra (XPS) were recorded using spectrometer model JEOL JPS-9200 (Al Kα, irradiation, hν = 1486.6 eV, 200 W). The samples under study were supported onto double side conducting copper scotch tape under Ar atmosphere. Binding energy (BE) scale was preliminarily calibrated by the position of the peak Cu2p3/2 (BE = 932.67 eV) core levels. The survey spectra were recorded at pass energy of the analyzer of 50 eV, while that for the narrow spectral regions was 20 eV.

## 2.6. MTA catalytic testing conditions

Zn modified ZSM-5 zeolites were tested as catalysts in the methanol conversion to light aromatics at different reaction temperatures at 400, 425 and 450 °C in a Microactivity reaction set (PID Eng & Tech) consisting of a fixed bed reactor completely automated and controlled from a computer. The reactor outlet is connected to a gas chromatograph to analyze the reaction products. N$_2$ was used as a stripping gas under a controlled flow. The methanol was fed as a liquid using an HPLC pump (Gilson 307). The methanol was converted to the gas phase and mixed with the N$_2$ stream in a preheater at 180 °C to generate a gas mixture with a constant molar ratio of methanol/N$_2$ of 4. Before the reaction, the catalysts were activated at 550 ° C for 1 h low air flow to remove any trace of organic molecules or moisture adsorbed within the pores of the catalyst. Typically, the sample was compacted and sieved in a 20-30 mesh, corresponding to a particle size between 0.84 and 0.59 mm. The weight of the catalyst and the flow of methanol were optimized to achieve different values of WHSV (4.74 and 9.48 h$^{-1}$ ). The reaction products were analyzed online by gas chromatography with a VARIAN CP3800 chromatograph. The device is equipped with two columns: (i) a Petrocol DH50.2 capillary column connected to an FID detector, and (ii) a Hayesep Q packed column (2 m length, 3.17 mm (1/8 ") diameter external and 2 mm internal diameter) connected to a TCD detector, to analyze hydrocarbons and oxygenated products, respectively.

## 3.  Results and discussion

### 3.1.  Catalyst characterizations

Figure S1 (supplementary information) shows the XRD patterns of the H-ZSM-5. All these zeolites exhibit typical diffraction peaks of MFI structure, composed of aggregates of nanosized crystalline units [17]. The characteristic peaks of ZnO at 31.8° and 36.3° were not observed in zeolites with Zn content [18], suggesting that Zn species were highly dispersed on ZSM-5 zeolite after the incorporation of zinc. Almutairi and coworkers [19] reported that Zn species dispersed on the external surface of ZSM-5 and stabilizied at the cation-exchange sites, which could cause lattice distortion of ZSM-5. Hence, Zn species partly interacted with the ZSM-5 framework and influenced the lattice structure of ZSM-5.
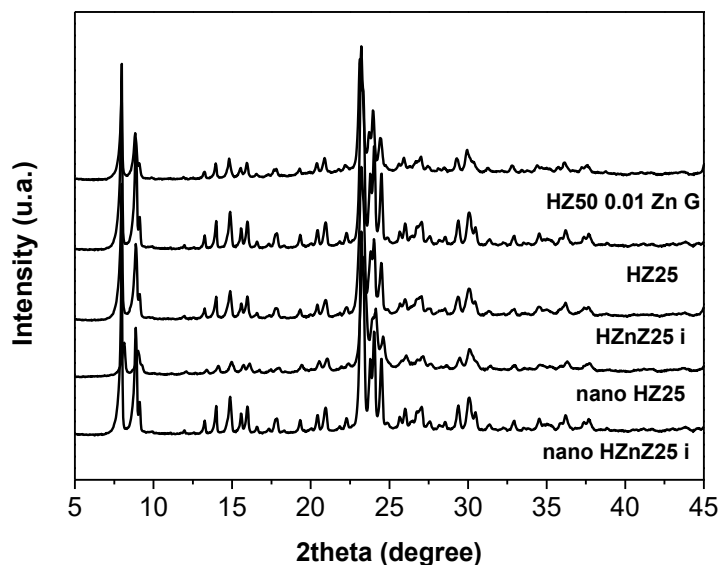


Figure S1. XRD patterns of Zn-containing HZSM-5 zeolites prepared by different methods, from 5 to 45° 2Ө.

Figure 1a and 1b shows SEM images of HZ50 0.01 Zn-G and HZ25 zeolites, respectively. It can be seen that the two catalysts present different particle size and morphology. HZ50 0.01 Zn-G image shows spherical particles with a certain roughness of size around 8 μm of diameter (Figure 1a). As seen in the figure 1b, HZ25 zeolite appeared as irregular hexagonal sheets crystal morphology with a mean particle size of more than 2 μm. This type of morphology is referred to as unilamellar [20]. SEM images of nano HZnZ25-i (ratio Si/Al 25) zeolite show spherical and uniform particles (60-80 nm range in diameter), and very rough surface (Figure S2a). The high magnification SEM image (Figure S2b) further reveals that they are highly mesoporous, attributed to the agglomerate of nanoparticles of 60-80

nm. The different morphologies of obtained zeolites were caused to a large extent by synthesis conditions even when the same template was used.
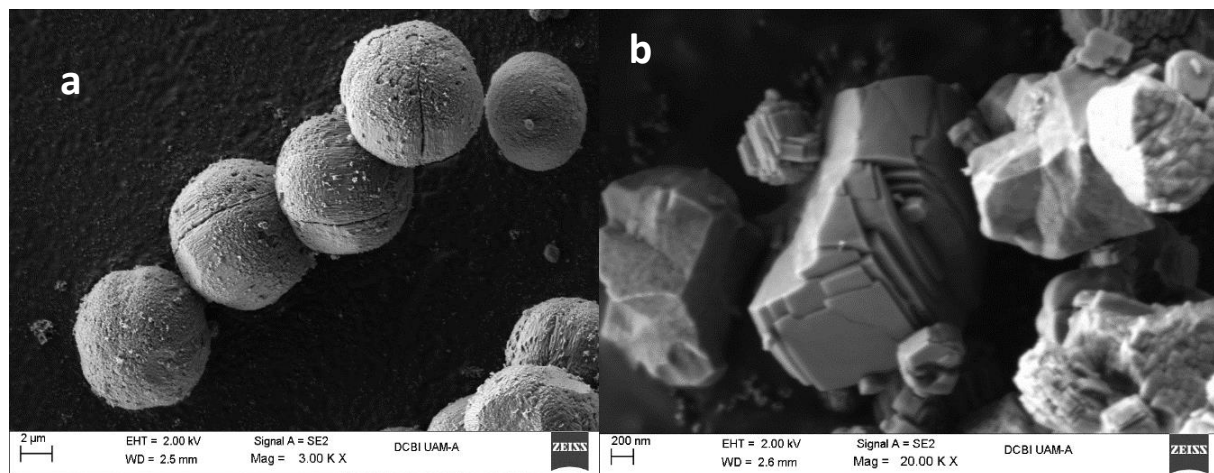


Figure 1. SEM images of the samples: a) HZ50 0.01 Zn-G d) HZ25 (acid zeolite). The images have a magnification of 3,000 and 20,000, respectively.
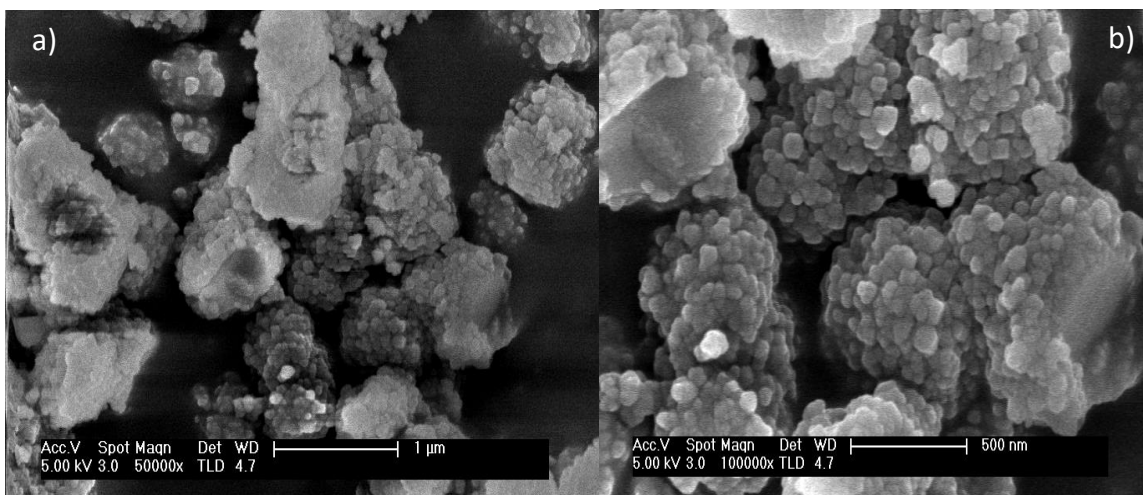


Figure S2. SEM images of the samples of nano HZnZ25- I to 5000 and 10000x

The TEM images in Figure 2 the formation of nanocrystals is clearly observed (ca. 60-80 nm range), and no chunks of Zn specials can be observed on the external surface of the zeolite crystals in each sample. This could be due to the

incorporation of Zn into the zeolite framework and the high dispersion of the extra-framework zinc species. This result agrees with the observed in $^{27}$Al NMR due to the reduction of the peak assigned to the substitution of Zn by Al extra-framework. The electron diffraction spot pattern of a selected area in HRTEM image (inset of Figure 2) evidences this fact. Other SEM figures show in figure S3 in supplementary material. The jointed nanocrystals create many inter-lattice mesopores in zeolite crystalline frameworks (Figure S3b and S3c). Smaller zeolite crystals should favor these reactions as the number of pore mouths (active sites) is increased.
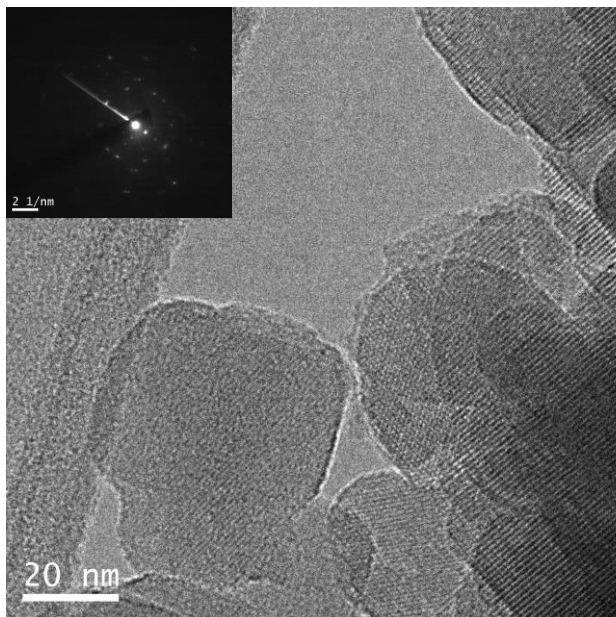


Figure 2. TEM image of the samples of nano HZnZ25-i. One sets of particles population is detected in the range 60 to 80 nm

are shown. A single loss of mass less than 100 °C is observed, which corresponds to the physisorption of water retained in the samples. No other significant weight losses are observed at higher temperature which indicates that the SDA was eliminated.
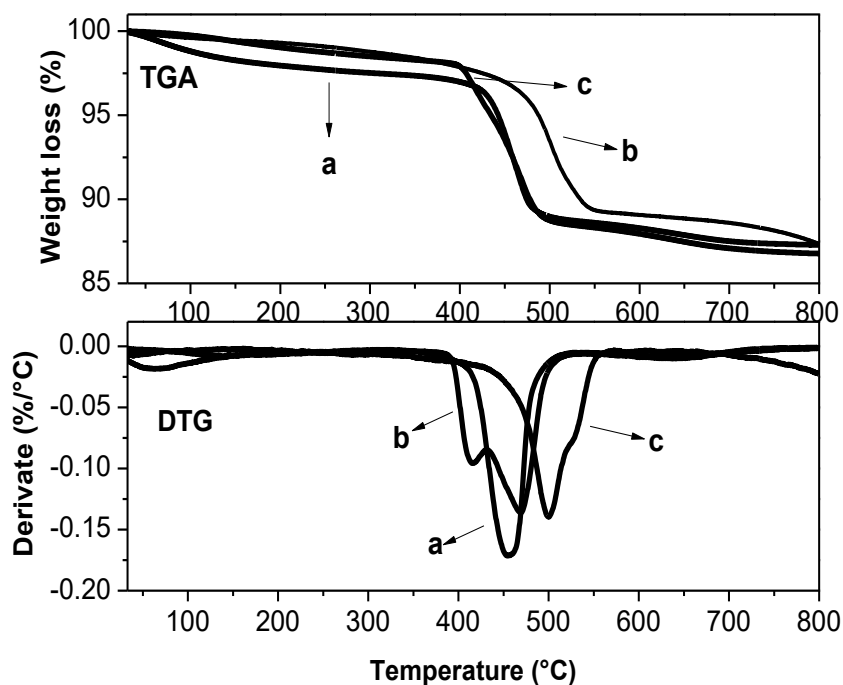


Figure S4. Thermal analysis of the ZSM-5 uncalcined materials TGA (top) and DTG (bottom) a) Z25, b) nano Z25 and c) Z50 0.01 Zn-G

Table 1. Textural properties of zinc-containing ZSM-5 zeolites prepared

| Catalyst | $S_{BET}/m^2 \cdot g^{-1}$ | $S_{micro}/m^2 \cdot g^{-1}$ | $S^*_{external}/m^2 \cdot g^{-1}$ | $V_{micro}/cm^3 \cdot g^{-1}$ |
|---|---|---|---|---|
| nano HZnZ25-i | 468 | 350 | 118 | 0.123 |
| nano HZ25 | 428 | 350 | 78 | 0.135 |
| HZnZ25-i | 369 | 293 | 76 | 0.114 |
| HZ25 | 403 | 247 | 156 | 0.101 |
| HZ50 0.01 Zn-G | 339 | 250 | 89 | 0.124 |

**\*** Calculed by t-plot method

The amount of Si, Al and Zn in the ZSM-5 zeolites of the calcined samples were determined by ICP-OES analysis (Table 2). It is observed that the incorporation of Zn is efficient both by ion exchange and in the synthesis gel. The acid nanocrystalline zeolite exchanged with zinc had the highest Zn concentration (1.1 wt %). The relation Si/Al to real was measured in all the catalysts, being less than the theoretical in all cases with relatively low Zn/Al ratios. The Si/Al ratio was reproducible through multiple repeats of our synthetic procedure indicating that the Al atoms in the synthetic solutions were incorporated into the framework structures of the ZSM-5 zeolites during the hydrothermal synthesis.

Table 2. Chemical composition (wt%) determined by ICP-OES of samples

| Catalyst | Theoretical molar ratio Si/Al | % wt Si | % wt Al | Real molar ratio Si/Al | % wt Zn | Ratio Zn/Al |
|---|---|---|---|---|---|---|
| nano HZnZ25-i | 25 | 38.46 | 1.80 | 20.53 | 1.1 | 2.52 |
| nano HZ25 | 25 | 34.37 | 2.04 | 16.21 | 0.0 | - |
| HZnZ25-i | 25 | 35.98 | 1.08 | 21.94 | 0.88 | 0.34 |
| HZ25 | 25 | 36.15 | 1.64 | 20.88 | 0.0 | - |
| HZ50 0.01 Zn-G | 50 | 36.09 | 0.76 | 45.73 | 1.08 | 0.59 |

The acid properties of catalysts were determined by $NH_3$-TPD technique, as presented in Figure 3. The spectra of all samples exhibit two peaks characteristic throughout the temperature range in all zeolites. The low-temperature (LT) region of 200–300 °C and the high temperature (HT) region of 400–500 °C, which are attributed to the $NH_3$ adsorbed on the acidic hydroxide group Si–OH–Al [26]. The LT peak is assigned to the weakly held ammonia adsorbed on acid sites to the zeolite [26-28]. The weak adsorption sites of ammonia are inactive in MTA reactions [29]. On the other hand, the HT peak above 400 °C is due to the desorption of $NH_3$ from strong acid sites. The incorporation of zinc species on HZSM-5 exhibits a significant influence on the distribution of strong acid sites. It is clearly observed, the intensity of HT peak increased by Zn loading because of the exchange of $H^+$ with $Zn^{2+}$, indicating the interaction between the $Zn^{2+}$ ions and Bronsted acid sites on Zn-modified ZSM-5 zeolites giving cationic species of Zn, which

^{27}Al and ^{29}Si MAS NMR measurements were performed to investigate the different environments of the corresponding atom. The ^{27}Al MAS NMR spectra of all the samples are showed in Figure 4. Two peaks at 54 ppm and 0 ppm, corresponding to tetrahedral Al (Al$_F$) entering the zeolite framework and extra-framework octahedral Al atoms (Al$_{EF}$), respectively. The signal at 0 ppm are ascribed to extra-framework aluminum from either cationic aluminum hydroxide species/hydroxylated alumina-like clusters inside the channel structure or as framework defects, where hydroxyl groups and water are partly bonded [17,33]. However, the peak intensity of Al$_{EF}$ decreases slightly due incorporation of Zn in the HZnZ25-i zeolite (Figure 4b). This indicates Al$_{EF}$ sites are incorporated into the framework structure and that defect sites are annealed by the ion exchange treatment, since the amounts of octahedral Al is reduced [17]. This observation is also occurred in figure 4c where is observed that after the incorporation of Zn in the nanocrystalline zeolite (nano HZnZ25-i) the amounts of Al(V) and Al(VI) are reduced after the ion exchange treatment due Al$_{EF}$ is incorporated into the framework after calcination at 550 °C. This result explains the excellent catalytic activity of nano catalyst HZnZ25-i by presenting a greater distribution of strong acid sites in comparison with the zeolite acid nano HZ25.
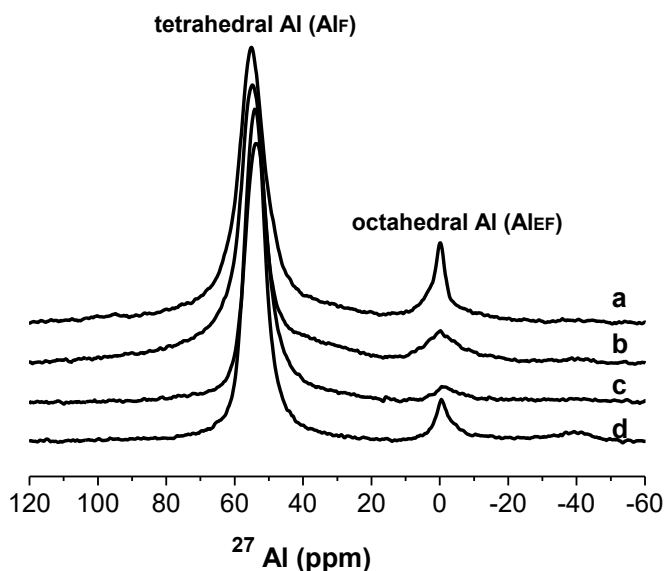


Figure 4. ^{27}Al MAS NMR spectra of HZSM-5 materials a) HZ25, b) HZnZ25-i, c) nano HZnZ25-i and d) nano HZ25

The ^{29}Si MAS NMR spectra (Figure 5) were provides information about silicon atoms with different bonding environments in the zeolite framework with silicon atoms connected to silicon, aluminum, or other atoms via oxygen bridge [34]. The deconvolution of [29]Si spectrum may result in two peaks centered. The resonances between -112 and -115 ppm due to its amorphous state with silicon atoms connected with multiple hydroxyl groups Si (4Si, 0Al). The

two bands around -105 and -109 ppm correspond to Si (3Si, 1Al) sites or $(AlO)Si(OSi)_3$, that is, Si atoms with one neighboring Al atom [35,36]. That last signal of the nano HZn25-i samples decreased with the Zn content, which indicated that Zn atom was easier to incorporate into the framework of the ZSM-5 zeolite and resulted in the larger amount of Brønsted acid sites formed by $(ZnO)Si(OSi)_3$ or $(AlO) Si(OSi)_3$ [26], indicating that Zn is incorporated in the structure mainly over the Brønsted sites.
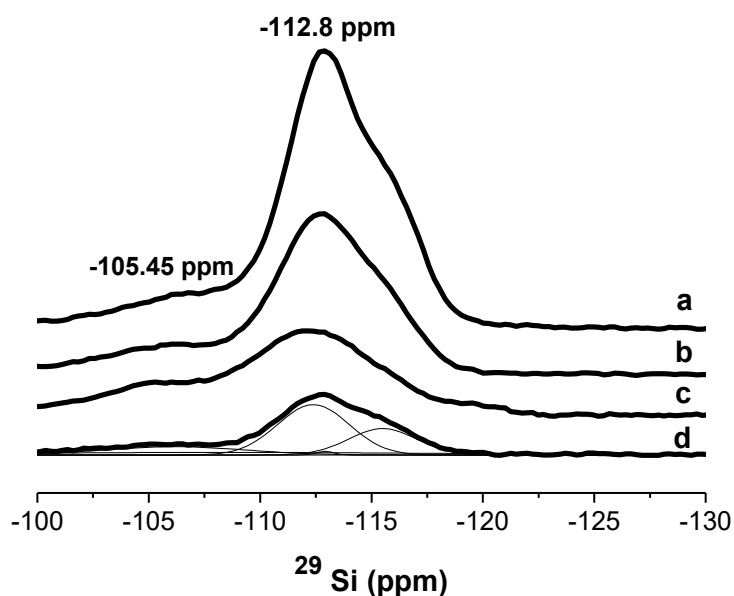


Figure 5. $^{29}$Si MAS NMR spectra of a) HZ25, b) HZnZ25-i, c) nano HZnZ25-i and d) nano HZ25

Figure S7 (supplementary material figure 7) presents Zn 2p3/2 core-level spectra obtained for samples. Depending on the preparation method, the distinct variation of the XPS spectra in shape and position demonstrates that the preparation method for introducing zinc species has a significant influence on the existent state of the surface zinc species. In the case of HZ50 0.01 Zn-G sample shows a Zn 2p3/2 peak at 1022.1 eV represents the formation of Zn–O bonds [34]. In the case of HZnZ25-i, the Zn 2p3/2 peak is shifted towards higher binding energies (around 1024.28 eV) suggest the presence of the zinc species having tighter interaction with the parent zeolite framework. This can be reasonably assigned to $Zn^{2+}$ cations in the cation exchanged sites of HZnZ25-i zeolite. Chen and coworkers attributed the high binding energy peak to $ZnOH^+$ species [37], which is formed from the strong interaction between the zinc species and the protonic acid sites. On the other hand, Tamiyakul and coworkers [38] have concluded that the Zn species localized at the ionic exchanged sites show a high binding energy of about 1024 eV because the lattice oxygen of the zeolite exhibits higher electronegativity than the $O^{2-}$ ligand in bulk zinc oxide.
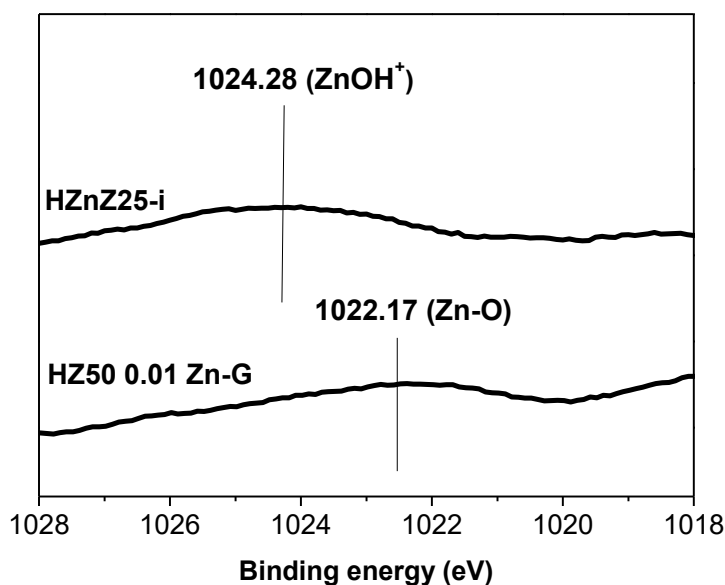
Figure S7. The Zn 2p3/2 XPS spectra of the studied samples: HZnZ25-i and HZ50 0.01 Zn-G

## 3.2. Catalytic Evaluation

The catalytic performances of HZSM-5 and Zn-modified HZSM-5 in MTA reaction in 1 h of reaction and WHSV of 9.48 $h^{-1}$ were listed in Table 4. The introduction of zinc species as well as the synthesis method exhibits a significant influence on the catalyst lifetime, methanol conversion, and product distribution. As reported by Jia and co-workers [39], acid species Lewis type ($^{+}$Z-O$^{...}$H$^{...}$O-Zn$^{2+}$) are able to activate dehydroaromatization of methanol by exchange of Zn in an acid zeolite, which is formed from the strong interaction between the zinc species and the intrinsic acid sites. In 1 h of reaction HZ25 catalyst presented 99.71% methanol conversion, 13.44 % BTX selectivity, and HZnZ25-i exhibited 93.60 % methanol conversion, with a higher BTX selectivity (21.54 %), which indicates that the incorporation of zinc by ion exchange increases the formation of aromatic compounds with the zeolite synthesized by hydrothermal conventional treatment. Acid zeolite HZ25 showed high selectivity towards light olefins $C_2$-$C_4$ (48.41%). Dyballa and coworkers [40] demonstrated that HZSM-5 zeolite exhibits high selectivity to olefins in the reaction of methanol to olefins (MTO). They indicate that the formation of olefins depends significantly on the presence of a high density of Bronsted acid sites.

On the other hand, nano HZ25 catalyst shows 99.88 % methanol conversion and 20.44 % BTX selectivity, however, the nano catalyst HZnZ25- i exchanged with Zn with a crystal size in the 60-80 nm range, showed a higher BTX

selectivity with a methanol conversion at 1 h of reaction. We reported that activity of Zn-modified zeolites in the MTA reaction with the Zn/ZSM-5 zeolite prepared by ion exchange and demonstrated significantly higher selectivity for aromatics compared with acid ZSM-5 zeolite [41,42]. The generation of nanocrystalline zeolites influences the optimization of the acid properties of ZSM-5 zeolite to enhance the catalytic activity [15]. The contribution of strong acid sites on the external surface of nano-ZSM-5 are significantly responsible of high shape-selectivity transformation [43]. It was shown that the zeolite with a crystal size in the 60-80 nm range (nano HZnZ25-i) showed better catalytic activity. Konno and coworkers [44] showed that the generation of nano-sized ZSM-5 zeolites with shorter diffusion length favoured the adsorption and desorption of reactants in the micropores compared with the micro-sized zeolite (2 µm), the MTA activity increased with the decrease of crystal size. Moreover, the selectivity aromatics with large molecular size ($C_9$-$C_{12}$) over nano HZnZ25-i was lower than that over HZnZ25-i. These are attributed to the external surface and the excellent porous shape-selectivity of nanocrystalline zeolites [25]. Similarly, Rownaghi and Hedlund [43] reported that nano zeolite displayed more improved BTX yield and catalytic stability than the conventional one, mainly because of reduction of the micropore diffusion path length and an increase of the external surface area by decreasing the zeolite crystal size. On the other hand, the improved selectivity of BTX for nano zeolite should mainly be due to the smaller crystal species which made the acid sites more accessible for reactant [45]. As a result, the oligomerization, cyclization and hydrogen transfer steps occurred easily in MTA reaction which were closely related to the amount and distribution of both Brønsted acid sites and Lewis acid sites [46,47].

Table 4. Distribution of reaction products of Zn-Modified HZSM-5 (Al/Si 15 ratio) catalysts in the conversion of methanol.
Conditions: TOS 1 h, WHSV 9.48 $h^{-1}$, 450 °C

| Catalyst | HZ25 | HZnZ25-i | Nano HZ25 | Nano HZnZ25-i |
|---|---|---|---|---|
| Crystal size | 2 µm | 2 µm | 80 nm | 80 nm |
| Methanol conversion (%) | 99.71 | 93.6 | 99.88 | 97.42 |
| Selectivity to products (% mol) | | | | |
| Olefins $C_2$-$C_4$ | 48.41 | 38.39 | 36.69 | 38.33 |
| Paraffins + olefins $C_5^+$ | 27.85 | 19.76 | 25.46 | 15.93 |
| Bencene | 0.43 | 0.45 | 0.88 | 1.25 |
| Toluene | 2.66 | 3.91 | 4.91 | 8.74 |
| Xilenes | 10.31 | 17.18 | 14.65 | 19.59 |
| $C_9$-$C_{12}$ | 10.35 | 20.30 | 17.41 | 16.16 |
| **BTX total** | **13.44** | **21.54** | **20.44** | **29.58** |

3.2.1.  Effect of temperature on the MTA reaction

Figure S8a and S8b show the effects of the reaction temperature on the reactivity of nano HZnZ25-i with a WHSV 9.48 h$^{-1}$. Figure 5a shows that the methanol was nearly completely converted to 400 and 425 °C until 3 h of reaction. The conversion of methanol drops to 18% after 9 h of reaction to 450 °C, however, BTX selectivity increased to short reaction times (32%) and subsequently decreased after 7 h to reaction. It is observed that the temperature affects the useful life of the catalyst, as the reaction temperature increases the catalyst tends to deactivate. On the other hand, with an increase of the reaction temperature, the selectivity to BTX increased (figure S8b). This indicates that the cokes on the nano HZnZ25-i probably do not cover the active sites and the channels for the reactants and BTX products are not blocked to a low temperature. In addition to temperature, particle size and particle density and kind of active sites on the crystallite surface will be of influence on catalyst lifetime [48,49].
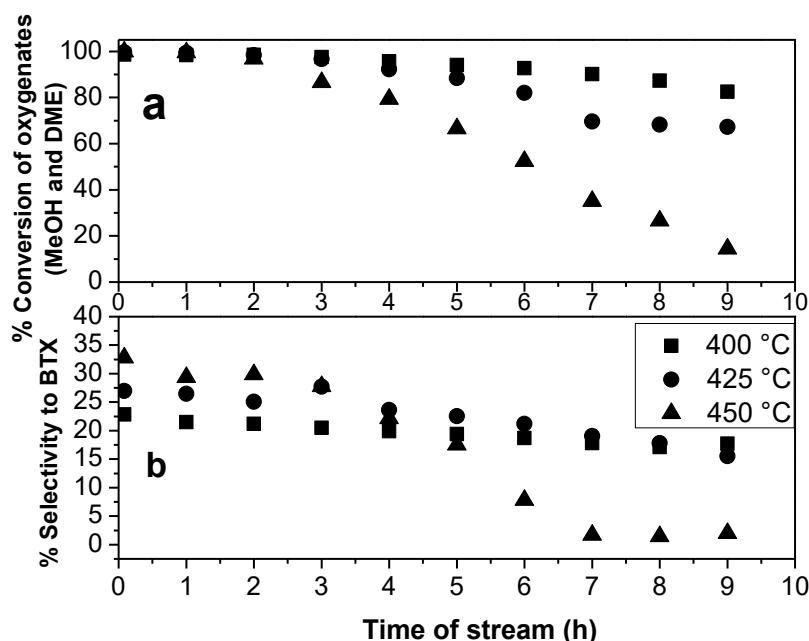


Figure S8. (a) % Conversion of oxygenates compounds (MeOH and DME) and (b) selectivity to BTX fraction over nano HZnZ25-i catalyst with WHSV of 9.48 h$^{-1}$, 0.25 g of catalyst and different temperatures 400 °C (■), 425 °C (●) and 450 °C (▲)

BTX selectivity increased with a higher contact time (WHSV 4.74 h$^{-1}$), corresponding to a methanol flux of 50 µml/min and a catalyst mass of 0.5 g. At 400 and 425 °C, the conversion of methanol is maintained around at 100% during the 9 h reaction (figure 6a). After 9 h of reaction the conversion of methanol drops to 84% at a temperature of 450 °C. With these conditions, the best BTX selectivity values are obtained at 450 °C, at short reaction times the selectivity is 32.6% and it drops to 25.4% at 9 h of reaction. At 400 and 425 °C the selectivity remained constant

throughout the reaction time around 24 and 28%, respectively (figure 6b). These results suggest that an increase in the reaction temperature, specifically at 450 ° C, favored the aromatization of methanol, however, to higher reaction temperature suppressed dehydrocyclization and promoted the formation of coke from a secondary reaction [48]. Hence, the BTX yield in MTA process was closely related to the acid amounts [46]. According to other works, these results of total aromatic selectivity (45.76%) are higher compared to those reported by Niu and coworkers [50] and Bi [12], in addition to our catalysts have better lifetime because we obtained shorter crystals size (60-80 nm range). Likewise, the BET area of our nano HZSM-5 catalysts were larger (400 $m^2*g$) compared to other publications [16] where they synthesized ZSM-5 zeolites of nanocrystalline size.
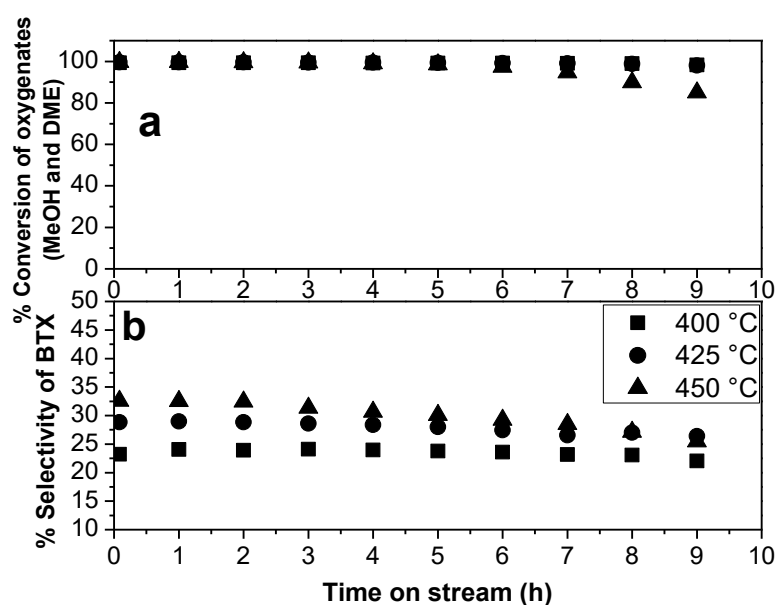


Figure 6. (a) % Conversion of oxygenates compounds (MeOH and DME) and (b) % selectivity to BTX fraction over nano HZnZ25-i catalyst with WHSV of 4.74 $h^{-1}$, 0.5 g of catalyst and different temperatures 400 °C (■), 425 °C (●) and 450 °C (▲)

### 3.2.2. Effect of the Zn incorporation form on the zeolites in the MTA reaction

The incorporation of zinc species by ion exchanging (HZnZ25-i) and synthesis gel (HZ50 0.01 Zn-G) has high influence on the catalytic stability methanol conversion, and products distribution to 450 °C (Figure 7a and 7b). Zn improved the formation of BTX aromatics in zeolite HZnZ25-i compared to pure acid zeolite HZ25. The enhanced aromatics formation observed for Zn would be the result of metal with the acid sites of the zeolites. It was observed that the reduction of the crystal size in the nanocrystalline zeolites improved the interaction of Zn with the acidity of

the ZSM-5 zeolite, improving diffusion processes by physical transport [12], which can dramatically increase the number of pore mouths and increase the accessibility of acid sites in the micropores. These results validated that the strong acid sites in a large amount in the core of the catalyst is crucial for the aromatic selectivity. Their catalytic activities were promoted with the increasing of mesopores and a smaller crystal size, which improving the diffusion efficiency and accessibility of acid sites for high selectivity BTX fraction. In this sense, nano HZ25 and nano HZnZ25-i catalyst show the longest lifetime to 9 h due to the coordination of proportion between Lewis acid sites and Brønsted acid sites and proper pore structure [48].
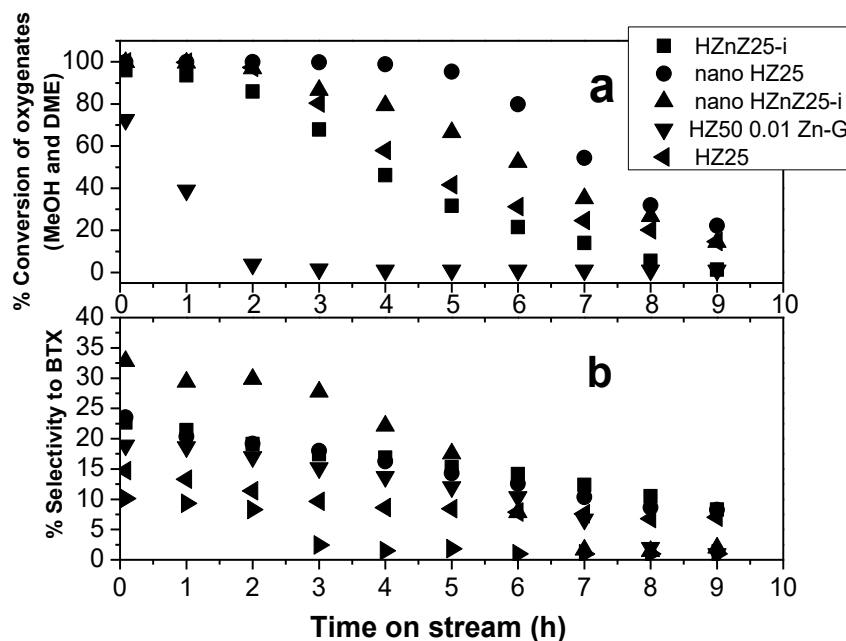


Figure 7. Results of catalytic activity of MTA reaction over HZSM-5 catalyst with different forms of zinc incorporation (a) conversion of oxygenates compounds (MeOH and DME) (b) selectivity to BTX fraction

Conditions reaction: WHSV of 9.48 $h^{-1}$, 450 °C, 0.25 g of catalyst

However, HZnZ50 0.01 Zn-G zeolite shows little stability, the lifetime is decreased to 2 h. This be ascribed to the accumulation of a small amount of nanometric ZnO clusters in the channels of HZ50 0.01 Zn-G zeolite, which avoid to the aromatics diffusion and may accelerate the catalyst deactivation due to coke deposition. Recently, Kim and coworkers [50] found coke was deposited on the external surfaces more than it was inside the micropores in the MTA reaction. The stability of catalysts decreases in the sequence of nano HZ25 >nano HZnZ25-i > HZ25 > HZnZ25-i > HZ50 0.01 Zn-G to 450 °C. Some authors [6,38,40,52-54] suggest that the incorporation of Zn by ion exchange method can be three types of Zn species; (i) isolated $Zn^{2+}$ ions stabilized at the cation-exchange sites of the zeolite, (ii) clusters resulting from the condensation of partially hydrolyzed $ZnOH^+$ extraframework cations, and (iii) more bulky intrazeolite or extrazeolite clusters of zinc oxide, which incorporated in the acid zeolite are responsible for the catalytic

activation at temperatures between 400 and 500 °C. However, it is not known for sure which of the three species are responsible for perform methanol activation.

   In other hand, it is clear that the stability increased at a temperature of 400 °C (Figure S9a and S9b). The conversion of methanol is maintained around 100% in all the catalysts throughout the entire reaction process, except for the sample HZ50 0.01 Zn-G, the catalyst is deactivated after 8 h of reaction due to coke formation.

In this case, deactivation is usually associated with diffusion limitations of heavy products by the formation of large Zn species formed in the micropores [13,39], this phenomenon indicates that the inactivation of aromatization reaction is mainly due to the decrease of strong acid sites and the cokes molecules covered that sites. In our work, improved aromatization of methanol results were observed when converting methanol using ZSM-5 zeolite Zn-modified compared to other metals previously studied by other authors. Ag-ZSM-5[7], Ag / HZSM-5 [55], Cu / Zn / HZSM-5 [56,57], $Mo_2C$ / ZSM-5 [8], $Ga_2O_3$ / HZSM-5 [58] and H-Ga- ZSM-5 (by exchange) [59] all gave good MTA ability but the BTX selectivity less than those obtained by us.
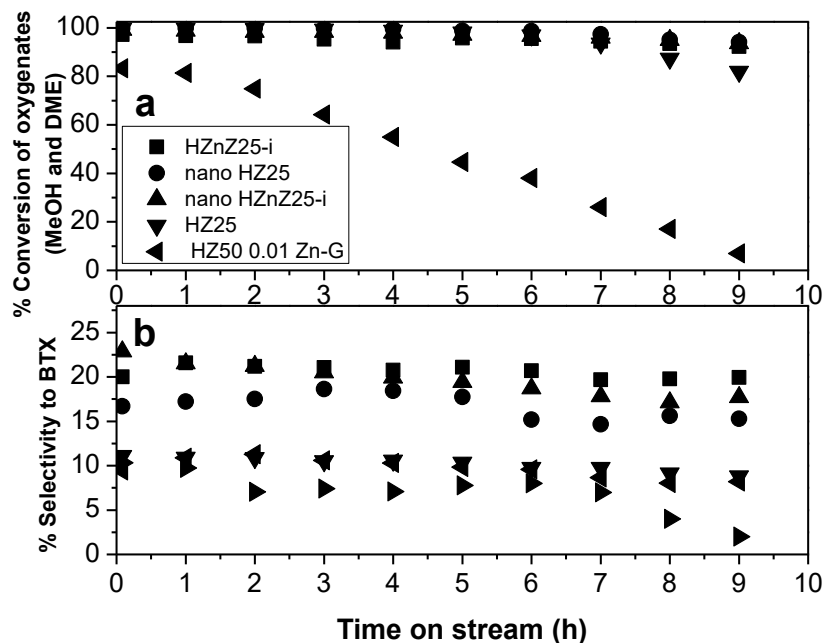


Figure S9. Results of catalytic activity of MTA reaction over HZSM-5 catalyst with different forms of zinc incorporation (a) conversion of oxygenates compounds (MeOH and DME) (b) selectivity to BTX fraction

Conditions: WHSV of 9.48 $h^{-1}$, 400 °C, 0.25 g of catalyst

### 4. Conclusions

The catalytic activity of Zn modified ZSM-5 catalysts was studied in methanol conversion to aromatics (MTA). The Zn incorporation method had obvious influences on the textural properties, morphology, acidic properties and catalytic performances. The BTX selectivity was effectively improved by introduction of Zn species by ion exchange, due to a greater distribution of strong acid sites, and the generation of strong acid sites, and these acidic sites are the active sites which are the main responsible of the methanol conversion to aromatics. The reaction temperature is an important variable in the MTA process. At 450 °C a better activation of acid sites is achieved in zeolite with Zn and therefore a high percentage of BTX selectivity is obtained.

The combination of physical characteristics such as very small crystal size, high external surface area, and strong acidity makes uniform nano ZSM-5 a potentially interesting catalyst in MTA processes. The generation of nanocrystallites of approximately in the 60-80 nm range in the nano zeolite HZnZ25-i drastically improved the catalytic activity. Nano zeolite increased the diffusion efficiency of molecules and the accessibility of acid sites, improving the BTX selectivity. Under the optimal conditions 450 °C and WHSV 4.74 h$^{-1}$, 0.5 g of catalyst and 50 µm/min of methanol nearly 100% methanol conversion and 32.5% selectivity BTX (with 9 h lifetime) was obtained. The temperature reaction has great influence on the catalytic activity, at 450 °C the best BTX selectivity is obtained, however, the catalyst is deactivated after 9 h of reaction. The stability of catalysts decreases in the sequence of nano HZ25 >nano HZnZ25-i > HZ25 > HZnZ25-i > HZ50 0.01 Zn-G to 450 °C and WHSV of 9.48 h$^{-1}$. Deactivation of catalyst is due of a small amount of ZnO clusters in the channels of HZSM-5 zeolite, which avoid to the aromatics diffusion and may accelerate the catalyst deactivation due to coke deposition that block the acid sites of the zeolite. Coke deposition was known to be the major reason for catalyst deactivation in MTA reaction.

### Acknowledgment

### References

[1] Fahim M, Alsahhaf T, Elkilani A (2010) Fundamentals of Petroleum Refining, 1$^{st}$ Ed., Elsevier Sci, Kuwait

[2] Wang N, Qian W, Shen K, Su C, Wei F (2014) Bayberry-like ZnO/MFI zeolite as high performance methanol-to-aromatics catalyst. Ind Eng Chem Res 53: 14932−14940

[3] Conte M, Lopez-Sanchez JA, He Q, Morgan DJ, Ryabenkova Y, Bartley JK, Carley AF, Taylor SH, Kiely CJ, Khalid K, Hutchings GJ (2012) Modified zeolite ZSM-5 for the methanol to aromatics reaction. Catal Sci Technol 2: 105–112

[4] Zhu X (2015). Hierarchical zeolites as catalysts for methanol conversion reactions Eindhoven: Technische Universiteit Eindhoven

[5] Haw JF, Song W, Marcus DM, Nicholas JB (2003) The Mechanism of Methanol to Hydrocarbon Catalysis. Acc Chem Res 36: 317-326

[6] Zhang GQ, Bai T, Chen TF, Fan WT, Zhang X (2014) Conversion of Methanol to Light Aromatics on Zn-Modified Nano-HZSM-5 Zeolite Catalysts. Ind Eng Chem Res 53: 14932−14940

[7] Inoue Y, Nakashiro K, Ono Y (1995) Selective conversion of methanol into aromatic hydrocarbons over silver-exchanged ZSM-5 zeolites. Micropor Mater 4: 379 383

[8] Barthos R, Bánsági T, Zakar TS, Solymosi F (2007) Aromatization of methanol and methylation of benzene over $Mo_2C$/ZSM-5 catalysts. J Catal 247: 368–378

[9] Yubing X, Puyu Q, Xinping D, Haiqiang L, Youzhu Y (2013) Enhanced Performance of Zn–Sn/HZSM-5 Catalyst for the Conversion of Methanol to Aromatics. Catal Lett 143: 798–806

[10] Zhou F, Gao Y, Ma H, Wu G, Liu C (2017) Catalytic aromatization of methanol over post-treated ZSM-5 zeolites in the terms of pore structure and acid sites properties. Molec Catal 438: 37–46

[11] Ni Y, Sun A, Wu Xi, Hai G, Hu J, Li T, Li G (2011) The preparation of nano-sized H[Zn, Al]ZSM-5 zeolite and its application in the aromatization of methanol. Micropor Mesopor Mater 143: 435–442

[12] Bi Y, Wang Y, Chen X, Yu Z, Xu L (2014) Methanol aromatization over HZSM-5 catalysts modified with different zinc salts. Chin J Catal 35: 1740–1751

[13] Gabrienko AA, Arzumanov SS, Toktarev AV, Danilova IG, Prosvirin IP, Kriventsov VV, Zaikovskii VI, Freude D, Stepanov AG (2017) Different Efficiency of $Zn^{2+}$ and ZnO Species for Methane Activation on Zn-Modified Zeolite. ACS Catal 1-45

[14] Pan D, Song X, Yang X, Gao L, Wei R, Zhang J, Xiao G (2018) Efficient and selective conversion of methanol to para-xylene over stable H [Zn,Al]ZSM-5/$SiO_2$ composite catalyst. Appl Catal A: Gen 557: 15–24

[15] Ji Y, Yang H, Yan W (2017) Strategies to Enhance the Catalytic Performance of ZSM-5 Zeolite in Hydrocarbon Cracking: A Review. Catalysts 7 (367): 1-31

[16] Petushkov A, Yoon S, Larsen SC (2011) Synthesis of hierarchical nanocrystalline ZSM-5 with controlled particle size and mesoporosity. Micropor Mesopor Mater 137: 92–100

[17] Pinilla-Herrero I, Borfecchia E, Holzinger J, Mentz UV, Finn J, Lomachenko KA, Bordiga S, Lamberti C, Berlier G, Olsbye U, Svelle S, Skibsted J, Beato P (2018) High Zn/Al ratios enhance dehydrogenation vs hydrogen transfer reactions of Zn-ZSM-5 catalytic systems in methanol conversion to aromatics. J Catal 362: 146–163

[18] Tian ZR, Voigt JA, Liu J, Mckenzie B, Mcdermott MJ, Rodriguez MA, Konishi H, Xu H (2003) Complex and oriented ZnO nanostructures. Nature Mater 2: 821-826

[19] Almutairi SM, Mezari B, Magusin PC, Pidko EA, Hensen EJ (2012) Structure and Reactivity of Zn-Modified ZSM-5 Zeolites: The Importance of Clustered Cationic Zn Complexes. ACS Catal 2: 71−83

[20] Wang Y, Song J, Baxter NC, Kuo GT, Wang S (2017) Synthesis of hierarchical ZSM-5 zeolites by solid-state crystallization and their catalytic properties. J Catal 349: 53–65

[21] Jin F, Wang X, Liu T, Xiao L, Yuan M, Fan Y (2017) Synthesis of ZSM-5 with the silica source from industrial hexafluorosilicic acid as transalkylation catalyst. Chin J Chem Eng 25: 1303–1313

[22] Thommes M, Kaneko K, Neimark A, Olivier J, Rodriguez-Reinoso F, Rouquerol J, Sing K (2015) Physisorption of gases, with special reference to the evaluation of surface area and pore size distribution (IUPAC Technical Report). Pure Appl Chem 87: 1051–1069

[23] van Laak AN, Sagala SL, Zecevic J, Friedrich H, de Jongh Petra E, de Jong, KP (2010) Mesoporous mordenites obtained by sequential acid and alkaline treatments – Catalysts for cumene production with enhanced accessibility. J Catal 276: 170–180

[24] Fang Y, Su X, Bai X, Wu W, Wang G, Xiao L, Yu A (2017) Aromatization over nanosized Ga-containing ZSM-5 zeolites prepared by different methods: Effect of acidity of active Ga species on the catalytic performance. J Energ Chem 26: 768–775

[25] Li J, Tong K, Xi Z, Yuan Y, Hu Z, Zhu Z (2016) High-efficient conversion of methanol to p-xylene over shape-selective Mg-Zn-Si-HZSM-5 catalyst with fine modification of pore-opening and acidic properties. Catal Sci Tech 6(13): 4802–4813

[26] Su X, Wang G, Bai X, Wu W, Xiao L, Fang Y, Zhang J (2016) Synthesis of nanosized HZSM-5 zeolites isomorphously substituted by gallium and their catalytic performance in the aromatization. Chem Eng J 293: 365–375

[27] Zhang J, Qian W, Kong C, Wei F (2015) Increasing para-Xylene Selectivity in Making Aromatics from Methanol with a Surface-Modified Zn/P/ZSM-5 Catalyst. ACS Catal. 5: 2982-2988

[28] Jia Y, Wang J, Zhang K, Chen G, Yang Y, Liu S, Ding C, Meng Y, Liu P (2018) Hierarchical ZSM-5 zeolite synthesized via dry gel conversion-steam assisted crystallization process and its application in aromatization of methanol. Powder Tech 328: 415–429

[29] Topsøe N, Pedersen K, Derouane E (1981) Infrared and temperature-programmed desorption study of the acidic properties of ZSM-5-type zeolites. J Catal 70: 41-52

[30] Joly JF, Ajot H, Merlen E, Raatz F, Alario F (1991) Parameters affecting the dispersion of the gallium phase of gallium H-MFI aromatization catalysts. Appl Catal A: Gen 79: 249-263

[31] Xiaoning W, Zhen Z, Li Z, Guiyuan J (2007) Effects of fight Rare earth on Acidity and Catalytic Performance of HZSM-5 Zeolite for Catalytic Clacking of Butane to Light Olefins. J Rare Earths 25: 321 - 328

[32] Reddy JK, Motokura K, Koyama T, Miyaji A, Baba T (2012) Effect of morphology and particle size of ZSM-5 on catalytic performance for ethylene conversion and heptane cracking. J Catal 289: 53–61

[33] Saito H, Inagaki S, Kojima K, Han Q, Yabe T, Ogo S, Kubota Y, Sekine Y (2018) Preferential dealumination of Zn/H-ZSM-5 and its high and stable activity for ethane dehydroaromatization. Appl Catal A: Gen 549: 76–81

[34] Wang Y, Song J, Baxter N, Kuo G, Wang S (2017) Synthesis of hierarchical ZSM-5 zeolites by solid-state crystallization and their catalytic properties. J Catal 349: 53–65

[35] Iwase Y, Motokura K, Koyama T, Miyaji A, Baba T (2009) Influence of Si distribution in framework of SAPO-34 and its particle size on propylene selectivity and production rate for conversion of ethylene to propylene. Phys Chem Chem Phys 11: 9268-9277

[36] Jakkidi K, Motokura K, Koyama T, Miyaji A, Baba T (2012) Effect of morphology and particle size of ZSM-5 on catalytic performance for ethylene conversion and heptane cracking. J Catal 289: 53–61

[37] Chen J, Feng Z, Ying P, Li C (2004) ZnO clusters encapsulated inside micropores of zeolites studied by UV Raman and laser-induced luminescence spectroscopies. J Phys Chem B 108(34): 12669-12676

[38] Tamiyakul S, Ubolcharoen W, Tungasmita DN, Jongpatiwut S (2015) Conversion of glycerol to aromatic hydrocarbons over Zn-promoted HZSM-5 catalysts. Catal Today 256: 325-335

[39] Jia Y, Wang J, Kan Z, Liu S, Chen G, Yang Y, Ding C, Liu P (2017) Catalytic Conversion of Methanol to Aromatics over Nanosized HZSM-5 Zeolite Modified by $ZnSiF_6 \cdot 6H_2O$. Catal Sci Technol 7: 1776–1791

[40] Dyballa M, Becker P, Trefz D, Klemm E, Fischer A, Jakob, H, Hunger M (2016) Parameters Influencing the Selectivity to Propene in the MTO Conversion on 10-Ring Zeolites: Directly Synthesized Zeolites ZSM5, ZSM-11, and ZSM-22. Appl Catal A: Gen 510: 233-243

[41] Gong T, Qin L, Lu J, Feng H (2016) ZnO modified ZSM-5 and Y zeolites fabricated by atomic layer deposition for propane conversion. Phys Chem Phys 18: 601-614

[42] Ono Y (1992) Transformation of Lower Alkanes into Aromatic Hydrocarbons over ZSM-5 Zeolites. Catal Rev Sci Eng 34: 179-226

[43] Rownaghi A, Hedlund J (2011) Methanol to Gasoline-Range Hydrocarbons: Influence of Nanocrystal Size and Mesoporosity on Catalytic Performance and Product Distribution of ZSM-5. Ind Eng Chem Res 50: 11872–11878

[44] Konno H, Tago T, Nakasaka Y, Ohnaka R, Nishimura J, Masuda T (2013) Effectiveness of nano-scale ZSM-5 zeolite and its deactivation mechanism on catalytic cracking of representative hydrocarbons of naphtha. Micropor Mesopor Mater 175: 25–33

[45] Zhang G, Bai T, Fei T, Fan W, Zhang X (2014) Conversion of Methanol to Light Aromatics on Zn-Modified Nano-HZSM-5 Zeolite Catalysts. Ind. Eng Chem Res 53: 14932−14940

[46] Ningning X, Donghui P, Yuanfeng W, Siquan X, Lijing G, Jin Z, Guomin X (2019) Preparation of nano-sized HZSM-5 zeolite with sodium alginate for glycerol aromatization. React Kinet Mechanisms Catal 127(1): 449–467

[47] Wan ZJ, Li GK, Wang CF, Yang H, Zhang DK (2018) Relating coke formation and characteristics to deactivation of ZSM-5 zeolite in methanol to gasoline conversion. Appl Catal A: Gen 549:141–151

[48] Zhao YH, Gao TY, Wang YJ, Zhou YJ, Huang GQ (2018) Zinc supported on alkaline activated HZSM-5 for aromatization reaction. React Kinet Mechanisms Catal 125 (2): 1085–1098

[49] Schulz H (2010) "Coking" of zeolites during methanol conversion: Basic reactions of the MTO-, MTP- and MTG processes. Catal Today 154: 183–194

[50] Niu X, Gao J, Miao Q, Dong M, Wang G, Weibin F, Qin Z, Wang J (2014) Influence of preparation method on the performance of Zn-containing HZSM-5 catalysts in methanol-to-aromatics. Micropor Mesopor Mater 197: 252–261

[51] Kim J, Choi M, Ryoo R (2010) Effect of mesoporosity against the deactivation of MFI zeolite catalyst during the methanol-to-hydrocarbon conversion process. J Catal 269: 219–228

[52] Khatamian M, Alaji Z, Khandar A (2011) Synthesis and Characterization of Polycrystalline ZnO/HZSM-5 Nanocomposites. J Iran Chem Soc 8: 44-54

[53] Kazansky V, Borovkov V, Serikh A, Van Santen R, Anderson B (2000) Nature of the sites of dissociative adsorption of dihydrogen and light paraffins in ZnHZSM-5 zeolite prepared by incipient wetness impregnation. Catal Lett 66: 39–47

[54] Olsbye U, Svelle S, Bjørgen M, Beato P, Janssens T, Bordiga S, Lillerud K (2012) Conversion of Methanol to Hydrocarbons: How Zeolite Cavity and Pore Size Controls Product Selectivity. Angew Chem Int Ed 51: 2–24

[55] Tian T, Qian WZ, Sun YJ, Cui Y, Lu YY, Wei F (2009) Aromatization of methanol on Ag/ZSM-5 catalyst. Modern Chem Ind 29 (1): 55-58

[56] Zaidi HA, Pant KK (2004) "Catalytic conversion of methanol to gasoline range hydrocarbons. Catal Today 96 (3): 155-160

[57] Zaidi, HA, Pant KK (2008) Activity of oxalic acid treated ZnO/CuO/HZSM-5 catalyst for the transformation of methanol to gasoline range hydrocarbons. Ind Eng Chem Res 47 (9): 2970-2975

[58] Freeman D, Wells RP, Hutchings GJ (2002) Conversion of methanol to hydrocarbons over $Ga_2O_3$/H-ZSM-5 and $Ga_2O_3$/$WO_3$ catalysts. J Catal 205 (2): 358-365

[59] Choudhary VR, Kinage AK (1995) Methanol-to-aromatics conversion over H-gallosilicate (MFI): influence of Si/Ga ratio, degree of $H^+$ exchange, pretreatment conditions, and poisoning of strong acid sites. Zeolites 15 (8): 732-738

## 8.2. Segundo artículo: Publicado

Your Submission TOCA-D-19-00112R1 - [EMID:7e55105b2c84d122] ▶ Recibidos x

**TOPICS in CATALYSIS (TOCA)** <em@editorialmanager.com>                 lun., 10 feb. 21:38 (hace 1 día)
para mí ▾

Dear Dr. García Ruiz,

We are pleased to inform you that your manuscript, "Synthesis of 10 and 12 ring zeolites (MCM-22, TNU-9 and MCM-68) modified with Zn and its potential application in the reaction of methanol to light aromatics and olefins", has been accepted for publication in
Topics in Catalysis.

You will receive an e-mail in due course regarding the production process.

Please remember to quote the manuscript number, TOCA-D-19-00112R1, whenever inquiring about your manuscript.

With kind regards,
Jose Escobar Aguilar
Guest Editor
Topics in Catalysis

Comments to the author (if any):

**ORIGINAL PAPER**

# Synthesis of 10 and 12 Ring Zeolites (MCM-22, TNU-9 and MCM-68) Modified with Zn and Its Potential Application in the Reaction of Methanol to Light Aromatics and Olefins

Misael García Ruiz[1] · Dora A. Solís Casados[2] · Julia Aguilar Pliego[3] · Carlos Márquez Álvarez[4] · Enrique Sastre de Andrés[4] · Diana Sanjurjo Tartalo[4] · Raquel Sáinz Vaque[4] · Marisol Grande Casas[4]

## Abstract

The effect on the incorporation of zinc of three zeolites TNU-9, MCM-22, and MCM-68 was investigated. The physico-chemical properties of zeolites were studied by X-ray diffraction, $N_2$-adsorption, temperature-programmed desorption of $NH_3$ (TPD), nuclear magnetic resonance of $^{27}Al$ and $^{29}Si$ (MAS NMR), scanning electron microscopy (SEM) and thermogravimetric analysis (TGA). Then all the samples were characterized and evaluated in the reaction of methanol to aromatics (MTA). The correlation of zinc incorporation method and acidic properties of zeolites with catalytic performance was investigated. The form of zinc incorporation, the acidity, the type of zeolitic structure and the reaction temperature had a great influence on the catalytic activity. Regarding the type of structure, the total aromatics selectivity in this work increased in the followed order for zeolites modified with Zn: MCM-68 > TNU-15 > MCM-22. The medium pore zeolite T9-15 (TNU-9 zeolite and Si/Al 15 ratio) catalysts with the ratio $ZnO/ZnO + Al_2O_3$ equal to 0.34 (T9-15 0.5 Zn) showed better stability with conversion of methanol completes during 9 h of reaction and 17% to BTX selectivity and 32% to total aromatics compounds at 450 °C and WHSV of 4.24 $h^{-1}$. In methanol conversion, the selectivity to aromatics over the T9-15 modified-Zn materials (TNU-9 zeolite and Si/Al 15 ratio) under study, increased in the followed order: T9-15 0.5 Zn > ZT9-15 > T9-15 > T9-15 0.2 Zn. The reaction temperature is an important variable in the MTA process. At 450 °C a better activation of acid sites is achieved in zeolite with Zn and therefore a high percentage of BTX selectivity is obtained for TNU-9 zeolite.

✉ Misael García Ruiz
  misagr89@gmail.com

1 Doctorado en Ciencia de Materiales de La Facultad de Química, Universidad Autónoma del Estado de México, Paseo Colón Esquina Paseo Tollocan S/N, C.P. 50000 Toluca, Mexico

2 Universidad Autónoma del Estado de México, Centro Conjunto de Investigación en Química Sustentable UAEM-UNAM, Personal Académico Adscrito a La Facultad de Química, UAEMex, Toluca, Mexico

3 Área de Química Aplicada, Departamento de Ciencias Básicas, UAM-A, San pablo 180, C.P. 02200 Mexico, Mexico

4 Instituto de Catálisis y Petroleoquímica, CSIC, C/Marie Curie 2, Campus Cantoblanco, 28049 Madrid, Spain

## 1 Introduction

Zeolites are crystalline aluminosilicate constituted by silica tetrahedron and alumina tetrahedron through oxygen bridges containing ordered micropores that enable shape-selective transformation [1]. Because of its high thermal stability and strong Brønsted acidity of zeolite catalysts, gives rise to many applications, for example in isomerization [2], alkylation [3] and aromatization reactions [4].

The conversion of methanol to hydrocarbons (MTH) over acidic zeolites has drawn considerable attention since its discovery in 1970s by Mobil Corporation. Depending on the product of reaction selectivity, this process was named as MTG (methanol to gasoline), MTO (methanol to olefins), MTP (methanol to propene) and MTA [methanol to aromatics (MTA)]. In this last process, aromatic compounds, especially benzene, toluene and xylene (BTX fraction) and light olefins, such as ethene and propene, are mainly produced

Springer

**Synthesis of 10 and 12 ring zeolites (MCM-22, TNU-9 and MCM-68) modified with Zn and its potential application in the reaction of methanol to light aromatics and olefins**

Misael García Ruiz*[a], Dora A. Solís Casados[b], Julia Aguilar Pliego[c], Carlos Márquez Álvarez[d], Enrique Sastre de Andrés[d], Diana Sanjurjo Tartalo[d], Raquel Sáinz Vaque[d], Marisol Grande Casas[d]

[a] Doctorado en Ciencia de Materiales de la Facultad de Química, Universidad Autónoma del Estado de México, Paseo Colón Esquina Paseo Tollocan S/N, Toluca Estado de México, México, C.P. 50000.

[b] Universidad Autónoma del Estado de México, Centro Conjunto de Investigación en Química Sustentable UAEM-UNAM. Personal Académico Adscrito a la Facultad de Química, UAEMex.

[c] Área de Química Aplicada, Departamento de Ciencias Básicas, UAM-A, San pablo 180, C.P. 02200, Cd de México.

[d] Instituto de Catálisis y Petroleoquímica, CSIC, C/Marie Curie 2, Campus Cantoblanco, 28049 Madrid, España

**Abstract**

The effect on the incorporation of zinc of three zeolites TNU-9, MCM-22, and MCM-68 was investigated. The physico-chemical properties of zeolites were studied by X-ray diffraction, $N_2$-adsorption, temperature-programmed desorption of $NH_3$ (TPD), nuclear magnetic resonance of $^{27}Al$ and $^{29}Si$ (MAS NMR), scanning electron microscopy (SEM) and thermogravimetric analysis (TGA). Then all the samples were characterized and evaluated in the reaction of methanol to aromatics (MTA). The correlation of zinc incorporation method and acidic properties of zeolites with catalytic performance was investigated. The form of zinc incorporation, the acidity, the type of zeolitic structure and the reaction temperature had a great influence on the catalytic activity. Regarding the type of structure, the total aromatics selectivity in this work increased in the followed order for zeolites modified with Zn: MCM-68 > TNU-15 > MCM-22. The medium pore zeolite T9-15 (TNU-9 zeolite and Si/Al 15 ratio) catalysts with the ratio $ZnO/ZnO+Al_2O_3$ equal to 0.34 (T9-15 0.5 Zn) showed better stability with conversion of methanol completes during 9 h of reaction and 17 % to BTX selectivity and 32 % to total aromatics compounds at 450 °C and WHSV of 4.24 $h^{-1}$. In methanol conversion, the selectivity to aromatics over the T9-15 modified-Zn materials (TNU-9 zeolite and Si/Al 15 ratio) under study, increased in the followed order: T9-15 0.5 Zn > ZT9-15 > T9-15 > T9-15 0.2 Zn. The reaction temperature is an important variable in the MTA process. At 450 °C a better

activation of acid sites is achieved in zeolite with Zn and therefore a high percentage of BTX selectivity is obtained for TNU-9 zeolite.

**Keywords**: Methanol conversion, Aromatics compounds, BTX fraction, Zeolites modified, Light olefins

### 1. Introduction

Zeolites are crystalline aluminosilicate constituted by silica tetrahedron and alumina tetrahedron through oxygen bridges containing ordered micropores that enable shape-selective transformation [1]. Because of its high thermal stability and strong Brønsted acidity of zeolite catalysts, gives rise to many applications, for example in isomerization [2], alkylation [3] and aromatization reactions [4].

The conversion of methanol to hydrocarbons (MTH) over acidic zeolites has drawn considerable attention since its discovery in 1970s by Mobil Corporation. Depending on the product of reaction selectivity, this process was named as MTG (methanol to gasoline), MTO (methanol to olefins), MTP (methanol to propene) and MTA (methanol to aromatics). In this last process, aromatic compounds, especially benzene, toluene and xylene (BTX fraction) and light olefins, such as ethene and propene, are mainly produced from the oil-based route to this date, the gradual depletion of oil reserves has resulted in a sustained tight supply and high cost of aromatics [5]. In recent years, the conversion of methanol to aromatics (MTA) has attracted great attentions because methanol can be easily produced via syngas from various sources, such as biomass, natural gas and coal [6]. One process that uses zeolites as shape-selective catalysts is the conversion of methanol to aromatics (MTA) and light olefins (MTO). For these methanol conversion technologies, ZSM-5 zeolite has been considered as an important catalyst [7]. As a crystalline aluminosilicate, ZSM-5 zeolite has well-defined microporous structure, large surface area and strong acidity [8], which contributes to high activity and selectivity for hydrocarbon production in MTH reaction [9]. In a previous article [10] we demonstrate the high catalytic activity of the modified-Zn ZSM-5 zeolite in the MTA process. The Zn/ZSM-5 catalyst obtained complete methanol conversions and high selectivity to the BTX fraction. On the other hand, we show that the crystal size has a significant influence on the catalytic activity improving the useful life of the catalyst. The ZSM-5 nanocrystalline zeolite showed a BTX selectivity of 32% with 80% conversions until 9 h reaction.

As demonstrated in previous studies [11], certain medium pore zeolites (with 10 and 12-membered channels), doped with different metals include Zn, La, Ga, Ag, Cu, Sn, Ni, Mo and Cr are capable of transforming methanol, however, the selectivity to a specific product versus time is different in each case.

Furthermore, it has been widely accepted that Zn species could greatly increase the selectivity of BTX in MTA reaction compared with other metal species. Specifically, Zn can be incorporated into zeolite by two methods; ion exchange (i) or in the synthesis gel (G) [12].

In this study, comprising different combinations of 10- and 12-ring pores, namely MCM-22 (MWW), TUN-9 (TNU) and MCM-68 (MSE), which have not been little studied in this type of reactions. Catalyst MCM-22 (MWW topology), which has unique pore architecture with two independent pore systems, 0.41 nm x 0.51 nm 2D (two-dimension) 10-ring sinusoidal pore system and large 3D 12-ring supercage system connected by 0.40 nm x 0.55 nm 10-ring windows The unique structure and the presence of supercage in MWW-type zeolites are considered essential in promoting activity and stability of the catalyst in methanol conversion reactions [13]. MCM-68 (framework type code: MSE) is a multipore zeolite with three-dimensional $2 \times 10 \times 10$-ring channel system, including a 12-ring ($6.4 \times 6.8$ Å) straight channel and two tortuous 10-ring ($5.2 \times 5.8$ Å and $5.2 \times 5.2$ Å) channels that intersect with each other [14]. Its four 10-ring windows may make H-MCM-68 more resistant to coke formation, because of their connection into the large 12-ring channels [15]. Finally, TNU-9 (Taejon National University No. 9), a new high-silica zeolite with 3D 10-ring channel system, has previously been synthesized by Suk Bong Hong and coworkers [16]. TNU-9 (TUN topology) consists of two different types of straight 10-ring channels running parallel to y-axis, with the dimension of $5.5 \times 6.0$ and $5.2 \times 6.0$ Å. The channels perpendicular to y-axis join these straight channels to form a 3D 10-ring channel system [17].

Due to the peculiar pore structure of these zeolites have been applied in many catalytic processes and is a potential catalyst in MTA and MTO reaction. Specifically, Zhang and coworkers [18] investigated H-MCM-22 catalyst in MTO reaction, they showed the light olefin selectivity seems to be related to the amounts of Brønsted acid, a comparison of Lewis acid which does not benefit to improve the catalytic stability. However, an important difficulty that a zeolite catalyst encounters is the heavy coke formation in the reaction process obtaining both longer lifetime and higher BTX selectivity is difficult. Therefore, the main challenge of our work is to improve the lifetime of the catalyst and produce high selectivity to aromatics. In this work, the effects of Zn incorporation and reactions on the catalytic performance of a Zn-modified of the three types of zeolites with different ration Si/Al in methanol conversion were investigated.

## 2. Experimental

### 2.1. Materials

The reagents used for the preparation of zeolites are tetraethyl orthosilicate (TEOS, 98%, Aldrich), fumed silica (Aerosil 200, Degussa), sodium hydroxide (NaOH), sodium aluminate (41 wt %$Al_2O_3$, 37 wt.% $Na_2O$), Bicyclo[2.2.2]oct-7-ene-2,3,5,6-tetracarboxylic dianhydride (> 95.0%, Sigma-Aldrich), hexamethyleneimine (HMI, 99 %, Sigma Aldrich), aluminum hydroxide hydrated ($Al(OH)_3$, Sigma-Aldrich), colloidal silica (40 wt% suspension in $H_2O$, LUDOX HS-40, Aldrich), Zinc nitrate hexahydrate ($Zn(NO_3)_2 \cdot 6H_2O$ reagent grade, 98%, Sigma-Aldrich), Aluminium nitrate ($Al(NO_3)_3 \cdot 9H_2O$ ACS reagent, ≥98%, Sigma-Aldrich), 1,4-dibromobutane (99%, Aldrich), 1-methylpyrrolidine (97%, Aldrich), methanol HPLC, ≥99.9% (Sigma-Aldrich) and Zinc acetate dihydrate ($Zn(CH_3COO)_2 \cdot 2H_2O$, 99% Sigma Aldrich).

### 2.2. Synthesis of MCM-22 zeolite

A sample of zeolite MCM-22 with Si/Al ratio of 30 and 50 was synthesized following the procedure described by Wu and coworkers [19] with some modifications. The gel was prepared with the molar composition $xSiO_2$: y $Al_2O_3$:0.075 $Na_2O$: 0.6 HMI: $zZnO$:35 $H_2O$, where x/y is ration Si/Al (30 and 50) and z represents the moles of Zn (in your case). First, sodium hydroxide and sodium aluminate were dissolved in deionized water in a Teflon glass and $Zn(NO_3)_2 \cdot 6H_2O$ (in the case) . Once dissolved, hexamethyleneimine (HMI) was added as structure directing agent (SDA) and finally was added fumed silica. The resulting mixture was vigorously shaken for 2 h to room temperature, after what the mixture was distributed in Teflon-lined, stainless steel autoclaves and heated at 160 °C for 11 days, both in conditions of agitation at 60 rpm (A) and in static conditions (S). After this period the autoclaves were removed from the oven, quenched in ice and the solid was filtered and washed with deionised water until pH 7. The product was dried at 110 °C overnight and calcined at 550 °C for 20 h in air atmosphere.

### 2.3. Synthesis of MCM-68 zeolite

MCM-68 zeolite was synthesized according to previous literature [20]. The SDA, $N,N,N_0,N_0$-tetraethylbicyclo[2.2.2]oct-7-ene-2,3:5,6- dipyrrolidinium diiodide ($TEBOP^{2+}(I^-)_2$) was synthesized exactly following the reported procedure [21] from commercially available bicyclo[2.2.2]oct-7-ene-2,3,5,6-tetracarboxylic anhydride (Aldrich) by three steps in 58% overall yield. The typical gel composition is

$xSiO_2$:0.1TEBOP$^{2+}$(I$^-$)$_2$:0.375KOH:yAl(OH)$_3$:30H$_2$O, where x/y represents the Si/Al molar ratio of 11. In a typical synthesis, colloidal silica, distilled water, and Al(OH)$_3$ were mixed and stirred at room temperature for 10 min, then KOH was added to the solution and stirred for another 15 min. After that, TEBOP$^{2+}$(I$^-$)$_2$ was added and the mixture was stirred for 3 h. Then the gel was transferred to a 50 mL Teflon-lined autoclave and placed in a 160 °C oven for 14 days in static conditions. The solid product obtained was separated by filtration, washed several times with distilled water, and dried overnight. The as-synthesized MCM-68 was calcined in a muffle furnace at 650 °C for 6 h to remove the SDA.

### 2.4. Synthesis of TNU-9 zeolite

TNU-9 zeolite was synthesized under hydrothermal conditions following the procedure given by Hong and coworkers [17] using 4-bis(methylpyrrodinium) pentane (1,4-MPP) as organic structure-directing agent (SDA). (1,4-MPP) in its bromide forms was prepared, purified, and characterized as described in previous paper [22]. This diquaternary ammonium salt was stored in a desiccator for use as an SDA.

In a typical synthesis, Al(NO$_3$)$_3$-9H$_2$O (98%, Sigma Aldrich) and NaOH (98 %, Sigma Aldrich) were dissolved in deionized water in a Teflon glass, and the mixture was vigorously stirred for 2 h, (1,4-MPP) was added once dissolved, fumed silica was added as a source of silica, the gel was mixed vigorously for 2 h at room temperature. The gel was placed in autoclaved at 160 °C with continuous stirring at 60 rpm for 10 days. The final synthesis gels had the following chemical composition: $xSiO_2$: 11Na$_2$O: yAl$_2$O$_3$: 4.5(1,4-MPP): 1200H$_2$O, where x/y represents the Si/Al molar ratio of 15, 30 and 50. The solid was recovered by filtration, dried at 70 °C and was calcined under flowing air at 550 °C for 10 h to remove the occluded organic SDA.

On the other hand, the synthesis of zinc-substituted TNU-9 zeolites was performed using the previous procedure, however, the final composition of the gel was 30 SiO$_2$: 11 Na$_2$O: xZnO: yAl$_2$O$_3$: 4.5 (1,4-MPP): 1200H$_2$O, where x is the amount of zinc oxide placed in the synthesis gel using zinc acetate dihydrate (Zn(CH$_3$COO)$_2$ ·2H$_2$O, 99% Sigma Aldrich) and Si/Al 15 ration. For these gels, the amount of ZnO was varied for a x/x+y of 0.33 y 0.16 ration, which corresponds to 0.5 and 0.2 moles of ZnO, respectively.

2.5. Preparation of acid zeolites H-MCM-22, H-MCM-68 and H-TNU-9 and ion exchange with Zn

The Na-Zeolites were converted to H-Zeolites (acid form) by refluxing twice with 1 M $NH_4NO_3$ solution at 80 °C for 3 h, followed by filtered and drying at 110 °C over night and calcination at 550 °C for 4 h in air. The acid zeolites previously synthesized were exchanged with a 0.025 M solution of $Zn(NO_3)_2•6H2O$ at 80 °C for 4 h. The zeolite was filtered, washed and dried at 70 ° C, finally the resulting powder was calcined at 550 ° C for 4 h with air flow. Table 1 lists the results from syntheses performed and its conditions.

Table 1. Synthesized zeolites and their synthesis conditions

| Zeolite | Ration Si/Al | Synthesis conditions | Zn incorporation method | Denoted |
|---------|--------------|----------------------|-------------------------|---------|
| MCM-22 | 30 | Agitation | Synthesis gel | M22-30A-G |
|  | 30 | Static | Synthesis gel | M22-30S-G |
|  | 30 | Static | ion exchange | ZM22-30S |
|  | 30 | Static | Synthesis gel | ZM22-30S-G |
|  | 30 | Agitation | ion exchange | ZM22-30A |
|  | 50 | Agitation | N/A | M22-50A |
|  | 50 | Static | N/A | M22-50S |
| MCM-68 | 11 | Static | ion exchange | ZM68-11 |
| TNU-9 | 15 | Agitation | N/A | T9-15 |
|  | 15 | Agitation | ion exchange | ZT9-15 |
|  | 15 | Agitation | Synthesis gel | T9 0.5 Zn |
|  | 15 | Agitation | Synthesis gel | T9 0.2 Zn |
|  | 30 | Agitation | N/A | T9-30 |
|  | 30 | Agitation | ion exchange | ZT9-30 |
|  | 50 | Agitation | N/A | T9-50 |
|  | 50 | Agitation | ion exchange | ZT9-50 |

2.6. Catalyst characterization

Powder X-ray diffraction (PXRD) patterns were collected with an XPert Pro PANalytical diffractometer (CuKα1 radiation = 0.15406 nm). Scanning electron microscopy (SEM) images were recorded on a Hitachi S-3000N microscope. Transmission electron microscopy (TEM) study was carried on a JEOL 2100F

microscope opering to 200KV. Nitrogen adsorption/desorption isotherms were measured at $-196$ °C in a Micromeritics ASAP 2020 device. Before the measurement, the previously calcined sample was degassed at 350 °C under high vacuum for at least 10 h. Surface areas were estimated by the BET method whereas microporous and external surface areas were estimated by applying the t-plot method.

Solid-state magic-angle spinning (MAS) NMR experiments were conducted on a Bruker Avance 300 (11.75 T) spectrometer operated with frequency at 130.32 MHz and spinning rate at 10 KHz. The 27Al NMR spectra were recorded using a pulse width of 0.5 μs (π/12 flip angle), 2400 scans and a recycle delay of 1 s.

The Al, Si and Zn concentrations of samples were obtained by inductively coupled plasma-optical emission spectroscopy (ICP-OES) with a Optima 3300 DV Perkin Elmer. Temperature programmed desorption of ammonia ($NH_3$-TPD) was conducted using a Micrometrics Autochem II chemisorption analysis equipment. Typically, 100 mg of sample pellets (30–40 mesh) were pretreated at 550 °C for 1 h in helium flow (25 mL/min) and then cooled to the adsorption temperature (177 °C). A gas mixture of 5.0 vol.% $NH_3$ in He was then allowed to flow over the sample for 4 h at a rate of 15 mL/min. Afterwards, the sample was flushed with a 25 mL/min helium flow for 30 min while maintaining the temperature at 177 °C to remove weakly adsorbed $NH_3$, and finally the temperature was increased to 550 °C at a rate of 10 °C/min. Thermogravimetric analysis (TGA) were carried out at a heating of 30 °C to 900 °C with a rate of 20 °C/min under air flow and registered in a PerkinElmer TGA7 instrument.

### 2.7. MTA catalytic testing conditions

Zn modified zeolites were tested as catalysts in the conversion of methanol at different reaction temperatures at 400, 425 and 450 ° C in a Microactivity reaction set (PID Eng & Tech) consisting of a fixed bed reactor completely automated and controlled from a computer. The reactor outlet is connected to a gas chromatograph to analyze the reaction products. $N_2$ was used as a stripping gas under a controlled flow. The methanol was fed as a liquid using an HPLC pump (Gilson 307). The methanol was converted to the gas phase and mixed with the $N_2$ stream in a preheater at 180 ° C to generate a gas mixture with a constant molar ratio of methanol/$N_2$ of 4. Before the reaction, the catalysts were activated at 550 ° C for 1 h low air flow to remove any trace of organic molecules or moisture adsorbed within the pores of the catalyst. Typically, the sample was compacted and sieved in a 20-30 mesh, corresponding to a particle size between

0.84 and 0.59 mm. The weight of the catalyst and the flow of methanol were optimized to achieve different values of space velocities (WHSV).

The reaction products were analyzed online by gas chromatography with a VARIAN CP3800 chromatograph. The device is equipped with two columns: (i) a Petrocol DH50.2 capillary column connected to an FID detector, and (ii) a Porapack Q 80–100 mesh packed column (2 m length, 3.17 mm (1/8 ") diameter external and 2 mm internal diameter) connected to a TCD detector, to analyze hydrocarbons and oxygenated products, respectively.

## 3. Results and discussion

### 3.1. X-Ray Diffraction

Figure 1 shows that all the parent H-MCM-22 and modified-Zn samples have a typical MWW structure [18]. H-MCM-22 zeolites with different methods of Zn incorporation display high intensities of the XRD patterns, showing high crystallinity, a diffraction line at $2\theta = 7.08°$ associated to 0 0 2 diffraction plane, characteristic of a layered structure of MWW sheets stacking along the c-direction, is observed. Three well resolved diffraction lines due to 1 0 0, 1 0 1 and 1 0 2 planes are also detected. Concerning the M22-30S product, the presence in its XRD pattern of an intense peak at $2\theta= 9.45$, 22.4 and 25.7°, suggests that, besides MCM-22, another phase is formed during crystallisation. It is known [23,24], formation of ferrierite phase besides MCM-22 has been reported over static synthesis conditions. Figure 1b presents XRD patterns for TUN zeolites synthesized with different Si/Al ratios (15, 30 and 50) exchanged with Zn and the acid sample T9-30 to verify there is not characteristic peaks of ZnO suggesting that Zn species were highly dispersed on TNU-9 zeolite [25]. All four X-ray patterns evidence high crystallinity and phase purity of these samples confirming that no structural changes proceeded during the post-synthesis treatments. The structure of zeolites was preserved after all treatments with Zn and no significant changes were observed in the individual XRD patterns. The XRD patterns of different MCM-68 samples are presented in Figure 1c. The zeolites of as-synthesized M68-11 and ZM68-11 showed a typical MSE topology with good crystallinity. The XRD patterns of ZM68-11 sample was consisted of the typical reflections at 6.79°, 8.06°, 9.66°, 19.36°, 21.62°, 22.50°,26.14° and 27.50°. MSE topology with Zn no obvious decrease in crystallinity compared with M68-11, suggesting that ZM68-11 zeolite structure was very well preserved after treatment [26].
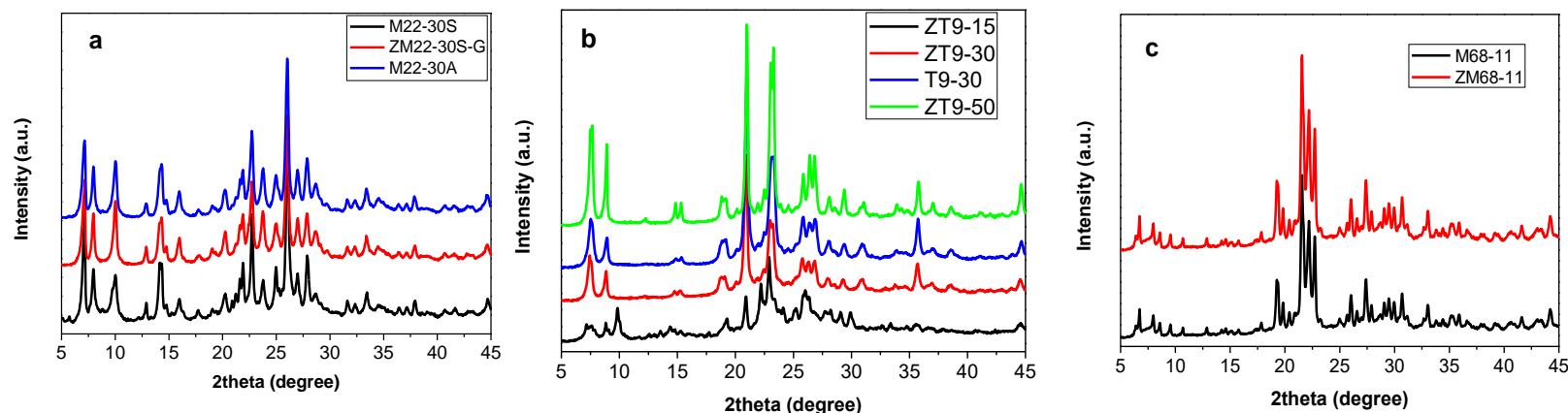
Figure 1. XRD patterns of HMCM-22, HMCM-68 y HTNU-9 zeolites selected

### 3.2.    N$_2$ adsorption–desorption

The N$_2$ adsorption–desorption isotherms of all MCM-22 modified samples are shown in Figure 2a. All the curves can be classified as a type I + IV isotherm, pointing out that in these solids, along with the characteristic microporous zeolite framework there is a mesoporous structure. Nitrogen adsorption–desorption isotherms of TNU-9 acids and modified with Zn are shown in Figure 2b. The TNU-9 samples show the type I isotherm with a high nitrogen uptake at low relative pressures, which is characteristic for purely microporous materials [27].

The adsorption isotherms did not practically change their shape and all samples possess practically the same micropore volume (0.107–0.152 cm$^3$/g). The distinctive increase in adsorption capacity at p/po=0.4–0.9, reveals that the presence of mesopores, whereas ZT9-15 sample shows an increase in quantity adsorbed at high pressures due to the presence of crystals of smaller size as observed by SEM. Finally, N$_2$ adsorption-desorption isotherms of various zeolites are shown in Figure 2c. Clearly, ZM68-11 exhibited type I isotherm with a very steep rise in N$_2$ amount adsorbed in the low relative pressure (p/po) range and a small hysteresis loop of type H3 in the high p/po range of 0.9–1.0, indicating its typical microporous feature as well as the existence of some mesopores and/or macropores derived mainly from the pile-up of zeolite crystals [20].

BET surface areas, microporous surface areas, microporous volumes and external surface areas of acid zeolites and exchanged zeolites are listed in Table 2.  Both the surface area and total pore volume decreased

after zinc treatment, suggesting that species ZnO may have been highly dispersed on the external surfaces or in the channels of the zeolites, especially for ZM22-30A-G (232 $m^2 \cdot g^{-1}$) by direct synthesis and ZT9-50 (312 $m^2 \cdot g^{-1}$) by ion exchange. TUN-9 samples the surface area and the micropore volume decrease as the Si/Al ratio increases. The large surface area is the result of a purely microporous framework with molecular dimensions for shape selectivity which is a characteristic of zeolites. A large external surface area produces to number of pore mouths and increase the accessibility of acid sites in the micropores, which delay the deactivation by coke formation [28].
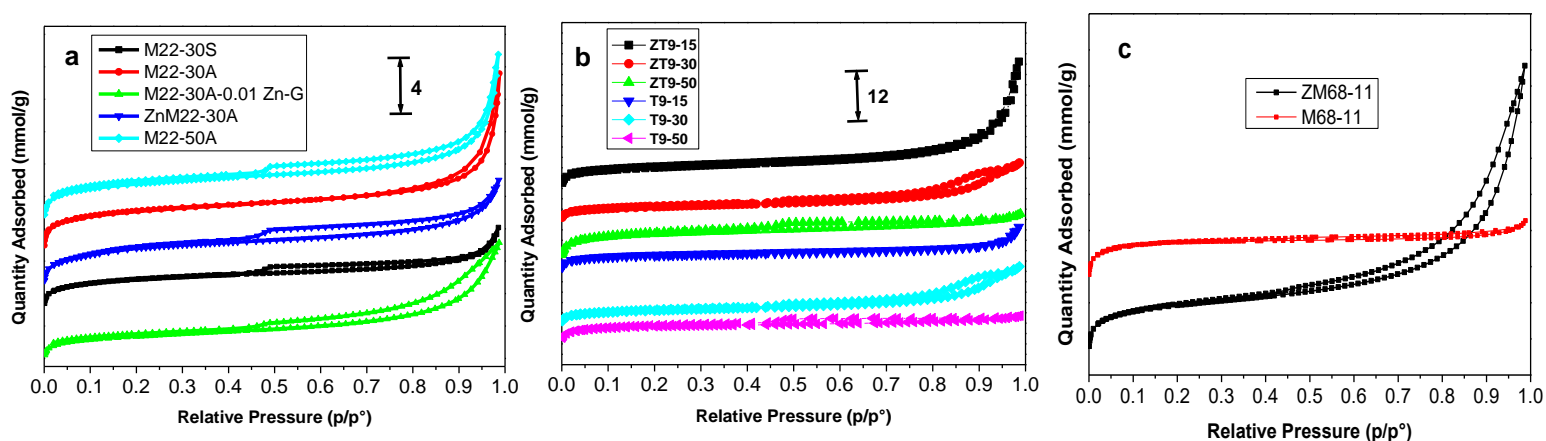


Figure 2. N$_2$ adsorption–desorption isotherms a) MCM-22 b) TNU-9 and c) MCM-68 zeolites

The surface area and micropore volume of these zeolites are listed in Table 2, which were calculated using the BET and t-plot methods, respectively. The large surface area is the result of a purely microporous framework with molecular dimensions for shape selectivity. The external surface area and micropore surface area of zeolites all decreased after the introduction of Zn species, indicating the Zn species were loaded on the external surface and into the channels of Zn modified zeolites simultaneously [24,26].

Table 2. Textural properties of zeolites prepared

| Catalyst | $S_{BET}/m^2 \cdot g^{-1}$ | $S_{micro}/m^2 \cdot g^{-1}$ | $S_{external}/m^2 \cdot g^{-1}$ | $V_{micro}/cm^3 \cdot g^{-1}$ |
|---|---|---|---|---|
| M22-30A | 526 | 453 | 73 | 0.191 |
| M22-30S | 356 | 301 | 55 | 0.132 |
| ZM22-30AG | 232 | 48 | 184 | 0.0717 |
| ZM22-30S | 208 | 161 | 47 | 0.0633 |

| | | | | |
|---|---|---|---|---|
| M22-50A | 450 | 64 | 386 | 0.1484 |
| M22-50S | 324 | 121 | 203 | 0.0809 |
| ZM22-50S | 469 | 381 | 88 | 0.1477 |
| M68-11 | 610 | 578 | 32 | 0.2173 |
| ZM68-11 | 429 | 348 | 81 | 0.1349 |
| T9-15 | 484 | 414 | 70 | 0.1596 |
| ZT9-15 | 517 | 401 | 116 | 0.1597 |
| T9 0.5 Zn | 320 | 250 | 70 | 0.0978 |
| T9 0.2 Zn | 470 | 395 | 75 | 0.1524 |
| T9-30 | 361 | 268 | 92 | 0.1058 |
| ZT9-30 | 361 | 276 | 85 | '0.1083 |
| T9-50 | 346 | 308 | 38 | 0.1176 |
| ZT9-50 | 312 | 269 | 43 | 0.1035 |

### 3.3.    Scanning Electron Microscopy (SEM)

SEM images of MCM-22 samples in stirring conditions are shown in Figure 3. For the M22-30A samples the SEM images confirm the crystallisation of pure MCM-22 in such conditions, which appears in the form of very thin particles in the form of a rose forming relatively small lamellar particles [24]. However, the samples synthesized hydrothermally in static conditions show different morphology (Figure 4). The samples have a morphology spherical particle with a small hole at the center due to the coupling of sheets of structure MWW. Previous reports show that the conditions of synthesis drastically influence the morphology of the MCM-22 zeolites. Scanning electron images of parent and modified TUN zeolites are given in Figure 5. The SEM pictures of ZT9-15 show a rod-like morphology and a crystal size in the range of 1–1.5 µm (Figure 5a). The ZT9-30 sample present 0.2 m spherical crystallites formed by stacked sheets (Figure 5b). Finally, sample ZT9-50 shows a totally different morphology, large crystals of 16 µm with intercrystalline growths inside them. The large crystals of this catalyst tend to have an inefficient diffusion of reactant molecules and products in the MTA process. The ration Si/Al influences in a considerate way distribution of crystals sizes and shapes of TUN zeolite (Figure 5c). Figure 5d shows the SEM images of these MSE type zeolites. It could be found that ZM68-11 exhibited cuboid shaped crystallites with sizes of about 100–200 nm, which was like the previous report [26]. In this study, the crystal size decreased in the order ZM68-11> ZT9-15>M22-30A which is also in agreement with the observed relative stability.
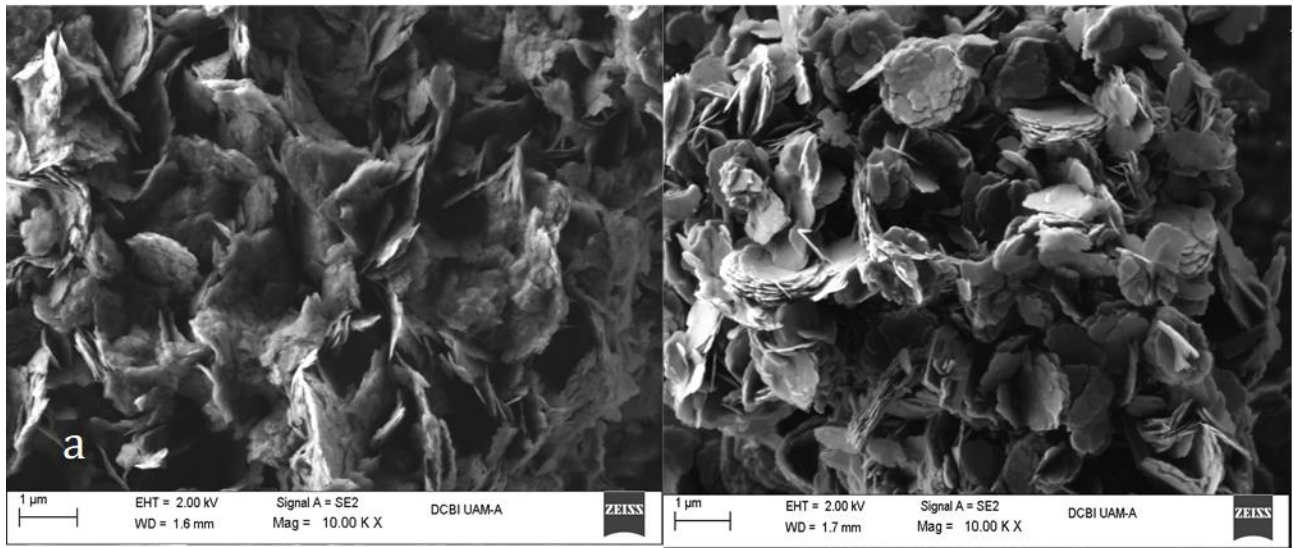
Figure 3. SEM images of the M22-30A samples (stirring conditions)
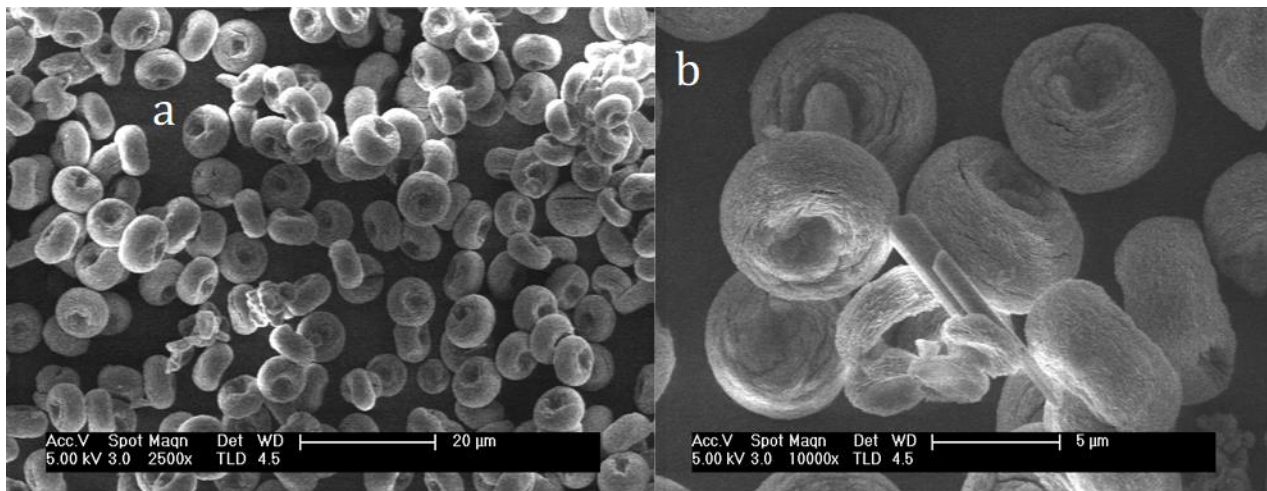


Figure 4. SEM images of the M22-30S sample (static conditions)

pores of zeolite MCM-22 with a percentage of weight loss of 3.75%. The second weight loss (2.18 %) at 325 °C is due to the decomposition of the imine that acts as a load compensator in the zeolitic structure. The last loss occurs due to the oxidation of different condensation products within the structure of the MCM-22 with a weight loss greater than 11.61 %.

In the air TGA of the M68-11 zeolite (blue line) prior to calcination (Figure 6b), three maxima were observed at 340, 450 and 645 °C, which agrees with previous reports [29]. These weight losses are due to exothermic processes produced by the combustion of SDA in the air atmosphere. A similar case occurred with the sample not calcined T9-15 (red line), where it had three weight losses at 175, 320 and 492 ° C as a result of SDA combustion. The ATG y DTG results of the zeolites after the calcination process are presented in Figure S1a and S1b (supplementary information S1), respectively. In all cases a single loss of mass less than 100 °C is observed, which corresponds to the physisorption of water retained in the samples. No other significant weight losses are observed at higher temperature which indicates that the SDA was eliminated.
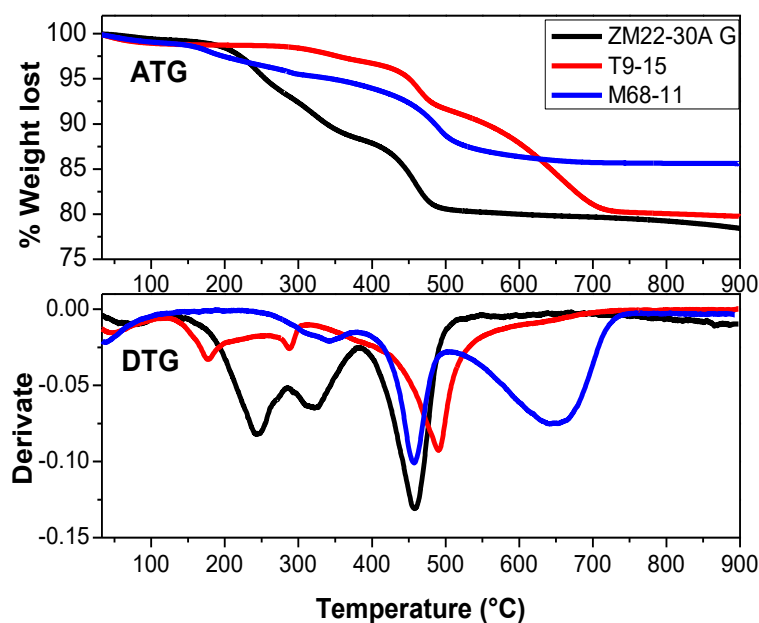


Figure 6. Thermal analysis of three structure zeolitic not calcined: a) ATG and b) DTG
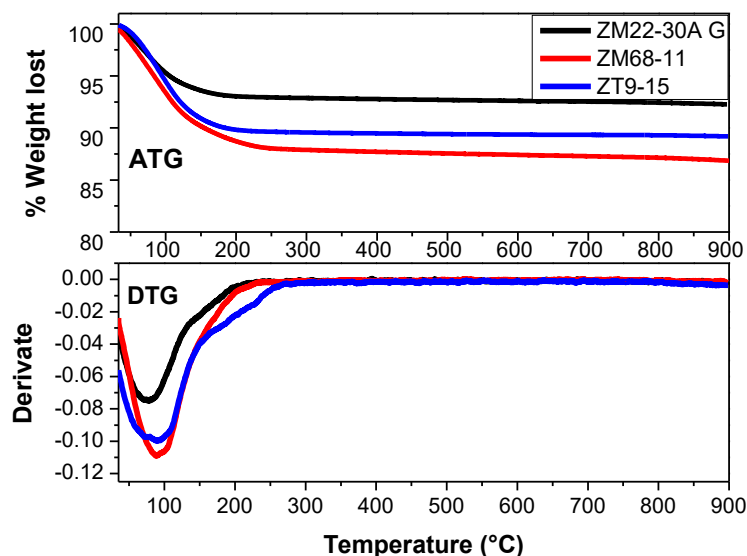
Figure S1. Thermal analysis of the materials calcined a) ATG and b) DTG

### 3.5.     ICP-OES Chemical Composition Analysis

The amount of Si, Al and Zn in the exchanged zeolites of the calcined samples were determined by ICP-OES analysis (Table 3). It is observed that the incorporation of Zn is efficient both by ion exchange and in the synthesis gel. The concentration of Zn was found to be close to 1% wt in all zeolites modified with Zn both by ion exchange and in synthesis gel. The relation Si/Al to real was measured in all the catalysts, being less than the theoretical in all calcined samples, which suggests that the exchange treatment and subsequent calcination to some extent anneals structural defects and incorporates a part of the extra-framework Al species ($Al_{EF}$) in the framework again.

Table 3. Chemical composition (wt%) determined by ICP-OES of samples.

| Catalyst | Theorical Si/Al ratio | % wt | | | Real Si/Al ratio |
|---|---|---|---|---|---|
| | | % Si | % Al | % Zn | |
| M22-30A | 30 | 36.67 | 1.20 | - | 29.65 |
| M22-30S | 30 | 35.92 | 1.56 | - | 22.13 |
| ZM22-30S | 30 | 41.08 | 1.33 | 0.74 | 29.78 |
| ZM22-30A-G | 30 | 36.48 | 1.52 | 1.20 | 23.07 |
| M22-50A | 50 | 39.45 | 0.72 | - | 52.81 |
| M22-50S | 50 | 39.22 | 0.90 | - | 42.06 |
| M68-11 | 11 | 34.23 | 4.02 | - | 8.12 |
| ZM68-11 | 11 | 32.88 | 4.61 | 1.11 | 6.85 |
| T9-15 | 15 | 32.92 | 3.72 | - | 8.48 |
| ZT9-15 | 15 | 33.07 | 3.92 | 1.33 | 8.11 |
| T9 0.5 Zn | 15 | 31.17 | 3.02 | 2.11 | 10 |
| T9 0.2 Zn | 15 | 29.31 | 4.22 | 1.53 | 6.66 |
| T9-30 | 30 | 38.07 | 1.72 | - | 21.28 |
| ZT9-30 | 30 | 36.75 | 1.22 | 1.76 | 28.95 |
| T9-50 | 50 | 37.54 | 0.73 | - | 49.51 |
| ZT9-50 | 50 | 38.54 | 0.79 | 0.25 | 47.01 |

3.6.    Temperature-programmed desorption (NH$_3$-TPD)

The acidic properties of the three zeolite structures modified with Zn were determined by NH$_3$-TPD technique, as presented in Figure 7a. The spectra of all samples exhibit two peaks characteristic throughout the temperature range in all zeolites. The low-temperature (LT) region of 200–300 °C and the high temperature (HT) region of 400–500 °C, which are attributed to the NH$_3$ adsorbed on the acidic hydroxide group Si–OH–Al situated in the framework of zeolite [30]. The TPD profile of ZM22-30A-G (black line) is characterized by one broad and asymmetric desorption peak with maxima in the temperature region 340-350 °C, assignable to NH$_3$ desorption from strong acid sites [31]. ZT9-15 (red line) shows a peak centered at a temperature of 270 °C and another shoulder with a maximum at approximately 365 ° C, the first peak was noted as HL and the second with HT, low and high acidity, respectively. Finally, ZM68-11 zeolite (blue line) presented an intense peak at a temperature of 275 °C, corresponding to weak acidity.

center appeared. These Zn sites can performance as strong sites to catalyze the reaction and obtain high aromatic selectivity. Traditionally, the HT peak is attributed to $NH_3$ desorption from strong Brønsted and Lewis acid sites, which are associated with the $Al_F$ (framework Al) atoms and are of catalytic importance [36].
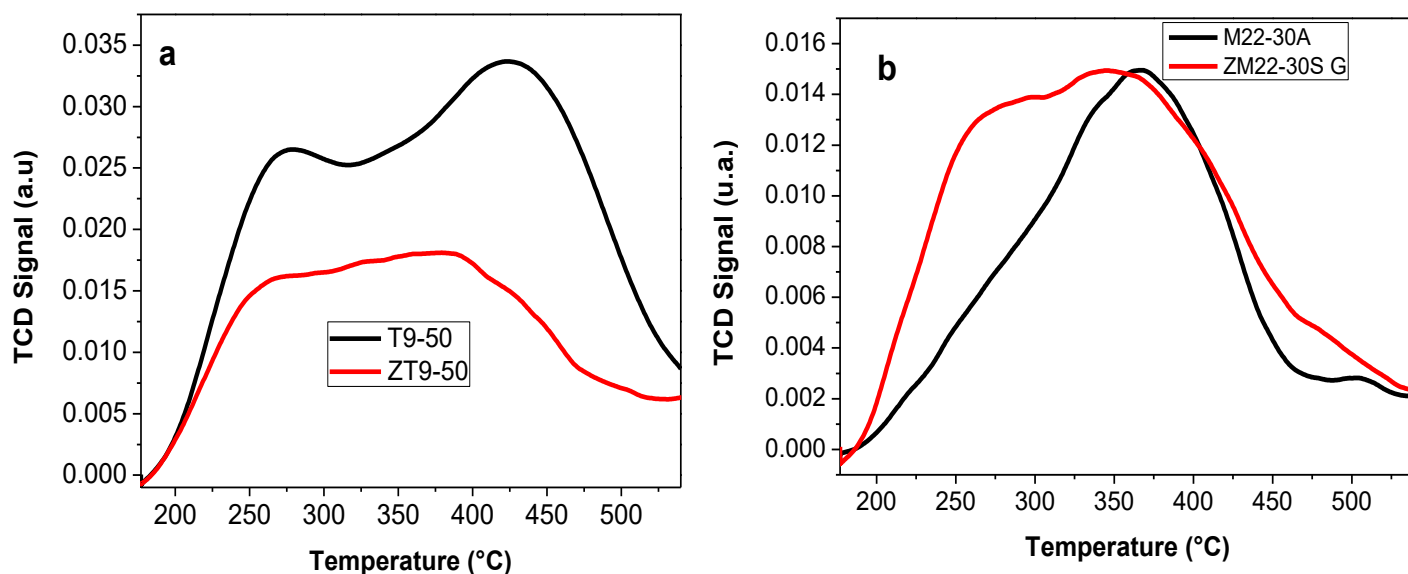
Figure S2. $NH_3$-TPD profiles of a) TNU-9 (Si/Al 50) zeolites and b) M22-30A modified

The specific peak area is proportional to the number of acid sites in the sample and can be determined by integration by convolution of the area under the curve of the spectra. The amounts of strong and weak acid sites are listed in Table 4. The acid site density increased in the order MCM-68 <TNU-9 <MCM-22.

Table 4. Acidity properties of materials

| Catalyst | Acidity ($\mu$mol NH$_3$/g) | | |
|---|---|---|---|
| | Weak acid (LT) | Strong acid (HT) | Total |
| M22-30A | 5134 | - | 5134 |
| M22-30S | 4918 | - | 4918 |
| ZM22-30AG | 6834 | - | 6834 |
| M22-50A | 5692 | - | 5692 |
| M22-50S | 6975 | | 6975 |
| ZM68-11 | 14549 | - | 14549 |
| T9-15 | 7929 | - | 7929 |
| ZT9-15 | 9978 | - | 9978 |
| T9 0.5 Zn | 9531 | - | 9531 |
| T9 0.2 Zn | 13388 | - | 13388 |
| T9-30 | 8983 | - | 8983 |
| ZT9-30 | 1729 | 4595 | 6324 |
| T9-50 | 8162 | - | 8162 |
| ZT9-50 | 3235 | 6184 | 9419 |

3.7.    Solid state NMR spectroscopy ($^{27}$Al and $^{29}$Si MAS NMR)

Figure 8a shows the $^{27}$Al MAS NMR spectra of M22-30A, M22-30A 0.01 Zn-G, and ZnM22-30A. Figure shows two peaks at 54 ppm and 0 ppm, corresponding to tetrahedral Al (Al$_F$) entering the zeolite framework and extra-framework octahedral Al atoms (Al$_{EF}$), respectively.  The small shoulder around 56 ppm is attributed to the Al species located at crystallographically different T sites [37]. However, the peaks intensity of Al$_{EF}$ y Al$_F$ decreased slightly due incorporation of Zn. That result demonstrate that the Zn cations could cover Al sites in octahedral and tetrahedral positions.

Figure 8b shows the $^{27}$Al MAS NMR spectra of the acid form of TNU-9 (Si/Al 15) and modified with Zn. The both spectra feature a strong chemical shift at 54 ppm and a weak chemical shift at 0 ppm, corresponding to tetrahedrally coordinated aluminum in the framework and octahedrally coordinated aluminum extra-framework, respectively [38]. The signal at 0 ppm are ascribed to extra-framework aluminum from either cationic aluminum hydroxide species/hydroxylated alumina-like clusters inside the channel structure or as framework defects, where hydroxyl groups and water are partly bonded [39,40]. It

is observed that after the exchange with Zn the peak corresponding to the $Al_{EF}$ decreases, which indicates that the Zn could occupy sites in octahedral positions of the Al. This indicates $AL_{EF}$ sites are incorporated into the framework structure and that defect sites are annealed by the ion exchange treatment, since the amounts of octahedral Al is reduced [39].
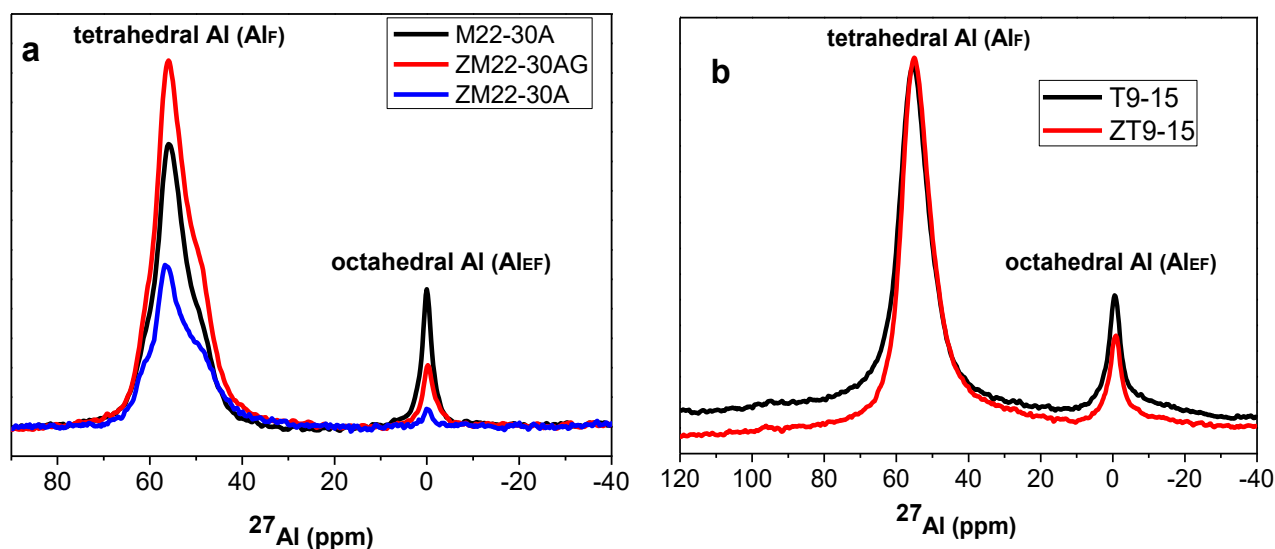


Figure 8. $^{27}$Al MAS NMR spectra of (a) MCM-22 modified (Si/Al 30) materials and (b) acid and Zn-modified TNU-9 zeolite (Si/Al 15)

The $^{29}$Si MAS-NMR spectra of MCM-22 structure and modified samples are presented in Figure 9a. According to the literature, in the MCM-22 framework there are 8 crystallographically non-equivalent T-atoms [33] giving equal number of $^{29}$Si MAS-NMR resonances. The Q4 environments (that is, T(TO)$_4$ groups) resonant at ca. −105, −110, −111, −112, −114, −115 and −119.5 ppm, while the Q3 sites (that is, T(TO)$_3$(OH) groups) give peaks at −104 and −100 ppm [24, 40-42].
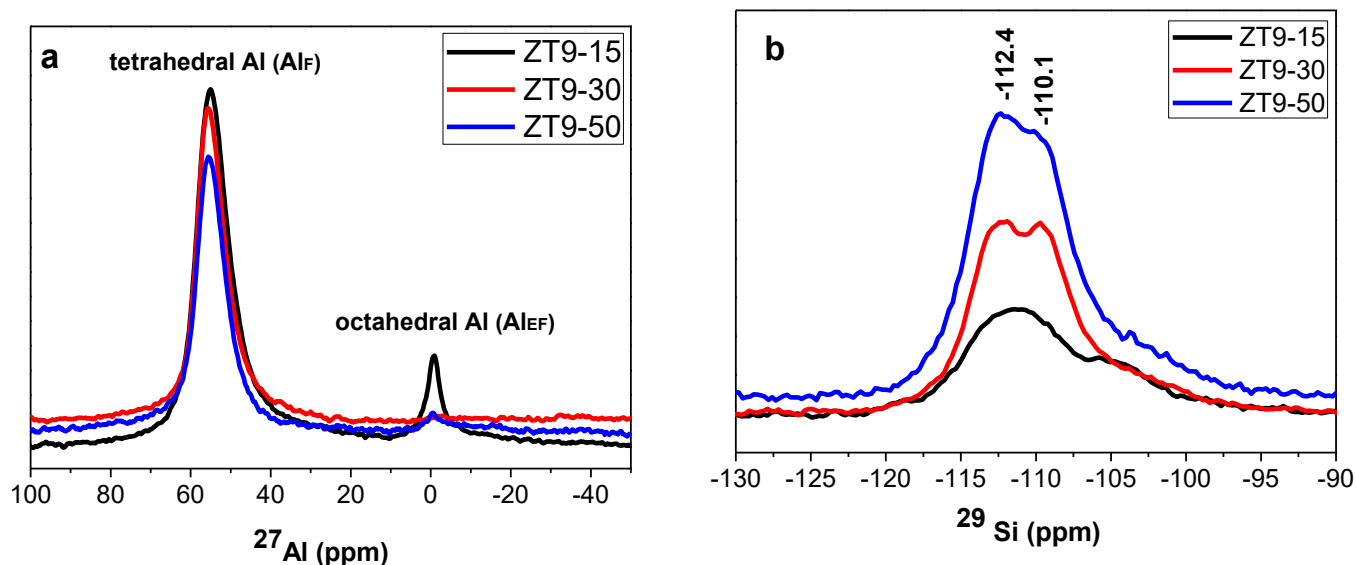
Figure S3. a) $^{27}$Al MAS NMR spectra of modified-Zn TNU-9 materials and (b) $^{29}$Si MAS NMR spectra of modified-Zn TNU-9 materials

## 3.8. Catalytic Evaluation

From literature it is known that catalyst stability in the MTA reaction is also influenced by acid site density, crystal size and acid site strength [44]. The catalytic activity and selectivity of T9-15 and ZT9-15 samples are shown in Figure 10a y 10b, with conditions of 400 °C, WHSV 4.24 h$^{-1}$ and 0.5 g of catalysts. The introduction of zinc species as well as the synthesis method exhibits a significant influence on the catalyst lifetime, methanol conversion, and product distribution. Both catalysts showed high conversion initial at 400 °C (Figure 9a), full conversion of oxygenates (both methanol and intermediate dimethylether, DME) was obtained, however, the clear distinction into both of stabilities, with ZT9-15 deactivating rapidly after 5h of reaction and T9-15 deactivating slowly, only correlates with the presence of Zn and the formation new acid sites produced by divalent metal. The 3D channel system with cavity structure allows TNU-9 to better generate, accommodate and diffuse of aromatics in the reaction. The presence of cavities in TNU-9 can accommodate more Zn species in the channels associated to Brønsted acid sites [45,46]. Selectivity to short chain olefins (C2 to C4) reached a nearly constant level close to 40% after until 5 h on stream (Figure 9b). The selectivity to total aromatics improved significantly with the incorporation of Zn into the ZT9-15 zeolite during the 5 h reaction.

mainly C9-C12 (aromatics with carbon number nine and higher). Heavy aromatics act as coke precursors, thus, their formation should be limited. The MCM-22 zeolite has a 10-ring system, so that the reaction proceeds higher olefins and paraffins selectivity and lower aromatics selectivity (20.05 %), this due to the peculiar pore structure of MCM-22 zeolite (10 and 12 MR channels). This result indicates that the cavity size of 3D 10-ring zeolites is of primary importance for their stability as MTH catalysts. It should be noted that, when considering the pore size of TNU-9 have clearly larger channels than the other topologies. The 3D channel system with cavity structure allows TNU-9 to better generate, accommodate and diffuse of aromatics in the reaction. In addition, we have also found that the presence of supercage favors the diffusion and migration of Zn species into the channels associated to Brønsted acid sites and improves activity and stability in MTH process. The selectivity total aromatics over several catalysts under this study, followed the order: ZM68-11 > ZT9-15 > ZM22-30A.

Table 5. Distribution of reaction products of different structures in the conversion of methanol. Conditions: TOS 1 h, WHSV 4.24 h$^{-1}$, 400 °C

| Catalyst | ZT9-15 | ZM68-11 | ZM22-30A |
|---|---|---|---|
| Methanol conversion (mol %) | 99.70 | 90.36 | 99.27 |
| Selectivity to products (% mol) | | | |
| Olefins $C_2$-$C_4$ | 29.09 | 25.76 | 26.64 |
| Paraffins + olefins $C_5^+$ | 42.19 | 41.87 | 53.31 |
| Bencene | 0.18 | 0.07 | 0.03 |
| Toluene | 1.46 | 0.06 | 0.57 |
| Xilenes | 5.23 | 0.24 | 2.28 |
| **Total aromatics** | **28.72** | **32.36** | **20.05** |
| **BTX total** | **6.87** | **0.37** | **2.88** |

3.8.2. Effects of temperature on the catalytic performance of Zn/TNU-9 catalysts

The effect of temperature reaction on the catalytic performance of T9-15 0.5 Zn modified-Zn catalysts is shown in Figure 11a and b. It is observed that the temperature affects the useful life of the catalyst, as the reaction temperature increases the catalyst tends to deactivate. When increasing the temperature reaction, the conversion of methanol decreased after 5 h at 425 and 450 °C. At 400 °C, the conversion is constant during 9 h of reaction, in the opposite case at 450 ° C, where the conversion decreased to 20% after 8 h of reaction, indicating catalyst deactivation. These results suggest that the catalyst did not display perfect

catalytic stability in methanol reaction to 450 °C. A high temperature more carbonaceous deposits were formed, and the coke can cover the active sites, which may induce a short lifetime of the catalyst. However, with an increase of the reaction temperature, the selectivity to BTX increased at initial time (figure 11b). These results suggest that an increase in the reaction temperature, specifically at 450 °C, favored the aromatization of methanol, however, to higher reaction temperature suppressed dehydrocyclization and promoted the formation of coke from a secondary reaction [49], indicating that the cokes on the T9-15 0.5 Zn probably do not cover the active sites and the channels for the reactants and BTX products are not blocked to a low temperature. In addition to temperature, particle size and particle density and kind of active sites on the crystallite surface will be of influence on catalyst lifetime [49,50].

On other hand, comparison of the T9-15 catalysts with the ratio $ZnO/ZnO+Al_2O_3$ equal to 0.34 and 0.16 were made at 400 °C and WHSV of 4.24 $h^{-1}$ were realized. The first one (T9-15 0.5 Zn) showed better stability with conversion of methanol completes during 9 h of reaction. T9-15 0.2 Zn catalyst presented lower conversion of methanol after 9 h, around 80 % mol. Also, this last catalyst showed better BTX selectivity (17 %) at short reaction times (black line), T9-15 0.2 Zn (red line) presented a lower BTX selectivity (around 5 % during all the reaction). It the higher BTX selectivity over the T9-15 0.5 Zn catalyst is perhaps related to its distinctive channel systems, which can accommodate more Zn species in the zeolite channels associated to Brønsted acid sites. This suggests the highly dispersed nature of its zinc particles. The BTX formation over H-TNU-9 would occur mainly inside the two types of 10-ring channels along [010] rather than inside its large 12-ring cavities [17,48].
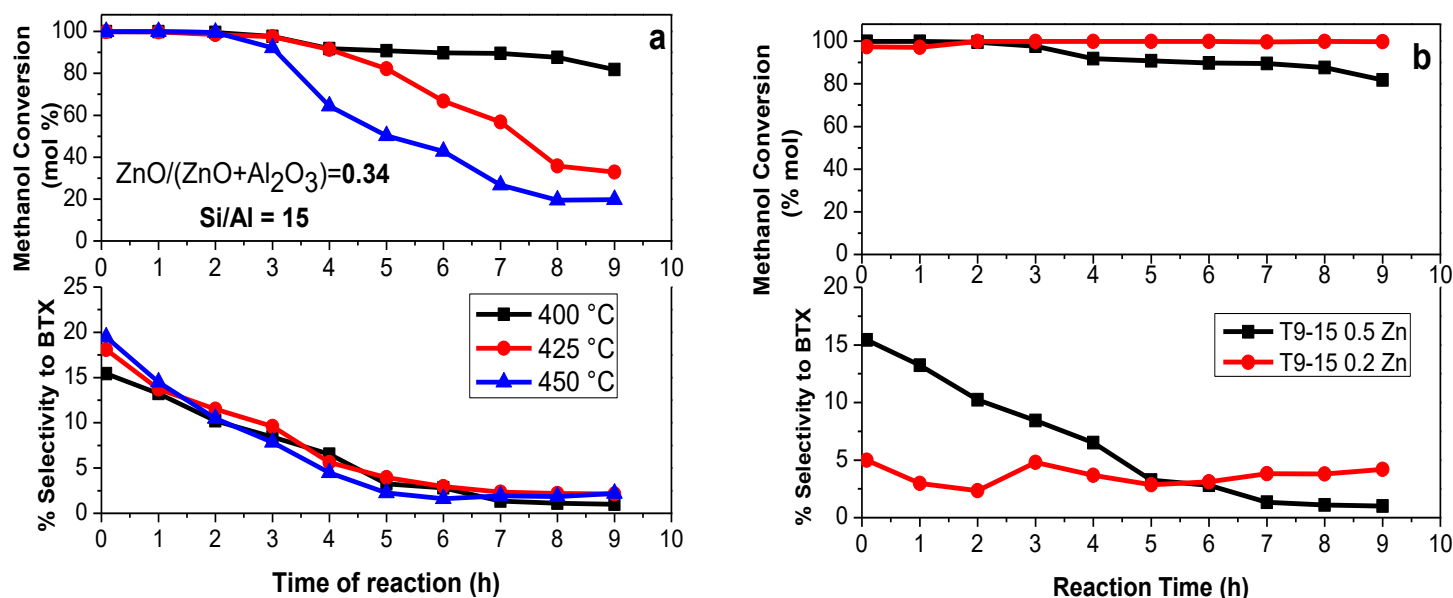
Figure 11. a) Methanol conversion and Selectivity to BTX with T9-15 0.5 Zn to 400, 425 and 450 °C b) Comparation selectivity to compounds vs. reaction time obtained with T9-15 and ZT9-15 catalysts. Test conditions: T = 400 °C, WHSV = 4.24 $h^{-1}$, 0.5 g of catalyst.

Figure 12a and 12b show the effects of the reaction temperature of T9-30 and ZT9-30 with a WHSV 4.24 h-$^1$, respectively. Figure 12a shows that the methanol was nearly completely converted to 400 and 425 °C until 5 h of reaction, decreasing to 85 % in both cases. The conversion of methanol decreased to 80 % after 5 h of reaction to 450 °C, however, total aromatics selectivity increased to short reaction time (80 %) and subsequently decreased after 5 h to reaction. So, at 450 °C the acid sites are activated in the MTA reaction. In contrast, the acid zeolite had a low selectivity to total aromatics to short time at three temperatures compared to the zeolite exchanged with Zn.
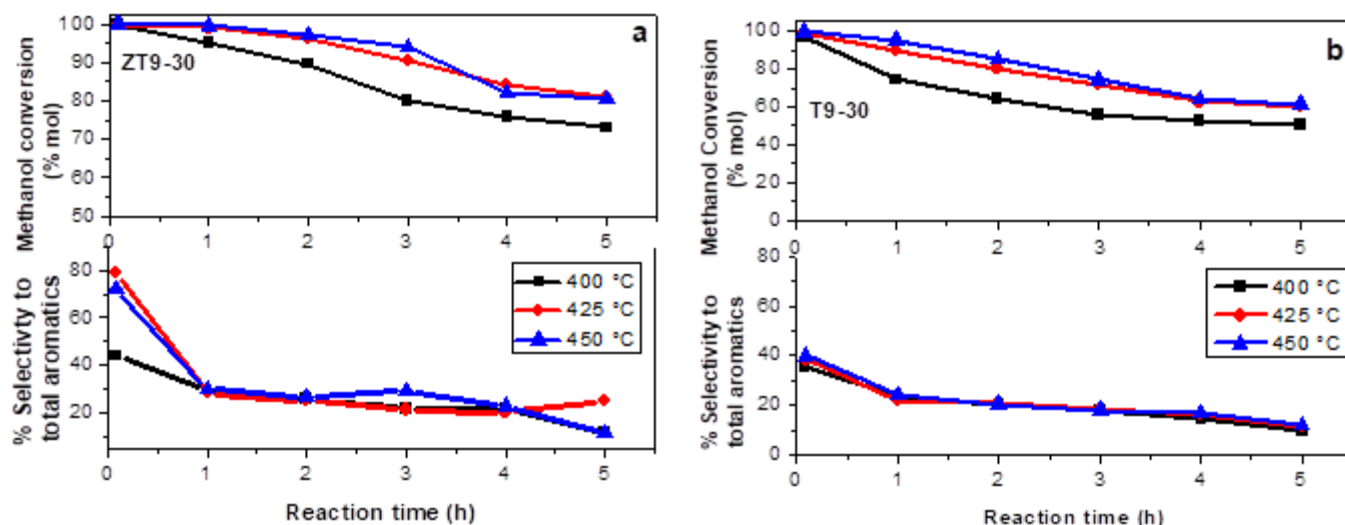
Figure 12. Methanol conversion and selectivity to total aromatics vs time of a) ZT9-30 and b) ZT9-30 (acid zeolite) to different temperature 400, 425 and 450 °C Test conditions: WHSV = 4.24 h$^{-1}$, 0.5 g of catalyst.

### 3.8.3. Effect of Zn incorporation method on TNU-9 catalysts

In this work the Zn has been incorporated to the zeolite by synthesis or by ion-exchange, as detailed in the experimental part. In a previous study, we have demonstrated that the impregnation method, commonly used to incorporate different cations or metals to catalysts, was not effective to improve the stability of Zn-modified catalysts for MTH [10]. These catalysts suffer a rapid deactivation probably because during the impregnation process an accumulation of a small amount of nanometric ZnO clusters occurs in the channels of zeolite, avoiding the aromatics diffusion and accelerating the catalyst deactivation due to coke deposition. In addition, the selectivity to aromatic compounds was considerably lower. The results of the conversion of methanol with different TNU-9 catalysts modified-Zn to 400 °C are presented in Table 6. In this study, the BTX selectivity at 1 h of reaction increased in the order T9-15 0.5 Zn > ZT9-15 T9-15 > T9-15 0.2 Zn, which is also in agreement with the observed relative stability. The least active and selective was TNU-9 acid zeolite providing the Si(OH)Al groups of the highest strength but accommodating the largest cavities on the intersection of 10-ring channels with lower selectivity BTX and total aromatics, 3.77 and 16.82 %, respectively [51]. HT9 0.5 Zn zeolite was the better catalyst for total aromatics and BTX

selectivity (12.58 %) due high acid density and high account of Zn, which is an aromatizing agent. This suggests that most of the acid sites in the proton form originates from the presence of both Al and Zn in framework positions using ratio $ZnO/ZnO+Al_2O_3$ equal to 0.34. In our work demonstrated that activity of Zn-modified TNU-9 zeolites in the MTA reaction improves by prepared using ratio $ZnO/ZnO+Al_2O_3$ of 0.34 (T9-15 0.5 Zn) and demonstrated significantly higher selectivity for aromatics compared with acid zeolite.

Table 6. Distribution of reaction products of HTNU-9 materials modified-Zn (Si/Al 15) in the conversion of methanol.
Conditions: TOS 1 h, WHSV 4.24 h$^{-1}$, 400 °C

| Catalyst | T9-15 | ZT9-15 | T9 0.5 Zn | T9 0.2 Zn |
|---|---|---|---|---|
| Methanol conversion (mol %) | 99.70 | 89.37 | 99.85 | 81.09 |
| Selectivity to products (% mol) | | | | |
| Olefins $C_2$-$C_4$ | 39.83 | 29.09 | 28.30 | 18.95 |
| Paraffins + olefins $C_5^+$ | 43.36 | 42.19 | 36.82 | 50.59 |
| Bencene | 0.06 | 0.18 | 0.73 | 0.10 |
| Toluene | 0.47 | 1.46 | 4.13 | 0.64 |
| Xilenes | 3.24 | 5.23 | 7.72 | 2.24 |
| **Total aromatics** | **16.82** | **28.72** | **34.88** | **30.56** |
| **BTX fraction** | **3.77** | **6.87** | **12.58** | **2.98** |

On the other hand, the incorporation of zinc species by ion exchanging (ZM22-30S-G) and synthesis gel (ZM22-30S) in MCM-22 zeolite has high influence on the catalytic stability methanol conversion, and products distribution to 400 °C (Figure S4a and S4b). The first one showed lower methanol conversion after 5 h of reaction (20 %), the exchanged zeolite presented better conversion of methanol values, 80 % mol during of 5 h of reaction. Which is usually associated with diffusion limitations of heavy products by the formation of large Zn species formed in the micropores [52].

However, the incorporation of zinc by ion exchange increases the formation of aromatic compounds (blue line) obtaining selectivity around 20 and 30 % during the reaction, contrary case ZM22-30S-G, which presented selectivity less than 20 %. In addition, the selectivity of light olefins and paraffins were showed, which were not modified with the incorporation of Zn in the zeolites.
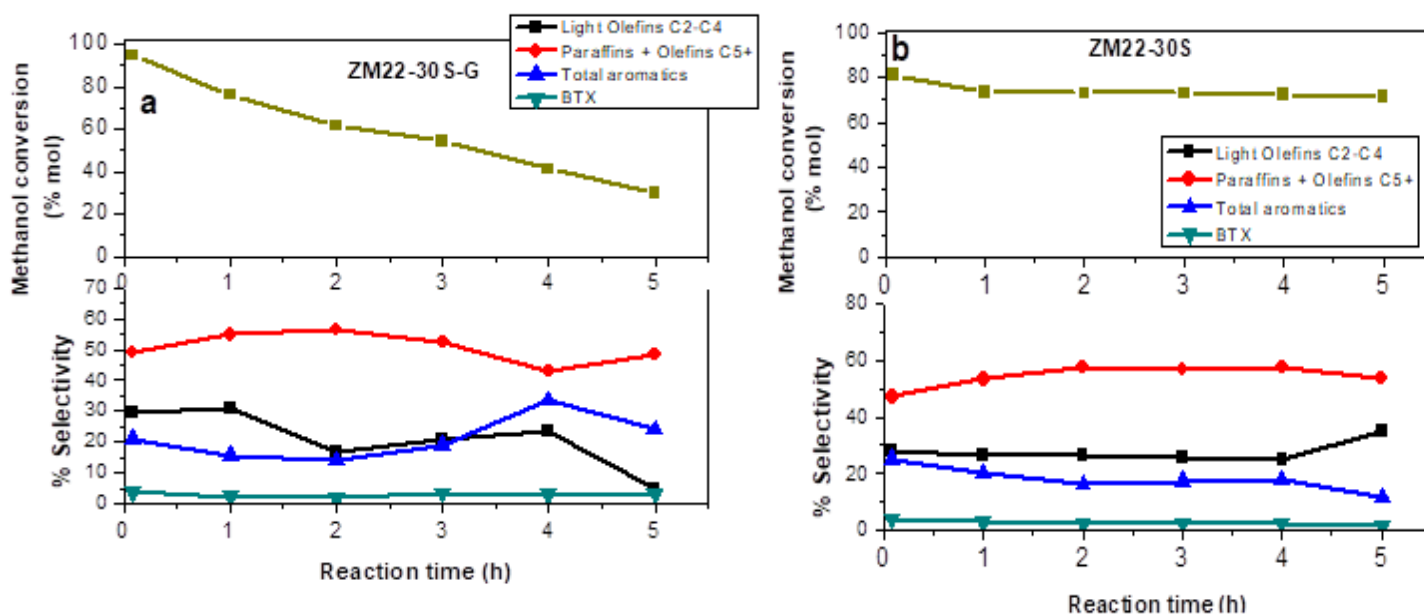
S4)



Figure S4. Incorporation form of Zn effect. Methanol conversion (% mol) and selectivity to total compounds vs time of a) ZM22-30-S-G and b) ZM22-30S. Test conditions: T= 400 °C, WHSV = 4.24 h-1, 0.5 g of catalyst

### 3.8.4. Effects of the morphology on the MCM-22 catalysts

From literature it is known that catalyst stability in the MTH reaction is also influenced by acid site density and this case the crystal size. The conversion of methanol and the distribution of reaction products of the MCM-22 zeolite with different synthesis conditions (agitation and static) and therefore with different morphology are shown in Figures 13a and 13b, respectively. The M22-30S zeolite showed higher conversion levels compared to the M22-30A zeolite due under static conditions (M22-30S) smaller particles (1.5 µm) are obtained, in contrast to static conditions when obtaining larger particles (about 7 µm) as observed by SEM. The generation of smaller crystals influences the optimization of the acid properties of zeolite to enhance the catalytic activity making shortens the length of diffusion of molecules [53,54]. In terms of selectivity, the zeolites were selective for obtaining light olefins and paraffins, this corresponds to what was reported by several researchers and low acidity measured by TPD-NH$_3$. Min and coworkers [55] found that contribution of supercages and their sinusoidal 10-ring channels are responsible for the high activity in the MTO reaction. Zhang and coworkers [56] also mention the light olefins selectivity seems to be related to the amounts of Brønsted acid sites present in the MCM-22 zeolite. Similarly, the selectivity to

olefins and paraffins benefits from the presence of smaller size such as zeolite M22-30A. In our work, improved aromatization of methanol results was observed when converting methanol using three zeolites Zn-modified compared to other works previously studied by other authors [44,56,57] and all gave good MTA ability but the BTX selectivity less than those obtained by us. Additionally, zeolite TNU-9 has been poorly studied in this reaction.
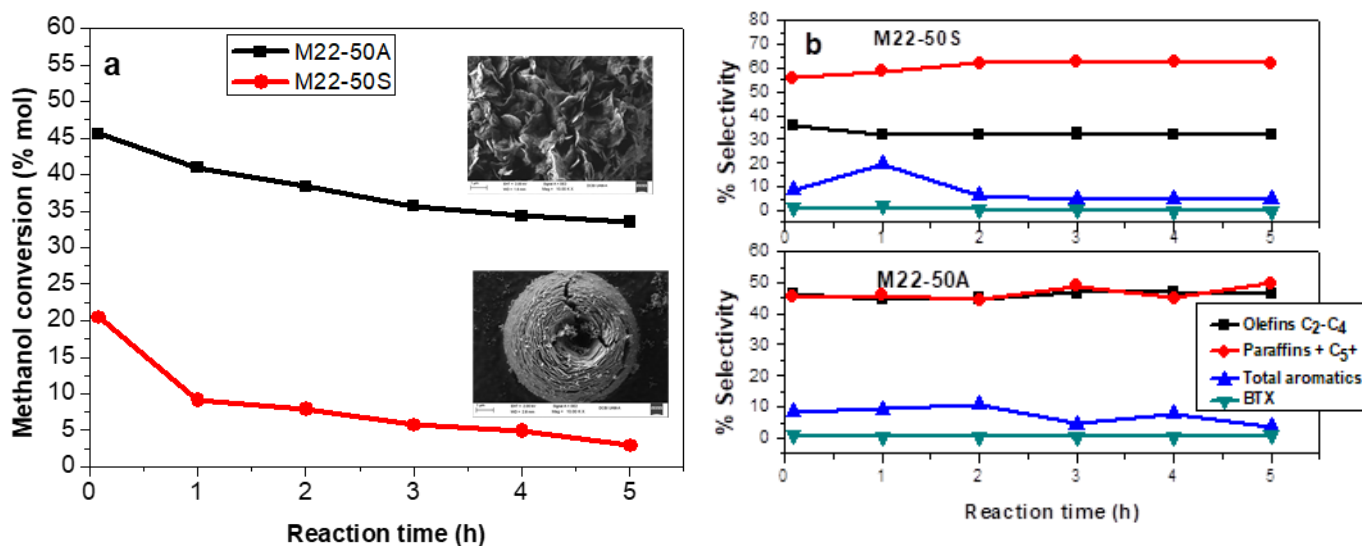


Figure 13. Morphology effect in catalytic activity a) Methanol conversion (% mol) M22-50A (agitation condition) and M22-50S (static condition) b) Selectivity to total compounds vs time. Test conditions: T= 400 °C, WHSV = 4.24 $h^{-1}$, 0.5 g of catalyst.

## 4. Conclusions

TNU-9, MCM-22 and MCM-68 are all active for the conversion of methanol at different temperatures, however, the distribution of reaction products was different for each zeolite. MTH reaction is also influenced by acid site density, crystal size and acid site strength. TNU-9 zeolite is an active catalyst for the studied reactions related to BTX aromatics, comparable to other zeolites studied in this work, mainly due to its acidic and topological characteristics. The Zn incorporation had influences on the textural properties, morphology, acidic properties and catalytic performances for all zeolites. T9-15 0.5 Zn zeolite showed a high content of total aromatics and therefore high selectivity to the BTX fraction. The BTX

selectivity was effectively improved by introduction of Zn species by ion exchange in the case of ZT9-30 zeolite, due to a greater distribution of strong acid sites, the generation of strong acid sites were the active sites for the conversion of methanol to aromatics. The reaction temperature has great influence on the catalytic activity in ZT9-30 zeolite, at 450 °C the best BTX selectivity is obtained, however, the catalyst is deactivated after 9 h of reaction. The crystal size parameter to affect the catalyst lifetime of the three topologies studied. In methanol conversion, the selectivity to aromatics over the T9-15 (Si/Al 15) zeolite catalysts under study, follow the order: T9-15 0.5 Zn > ZT9-15 T9-15 > T9-15 0.2 Zn. T9-15 catalysts with the ratio $ZnO/ZnO+Al_2O_3$ equal to 0.34 (T9-15 0.5 Zn) at 400 °C and WHSV of 4.24 $h^{-1}$ presented the best total aromatic selectivity (32 %) at 1 h of reaction. In terms of zeolite topology, aromatic selectivity increased in the following order. ZM68-11 > ZT9-15 > ZM22-30, however, MCM-68 zeolite modified-Zn produced mainly heavy aromatics, due to its high acidity and the space of its super-cages of up to 18 members. Finally, MCM-22 zeolites, regardless of morphology, were selective for obtaining light olefins and paraffins, due to its structure formed by supercages and their sinusoidal 10-ring channels, as well as its low acidity.

The different between the three tested topologies with respect to products selectivities and methanol conversion is a clear evidence of the importance of the channel dimensions in the MTH reaction. The zeolite MCM-68 presented a generation of heavy hydrocarbons (C9-C12) which were responsible for the generation of coke causing the rapid deactivation of the catalyst due to 12-member and clearly channels larger channels than the other topologies. The unique pore architecture and strong acid of zeolite TNU-9, with 10-ring channel systems, being slightly larger zeolite compared with MCM-22, can offer new opportunities for methanol conversion.

**Acknowledgment**

**Ethical statement**

All authors contributed to the study conception and design. Material preparation, data collection and analysis were performed by Dora A. Solís Casados, Julia Aguilar Pliego, Carlos Márquez Álvarez, Enrique Sastre de Andrés, Diana Sanjurjo Tartalo, Raquel Sáinz Vaque and Marisol Grande Casas. The first draft of the manuscript was written by PhD student, Misael Garcia Ruiz and all authors commented on previous versions of the manuscript. All authors read and approved the final manuscript.

We considerate the submitted is original and unique work and it has not been submitted to another journal simultaneity.

The work is single study and it's not up into several parts and results are presented clearly, honestly, and without, falsification or inappropriate the data manipulation, the study submitted is part of my doctoral thesis.

Conflict of Interest: The authors declare that they have no conflict of interest.

This work does not contain any studies with human participants or animals performed by any of the authors.

Finally, additional informed consent was obtained from all individual participants for whom identifying information is included in this chapter

As a student of PhD, conducting research and publishing my work is essential to my professional development and the advancement of my postgraduate studies.

# References

[1] Zhu, X (2015) Hierarchical zeolites as catalysts for methanol conversion reactions. Eindhoven: Technische Universiteit Eindhoven.

[2] Blomsma E, Martens JA, Jacobs PA (1997) Isomerization and Hydrocracking of Heptane over Bimetallic Bifunctional PtPd/H-Beta and PtPd/USY Zeolite Catalysts. J Catal 165(2) :241-248

[3] Fraenkel D, Cherniavsky M, Ittah B, Levy M (1986) Shape-selective alkylation of naphthalene and methylnaphthalene with methanol over H-ZSM-5 zeolite catalysts. J Catal 101, 2: 273-283

[4] Zhang GQ, Bai T, Chen TF, Fan WT, Zhang X (2014) Conversion of Methanol to Light Aromatics on Zn-Modified Nano-HZSM-5 Zeolite Catalysts. Ind. Eng. Chem. Res. 53: 14932−14940

[5] Zhang J, Qian W, Kong C, Wei F (2015) Increasing para-Xylene Selectivity in Making Aromatics from Methanol with a Surface-Modified Zn/P/ZSM-5 Catalyst. ACS Catal. 5(5): 2982–2988

[6] Wang T, Tang X, Huang X, Qian W, Cui Y, Hui X, Yang W, Wei F (2014) Conversion of methanol to aromatics in fluidized bed reactor. Catal Today 233: 8–13

[7] Baliban RC, Elia JA, Floudas CA (2013) Biomass to liquid transportation fuels (BTL) systems: process synthesis and global optimization framework, Energy Environ. Sci. 6: 267–287

[8] Appelt J, Heschel W, Meyer B (2016) Catalytic pyrolysis of central German lignite in a semi-continuous rotary kiln—performance of pulverized one-way ZSM-5 catalyst and ZSM-5-coated beads. Fuel Process. Technol. 144: 56–63

[9] Bjørgen M, Joensen F, Holm MS, Olsbye U, Lillerud KP, Svelle S (2008) Methanol to gasoline over zeolite H-ZSM-5: improved catalyst performance by treatment with NaOH. Appl. Catal. A Gen. 345: 43–50

[10] Garcia-Ruiz M, Solis-Casados DA, Aguilar-Pliego J, Márquez-Álvarez C, Sastre de Andrés E, Sanjurjo-Tartalo D, Sainz-Vaque R, Grande-Casas M (2020) ZSM-5 zeolites modified with Zn and their effect on the crystal size in the conversion of methanol to light aromatics (MTA). https://doi.org/10.1007/s11144-019-01716-4

[11] Yubing X, Puyu Q, Xinping D, Haiqiang L, Youzhu Y (2013) Enhanced Performance of Zn–Sn/HZSM-5 Catalyst for the Conversion of Methanol to Aromatics. Catal Lett. 143: 798–806

[12] Gabrienko AA, Arzumanov SS, Toktarev AV, Danilova IG, Prosvirin IP, Kriventsov VV, Zaikovskii VI, Freude D, Stepanov AG (2017) Different Efficiency of $Zn^{2+}$ and ZnO Species for Methane Activation on Zn-Modified Zeolite. ACS Catal. 7(3): 1-45

[13] Ma D, Shu Y, Han X, Liu X, Xu Y, Bao X (2001) Mo/HMCM-22 Catalysts for Methane Dehydroaromatization: A Multinuclear MAS NMR Study. J. Phys. Chem. B. 105: 1786-1793

[14] Dorset DL, Weston SC, Dhingra SS (2006) Crystal Structure of Zeolite MCM-68: A New Three-Dimensional Framework with Large Pores. J. Phys. Chem. B 110: 2045-2050

[15] Ni Y, Sun A, Wu X, Hai G, Hu J, Li T, Li G (2011) The preparation of nano-sized H[Zn, Al]ZSM-5 zeolite and its application in the aromatization of methanol Micropor Mesopor Mater 143: 435–442

[16] Hong SB, Lear EG, Wright PA, Zhou W, Cox PA, Shin CH, Park JH, Nam IS (2004) Synthesis, Structure Solution, Characterization, and Catalytic Properties of TNU-10: A High-Silica Zeolite with the STI Topology. J. Am. Chem. Soc. 126: 5817-5826

[17] Hong SB, Nam IS, Min HK, Shin CH, Warrender SJ, Wright PA, Cox PA, Gramm F, Baerlocher Ch, McCusker LB, Liu Z, Ohsuna T, Terasaki O (2007) TNU-9: a novel medium-pore zeolite with 24 topologically distinct tetrahedral sites. Zeolites to Porous MOF Materials – the 40th Anniversary of International Zeolite Conference

[18] Zhang L, Wang H, Liu G, Gao K, Wu J (2016) Methanol-to-olefin conversion over H-MCM-22 catalyst. Journal of Molecular Catalysis A: Chemical 411: 311–316

[19] Wu Y, Ren X, Lu Y, Wang J (2008) Crystallization and morphology of zeolite MCM-22 influenced by various conditions in the static hydrothermal synthesis. Micropor Mesopor Mater 112: 138–146

[20] Hao H, Chang Y, Yu W, Lou LL, Liu S (2018) Hierarchical porous MCM-68 zeolites: Synthesis, characterization and catalytic performance in m-xylene isomerization. Micropor Mesopor Mater 263: 135–141

[21] Calabro JC, Cheng RA, Crane Jr, Kresge CT, Dhingra SS, M.A. Steckel MA, Stern DL. Weston SC, U. S. Patent. 6049018, 2000

[22] Kubu M, Zones SI, Cejka J (2010) TUN, IMF and -SVR Zeolites; Synthesis, Properties and Acidity. Top Catal. 53: 1330–1339

[23] Corma A, Corell C, Pérez-Pariente J (1995) Synthesis and characterization of the MCM-22 zeolite. Zeolites 15(1): 2-8

[24] Delitala C, Alba MD, Becerro AI, Delpiano D, Meloni D, Musu E, Ferino I (2009) Synthesis of MCM-22 zeolites of different Si/Al ratio and their structural, morphological and textural characterization. Micropor Mesopor Mater 118: 1–10

[25] Tian ZR, Voigt JA, Liu J, Mckenzie B, Mcdermott MJ, Rodriguez MA, Konishi H, Xu H (2003) Complex and oriented ZnO nanostructures. Nat. Mater. 2: 821-826

[26] Li J, Lou LL, Yang Y, Hao H, Liu S (2015) Alkylation of phenol with tert-butyl alcohol over dealuminated HMCM-68 zeolites. Micropor Mesopor Mater 207: 27-32

[27] Hu J, Wu S, Liu H, Ding H, Li Z, Guan J, Kan Q (2014) Effect of mesopore structure of TNU-9 on methane dehydroaromatization. RSC Adv. 4: 26577–26584

[28] Ji Y, Yang H, Yan W (2017) Strategies to Enhance the Catalytic Performance of ZSM-5 Zeolite in Hydrocarbon Cracking: A Review. Catalysts 7 (367): 1-31

[29] Ernst S, Elangovan SP, Gerstner M, Hartmann M, Hecht T, Sauerbeck S (2004) Characterization and catalytic evaluation of zeolite MCM-68. Stud Surf Sci Catal 154: 2861-2868

[30] Su X, Wang G, Bai X, Wu W, Xiao L, Fang Y, Zhang J (2016) Synthesis of nanosized HZSM-5 zeolites isomorphously substituted by gallium and their catalytic performance in the aromatization. Chem. Eng. 293: 365–375

[31] Jung HJ, Park SS, Shin CH, Park YK, Hong SB (2007) Comparative catalytic studies on the conversion of 1-butene and n-butane to isobutene over MCM-22 and ITQ-2 zeolites. J. Catal. 245: 65–74

[32] Topsøe N, Pedersen K, Derouane E (1981) Infrared and temperature-programmed desorption study of the acidic properties of ZSM-5-type zeolites. J. Catal. 70: 41-52

[33] Wu P, Kan Q, Wang X, Wang D, Xing H, Yang P, Wu T (2005) Acidity and catalytic properties for methane conversion of Mo/HZSM-5 catalyst modified by reacting with organometallic complex. Appl. Catal. A-Gen 282: 39-44

[34] Joly JF, Ajot H, Merlen E, Raatz F, Alario F (1991) Parameters affecting the dispersion of the gallium phase of gallium H-MFI aromatization catalysts. Appl. Catal. A-Gen 79: 249-263

[35] Xiaoning W, Zhen Z, Chunming X, Aijun D, Li Z, Guiyuan J (2007) Effects of fight Rare Earth on Acidity and Catalytic Performance of HZSM-5 Zeolite for Catalytic Clacking of Butane to Light Olefins. J. of rare earths 25: 321 - 328

[36] Reddy JK, Motokura K, Koyama T, Miyaji A, Baba T (2012) Effect of morphology and particle size of ZSM-5 on catalytic performance for ethylene conversion and heptane cracking. J. Catal, 289: 53–61.

[37] Kolodziejski W, Zicovich-Wilson C, Corell C, Perez-Pariente J, Corma A (1995) $^{27}$Al and $^{29}$Si MAS NMR Study of Zeolite MCM-22.  J. Phys. Chem. 99(18): 7002–7008

[38] Song YQ, Feng YL, Liu F, Kang CL, Zhou XL, Xu LY, Yu GX (2009) Effect of variations in pore structure and acidity of alkali treated ZSM-5 on the isomerization performance. J. Mol. Catal. A-Chem. 310: 130–137.

[39] Pinilla-Herrero I, Borfecchia E, Holzinger J, Mentz UV, Finn J, Lomachenko KA, Bordiga S, Lamberti C, Berlier G, Olsbye U, Svelle S, Skibsted J, Beato P (2018) High Zn/Al ratios enhance dehydrogenation vs hydrogen transfer reactions of Zn-ZSM-5 catalytic systems in methanol conversion to aromatics. J.Catal. 362: 146–163

[40] Saito H, Inagaki S, Kojima K, Han Q, Yabe T, Ogo S, Kubota Y, Sekine Y (2018) Preferential dealumination of Zn/H-ZSM-5 and its high and stable activity for ethane dehydroaromatization. Appl. Catal. A-Gen. 549: 76–81

[41] Machado V, Rocha J, Carvalho AP, Martins A (2012) Modification of MCM-22 zeolite through sequential post-synthesis treatments. Implications on the acidic and catalytic behavior. Appl. Catal. A-Gen. 445– 446: 329– 338.

[42] Elyassi B, Zhang X, Tsapatsis M (2014) Long-term steam stability of MWW structure zeolites (MCM-22 and ITQ-1). Micropor Mesopor Mater 193: 134–144

[43] Wang P, Huang L, Li J, Dong M, Wang J, Tatsumi T, Fan W (2015) Catalytic properties and deactivation behavior of H-MCM-22 in the conversion of methanol to hydrocarbons. RSC Advances 5: 1-28

[44] Bleken F, Skistad W, Barbera K, Kustova M, Bordiga S, Beato P, Lillerud KP, Svellea S, Olsbye U (2011) Conversion of methanol over 10-ring zeolites with differing volumes at channel intersections: comparison of TNU-9, IM-5, ZSM-11 and ZSM-5. Phys. Chem. Chem. Phys., 13: 2539–2549

[45] Franch-Martí C, Alonso-Escobar C, Jorda JL, Peral I, Hernández-Fenollosa J, Corma A, Palomares AE, Rey F, Guilera G (2012) TNU-9, a new zeolite for the selective catalytic reduction of NO: An in situ X-ray absorption spectroscopy study. J.Catal 295: 22–30

[46] Al-Khattaf S, Ali SA, Aitani MA, Žilková N, Kubicka D, Cejka J (2014) Recent Advances in Reactions of Alkylbenzenes Over Novel Zeolites: The Effects of Zeolite Structure and Morphology. Catal Rev: Sci. Eng. 56: 333–402

[47] Gołąbek K, Tarach KA, Filek U, Góra-Marek K (2018) Ethylene formation by dehydration of ethanol over medium pore zeolites. Spectrochim Acta A 192: 464–472

[48] Liu H, Yang S, Wu S, Shang F, Yu X, Xu C, Guan J, Kan Q (2011) Synthesis of Mo/TNU-9 (TNU-9 Taejon National University No. 9) catalyst and its catalytic performance in methane non-oxidative aromatization. Energy 36: 1582-1589

[49] Zhao YH, Gao TY, Wang YJ, Zhou YJ, Huang GQ (2018) Zinc supported on alkaline activated HZSM-5 for aromatization reaction. React Kinet Mech Cat 125 (2): 1085–1098

[50] Schulz H (2010) "Coking" of zeolites during methanol conversion: Basic reactions of the MTO-, MTP- and MTG processes. Catal. Today 154: 183–194

[51] Gołąbek K, Tarach KA, Filek U, Góra-Marek K (2018) Ethylene formation by dehydration of ethanol over medium pore zeolites. Spectrochim Acta A 192: 464–472

[52] Olsbye U, Svelle S, Bjørgen M, Beato P, Janssens T, Bordiga S, Lillerud K (2012) Conversion of Methanol to Hydrocarbons: How Zeolite Cavity and Pore Size Controls Product Selectivity. Angew Chem Int Ed 51: 2–24

[53] Petushkov A, Yoon S, Larsen SC (2011) Synthesis of hierarchical nanocrystalline ZSM-5 with controlled particle size and mesoporosity. Micropor Mesopor Mat. 137: 92–100

[54] Ji Y, Yang H, Yan W (2017) Strategies to Enhance the Catalytic Performance of ZSM-5 Zeolite in Hydrocarbon Cracking: A Review. Catalysts 7 (367): 1-31

[55] Min KH, Park MB, Hong SB (2010) Methanol-to-olefin conversion over H-MCM-22 and H-ITQ-2 zeolites. J, Catal. 271: 186–194

[56] Zhang L, Wang H, Liu G, Gao K, Wu J (2016) Methanol-to-olefin conversion over H-MCM-22 catalyst. J. Mol. Catal. A-Chem 411: 311–316

## 8.3. Tercer artículo: enviado

**Submission Confirmation** ▶ Recibidos ×

**TOPICS in CATALYSIS (TOCA)** <em@editorialmanager.com>                    11:54 (hace 11 minutos)    ☆    ↩    ⋮

para mí ▾

Dear Dr. García Ruiz,

Thank you for submitting your manuscript,
"Synthesis and characterization of aluminophosphates type-5 and 36 doubly modified with Si and Zn and its catalytic application in the reaction to hydrocarbons reaction (MTH)", to Topics in Catalysis

The submission id is: TOCA-D-20-00017
Please refer to this number in any future correspondence.

During the review process, you can keep track of the status of your manuscript by accessing the journal's web site.

Your username is: Misael García Ruiz
If you forgot your password, you can click the 'Send Login Details' link on the EM Login page at https://www.editorialmanager.com/toca/.

With kind regards,

Journals Editorial Office TOCA
Springer

# Synthesis and characterization of aluminophosphates type-5 and 36 doubly modified with Si and Zn and its catalytic application in the reaction to hydrocarbons reaction (MTH)

Misael García Ruiz*[a], Dora A. Solís Casados[b], Julia Aguilar Pliego[c], Carlos Márquez Álvarez[d], Enrique Sastre de Andrés[d], Diana Sanjurjo Tartalo[d], Manuel Sanchez-Sanchez[d], Marisol Grande Casas[d]

[a] Doctorado en Ciencia de Materiales de la Facultad de Química, Universidad Autónoma del Estado de México, Paseo Colón Esquina Paseo Tollocan S/N, Toluca Estado de México, México, C.P. 50000.

[b] Universidad Autónoma del Estado de México, Centro Conjunto de Investigación en Química Sustentable UAEM-UNAM. Personal Académico Adscrito a la Facultad de Química, UAEMex.

[c] Área de Química Aplicada, Departamento de Ciencias Básicas, UAM-A, San pablo 180, C.P. 02200, Cd de México.

[d] Instituto de Catálisis y Petroleoquímica, CSIC, C/Marie Curie 2, Campus Cantoblanco, 28049 Madrid, España

**Abstract**

This paper presents a study of the synthesis of $AlPO_4$-5 and $AlPO_4$-36 materials doubly substituted by Si and Zn, as acid function and aromatizing function, respectively. The physicochemical properties of the zeotypes were studied by XRD, adsorption of $N_2$, temperature desorption programmed at $NH_3$, $^{31}P$ MAS NMR and SEM. The incorporation of Zn and Si has shown an important effect on the acidic, textural and morphological properties of the samples. The particle size has a significant effect on the catalytic activity in the reaction of methanol to hydrocarbons (MTH) in terms of methanol conversion and selectivity. It was observed that as the particle size decreases, the methanol conversion increases causing the catalyst to deactivate in a shorter time. The incorporation of Zn improved the selectivity to total aromatics by the aromatizing effect of Zn. The SAPO-5 (S5) material having a smaller particle size showed complete conversions of methanol. In contrast, the ZnAPO-5 (Z5) material showed low conversions but a high selectivity to total aromatics (41%). On the other hand, the material S36-2 presented a high selectivity to aromatics (58%) due to the high amount of Zn and Si. Both metals provided a certain acidic character to the materials.

**Keywords**: Methanol conversion, zeotypes, aromatics, BTX fraction, doubly substituted AlPO, MeAPSO materials.

## 1. Introduction

Aluminophosphates (AlPOs), first reported by Wilson in 1982 [1], constitute a large class of molecular sieves or zeotypes. Zeotypes are extensively investigated and applied in the field of catalysis because of their intrinsic properties such as high micropore areas, narrow micropore distribution, high thermal stability and capacity of being doped by different heteroatom ions, which generate heterogeneous active sites within structures with shape-selective ability [2]. These materials not only exhibit characteristics of zeolites but also show novel physicochemical properties that are linked to their unique composition and have potential applications in catalysis, adsorption, and ion-exchange [3].

Isomorphic substitution of framework $Al^{3+}$ and $P^{5+}$ ions by metal cations (V, Co, Mg, Ga, Fe, Zn, etc.) or silicon produces the MeAPO and SAPO family materials, respectively. The incorporation of cations can lead to Brønsted acid sites, which make these materials useful in acid-catalyzed reactions [4,5]. This acid property of SAPO is strongly dependent on the Si content, sitting and ordering in the lattice. When Si atoms are incorporated into the framework of an $AlPO_4$ at the phosphorous sites (mechanism SM2), a potential Bronsted site per Si atom would be generated. Simultaneous replacement of a pair of Al + P atoms by two Si atoms (mechanism SM3 in combination with mechanism SM2), according to the model SM3+SM2 proposed by Dwyer and coworkers [6] thus creating silicon islands. Depending on the relative rates of the SM3 and SM2 mechanisms, the size and terminating environment of the Si islands vary. when the SM2 mechanism dominates, the silicon islands grow to smaller sizes terminating with a $Si(OAl)_4$ environment that render the edge a negative charge which can host a proton, thus forming a Brønsted acid site [7]. Regarding zinc, taking into account its oxidation state, zinc is expected to be incorporated into the framework by the SM1 replacement mechanism (occupying an aluminum position).

On the other hand, there are other materials denominated MeAPSO, where Zn and Si are incorporated, replacing Al and P, respectively. These materials were studied in the present work where it is proposed that Zn acts as a flavoring agent and Si as an acidic agent. These materials were evaluated in the reaction of methanol to hydrocarbons (MTH). The conversion of methanol to hydrocarbons (MTH) over acidic zeolites has drawn considerable attention since its discovery in 1970s by Mobil Corporation [8]. Depending on the product of reaction selectivity, this process was named as MTG (methanol to gasoline), MTO (methanol to olefins), MTP (methanol to propene) and MTA (methanol to aromatics). In this last process, aromatic compounds, especially benzene, toluene and xylene (BTX fraction) are mainly produced from the oil-based route to this date, the gradual depletion of oil reserves has resulted in a sustained tight supply and high cost

of aromatics [9]. However, methanol can be expediently produced via syngas from multifarious carbon resources such as coal, natural gas and biomass [10].

MeAPSO materials can be considered potential catalysts for the MTA reaction, due to the presence of Zn and Si in the structure. In this study, the catalytic activity of two types of structures named MeAPSO-5 (AFI) and MeAPSO-36 (ATS) are compared. We will work with structures with channels of 12 members with large pores such as $AlPO_4$-5 or $AlPO_4$-36. $AlPO_4$-5 zeotype, first reported by Wilson and coworkers [1] has a three-dimensional structure with hexagonal symmetry (AFI structure), which contains one-dimensional channels oriented parallel to the caxis and delimited by 12-membered rings comprising alternating $AlO_4$ and $PO_4$ tetrahedra [11,12]. AFI-structured AlPO4-5 based materials have been extensively studied in catalysis, because of their large pore system as well as the large number of structure-directing agents (SDAs) able to lead their crystallization [13]. Specifically, the SAPO-5 has been previously studied by Terasaka and coworkers [14] in the MTO process. They produced predominantly propene followed by butenes with the complete conversion of methanol using SAPO-5 with different morphologies material.

$AlPO_4$-36 possesses a 12-ring channel system with annular side pockets. The channels are elliptical 1.01 nm $\times$ 0.92 nm in size and have a pore opening of $0.74 \times 0.66$ nm. The side pockets consist of two pairs of four rings and one boat-shaped hexagon. The presence of staggered annular side pockets inside the channels enlarges the diameter to 10.1 x 9.2 Å giving rise to high sorption capacities compared to similar $AlPO_4$ materials [15]. The MeAPSO-36 framework is acidic, and it possesses both Bronsted and Lewis acid sites. The incorporation of cobalt, magnesium, manganese, silicon, titanium, vanadium, and zinc into the framework of $AlPO_4$ can generate catalytically active centers and thus produce heterogeneous catalysts [16]. MeAPSO-36 molecular sieves have ATS topology, of which aluminum sites can partly substituted by zinc. $AlPO_4$-36 has not so far been prepared in pure aluminophosphate form but is readily synthesized in the presence of $Zn^{2+}$ or $Mg^{2+}$ using a tripropylamine template (TPA).

In this context the P or Al atoms of the network can easily be replaced by Si or Zn, respectively, generating acidity. In the present work, the aim is the synthesis of doubly substituted AlPOs, by Zn as a flavoring function and Si as an acid function. The amount of silicon and zinc incorporated in the materials was varied systematically, so that the composition of the synthesis gels can be directly related to the properties of the materials obtained. It is important to note that these types of materials have not been studied in the MTH process previously.

## 2. Experimental

### 2.1. Materials

The reagents used for the preparation of zeolites are tetraethyl orthosilicate (TEOS, 98%, Aldrich), aluminum hydroxide hydrated ($Al(OH)_3$, Sigma-Aldrich), zinc acetate dihydrate ($Zn(CH_3COO)_2$ $2H_2O$, 99% Sigma Aldrich), tripropylamine (TPA, 99%, Aldrich), N-methyldicyclohexylamine (MCHA, 99%, Aldrich ), Phosphoric acid ($H_3PO_4$, 85 wt. % in $H_2O$, Aldrich).

### 2.2. Synthesis of MeAPSO-36 materials

MeAPSO-36 was synthesized according to the reported procedure [5]. The gels were prepared using phosphoric acid ($H_3PO_4$, 85% in water, Aldrich), Hydrated aluminum hydroxide ($Al(OH)_3$-$xH_2O$, Aldrich) and tripropylamine (TPA, 99%, Aldrich) with a composition of 1.0 P: y Zn: 1-y Al: x Si: 0.8 TPA :10 $H_2O$.

In a typical synthesis $H_3PO_4$ and $Al(OH)_3$-$xH_2O$ were dissolved in deionized $H_2O$ under continue stirring for 15 min. Upon dissolution, zinc diacetate ($Zn(CH_3$-$COO)_2$-$2H_2O$) was slowly added to the solution under vigorous stirring until a homogeneous gel was achieved. Finally, the SDA was added to the gel dropwise and then rapidly with vigorous stirring by 1 h. Gels were then placed in Teflon (PTFE) lined stainless steel autoclaves and heated for 18 h at 160 °C. Then products were filtered, washed with distilled water, and dried at 100 °C for one night. As-prepared samples were calcined at 550 °C for 6 h under an air flow. Previously, the sample has been heating with a rate of 1 °C*$min^{-1}$ under a $N_2$ flow and maintained for 1 h at 550 °C under this atmosphere.

First, the molar ratio of zinc (y) was modified between 0 and 0.15, keeping the amount of silicon constant in the gels (x). Complementarily in a second stage, the amount of zinc that was incorporated in the synthesis gels (y = 0.1) was kept constant and the silicon content (x) of them was modified between 0 and 0.25. The gel composition and synthesis conditions are presented in Table 1.

Table 1. Synthesis of SAPO-5. Molar composition of gel:
1.0 P: y Zn: 1-y Al: x Si: 0.8 MCHA: 25 $H_2O$

| Sample | Denoted | amount of Zn in moles (y) | amount of Si in moles (x) | Product phase |
|--------|---------|---------------------------|---------------------------|---------------|
| A5-0.02 Zn-0.15 Si | S5-1 | 0.02 | 0.15 | AFI+TRI |
| A5-0.15 Zn-0.15 Si | S5-2 | 0.15 | 0.15 | AFI+TRI |
| A5-0.05 Zn-0.02 Si | S5-3 | 0.05 | 0.02 | AFI+TRI |
| A5-0.05 Zn-0.05 Si | S5-4 | 0.05 | 0.05 | AFI+TRI |
| A5-0.15 Si (SAPO-5) | S5 | - | 0.15 | AFI |
| A5-0.04 Zn (ZnAPO-5) | Z5 | 0.04 | - | AFI |

*2.3. Synthesis of MeAPSO-5 materials*

MeAPSO-5 samples were synthesized by hydrothermal treatment using N-methyldicyclohexylamine (MCHA) as SDA according to the reported procedure [13]. The gel composition was 1.0 P: y Zn: 1-y Al: x Si: 0.8 MCHA: 25 $H_2O$. The molar composition of the reaction mixtures and the synthesis conditions for the different MeAPSO-5 materials obtained are given in table 4. Samples were synthetized over similar condition to MeAPSO-36, however the synthesis temperature was 175 °C and 4h. Finally, the samples were calcined under the same conditions mentioned previously. The gel composition and synthesis conditions are presented in Table 2.

Table 2. Synthesis of SAPO-36. Molar composition of gel:
1.0 P: y Zn: 1-y Al : x Si: 0.9 TPA :10 $H_2O$

| Sample | Denoted | Amount of Zn in moles (y) | amount of Si in moles (x) | Product pase |
|--------|---------|---------------------------|---------------------------|--------------|
| A36-0.01 Zn (ZnAPO-36) | Z36 | 0.01 | - | ATS |
| A36-0.05 Zn-0.15 Si | S36-1 | 0.05 | 0.15 | ATS+AFI |
| A36-0.15 Zn-0.15 Si | S36-2 | 0.15 | 0.15 | ATS |
| A36-0.1 Zn-0.05 Si | S36-3 | 0.1 | 0.05 | ATS+AFI |
| A36-0.1 Zn-0.15 Si | S36-4 | 0.1 | 0.15 | ATS+AFI |
| A36-0.1 Zn-0.25 Si | S36-5 | 0.1 | 0.25 | ATS+AFI |

### 2.4. Catalyst characterization

Powder X-ray diffraction (PXRD) patterns were collected with an XPert Pro PANalytical diffractometer (CuKα1 radiation = 0.15406 nm). Scanning electron microscopy (SEM) images were recorded on a Hitachi S-3000N microscope. Transmission electron microscopy (TEM) study was carried on a JEOL 2100F microscope opering to 200KV. Nitrogen adsorption/desorption isotherms were measured at −196 °C in a Micromeritics ASAP 2020 device. Before the measurement, the previously calcined sample was degassed at 350 °C under high vacuum for at least 10 h. Surface areas were estimated by the BET method whereas microporous and external surface areas were estimated by applying the t-plot method.

Solid-state magic-angle spinning (MAS) NMR experiments were conducted on a Bruker Avance 300 (11.75 T) spectrometer operated with frequency at 130.32 MHz and spinning rate at 10 KHz. The 27Al NMR spectra were recorded using a pulse width of 0.5 µs (π/12 flip angle), 2400 scans and a recycle delay of 1 s.

The Al, Si, P and Zn concentrations of samples were obtained by inductively coupled plasma-optical emission spectroscopy (ICP-OES) with a Optima 3300 DV Perkin Elmer. Temperature programmed desorption of ammonia ($NH_3$-TPD) was conducted using a Micrometrics Autochem II chemisorption analysis equipment. Typically, 100 mg of sample pellets (30–40 mesh) were pretreated at 550 °C for 1 h in helium flow (25 mL/min) and then cooled to the adsorption temperature (177 °C). A gas mixture of 5.0 vol.% $NH_3$ in He was then allowed to flow over the sample for 4 h at a rate of 15 mL/min. Afterwards, the sample was flushed with a 25 mL/min helium flow for 30 min while maintaining the temperature at 177 °C to remove weakly adsorbed $NH_3$, and finally the temperature was increased to 550 °C at a rate of 10 °C/min. Thermogravimetric analysis (TGA) were carried out at a heating of 30 °C to 900 °C with a rate of 20 °C/min under air flow and registered in a PerkinElmer TGA7 instrument.

### 2.5. MTH catalytic testing conditions

Zeotypes materials were tested as catalysts in the conversion of methanol at 400 °C in a Microactivity reaction set (PID Eng & Tech) consisting of a fixed bed reactor completely automated and controlled from a computer. The reactor outlet is connected to a gas chromatograph to analyze the reaction products. $N_2$ was used as a stripping gas under a controlled flow. The methanol was fed as a liquid using an HPLC pump (Gilson 307). The methanol was converted to the gas phase and mixed with the $N_2$ stream in a preheater at

180 ° C to generate a gas mixture with a constant molar ratio of methanol/$N_2$ of 4. Before the reaction, the catalysts were activated at 550 ° C for 1 h low air flow to remove any trace of organic molecules or moisture adsorbed within the pores of the catalyst. The weight of the catalyst (sieved in a 20-30 mesh, corresponding to a particle size between 0.84 and 0.59 mm) and the flow of methanol were optimized to achieve different values of space velocities (WHSV).

The reaction products were analyzed online by gas chromatography with a VARIAN CP3800 chromatograph. The device is equipped with two columns: (i) a Petrocol DH50.2 capillary column connected to an FID detector, and (ii) a HayesepQ packed column (2 m length, 3.17 mm (1/8 ") diameter external and 2 mm internal diameter) connected to a TCD detector, to analyze hydrocarbons and oxygenated products, respectively.

### 3. Results and discussion

#### 3.1. *X-Ray Diffraction*

The XRD pattern of the substituted MeAPSO-36 material with different amounts of Si and Zn are show in Figure 1a. In all the samples, the peaks position and the intensities are identical to those reported for SAPO-36 [17], however, there are minor differences in the XRD patterns in each sample depending on the Zn and Si content of the samples. ATS structure is favored by the presence of zinc in the structure of MeAPSO-36, as well as low silicon content and high synthesis temperature, the S36-2 XRD pattern contains only ATS-type structure, due to the high amount of moles of Zn present in the sample. Wilson and coworkers [1] reported that the synthesis of MeAPO-36 the high concentration of metals such as zinc favors the crystallization of the MeAPSO-36 over that of its competitive co-phase structure type 5 (AFI). It is observed that as the amount of Zn increases in the peak samples corresponding to the AFI structure (marked with asterisks) it disappears, which indicates that the stability of the crystalline structure increased with the Zn content. Sample S36-5 has a low Zn content and a high Si content, so it showed an increase in the appearance of co-phase structure AFI.
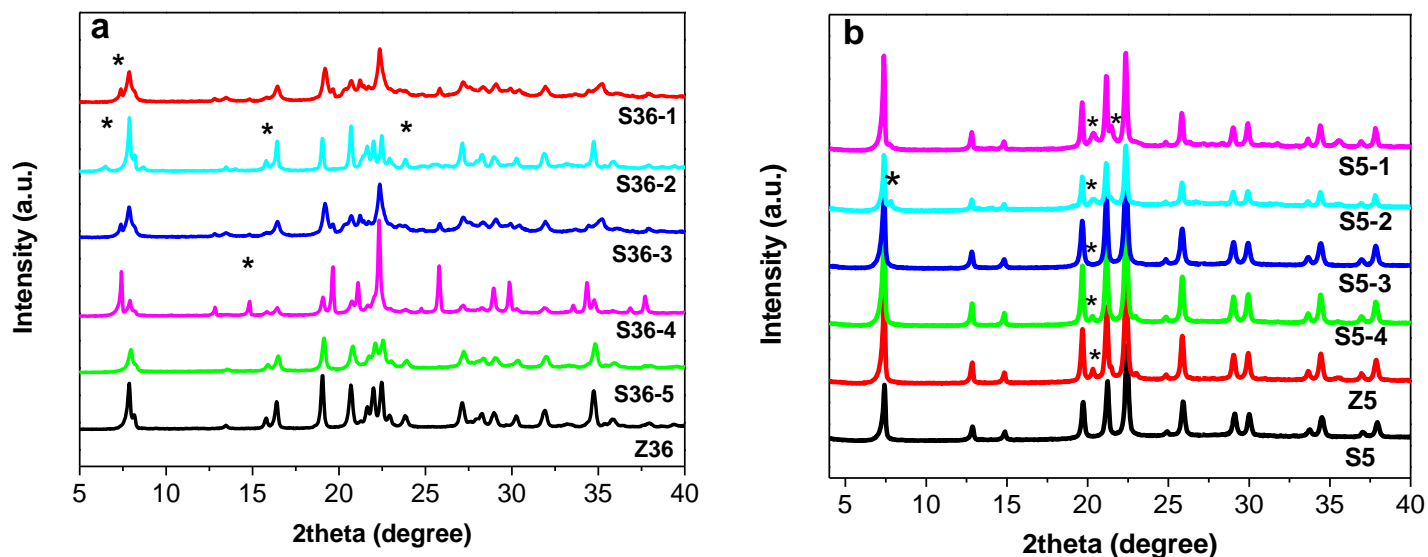
Figure 1. XRD patterns of (a) MeAPSO-36 and (b) MeAPSO-5 materials synthetized

For the other hand, the XRD patterns of the MeAPSO-5 samples are show in Figure 1b, S5 (SAPO-5) material shows a pattern of AFI structure without any impurity. In particular, the use of MCHA as the SDA for synthesis SAPO-5 samples, can forming AFI structure without any additional impurity phases. The other samples showed a small amount of impurity identified as the tridymite phase [18] coexisting with the AFI-type structure. The impurity phase was also observed by Chen and coworkers [19] when loading a higher amount of metal onto the AFI framework of $AlPO_4$-5. As high amount zinc the intensity of those diffraction peaks attributed to tridymite and berlinite significantly increase. The ratio of 0.9 moles of SDA is enough to form an $AlPO_4$-5 phase. It is known that AFI structure increases with an increase of pH or the SDA content [20].

### 3.2. N₂ adsorption–desorption

All as-prepared MeAPSO samples were studied by $N_2$ adsorption/desorption isotherms at 77 K in order to determine their textural properties. Isotherms of MeAPSO-5 and MeAPSO-36 samples are showed in figures S1a and S1b (material supplementary 1a and 1b), respectively. All the samples present type I isotherms (according to the IUPAC classification [21]), corresponding to microporous materials. The steep uptake at low relative pressures in MeAPSO-36 samples is due to adsorbent-adsorptive interactions in

narrow micropores and the subsequent formation of a monolayer (Figure S1a). The shape of the isotherm at higher relative pressures (up to $P/Po=1$) is due to unrestricted monolayer-multilayer adsorption. At higher relative pressures, the $N_2$ adsorption-desorption curve of MeAPSO-36 samples exhibits hysteresis H4-type, which is characteristic of molecular sieves with formation of inter or intracrystalline mesopores as will be observed by SEM analysis later [22,23].

Figure S1a presents the $N_2$ adsorption-desorption isotherm of MeAPSO-5 samples. Similarly, the $N_2$ adsorption capacity of all materials is high at low relative pressures, indicating the presence of a microporous structure with an H4-type hysteresis loop formed almost throughout the P/Po range although to a lesser extent compared to the MeAPSO-36 samples [24,25]. It may be considered that MCHA structure-directing agent constrained in the unidimensional 12-ring pore channels generated larger pores, giving mesoporous $AlPO_4$-5 [25].

The micropore volumes and BET areas for the samples prepared using different silicon and zinc contents are summarized in Table 3. It can be observed that all the samples have surface area in the range 550–650 $m^2/g$ for MeAPSO-5 materials. However, the MeAPSO-36 materials presented smaller areas in the range 200 and 320 $m^2/g$. These differences can be explained in base to the longer crystal size and the higher intercrystalline porosity in MeAPSO-36 materials in addition show very low non-microporous (external) surface, values characteristic of this type of materials. High silicon content led to a distinct decrease of BET surface area and microporous volume due to the existence of amorphous $SiO_2$ [26], however, our obtained BET surface area of SAPO-5 materials are larger than the literature reported values 286 $m^2/g$ [25]. This is mainly caused by the higher external surface areas, which may be attributed to mesopore formation. Therefore, the coexistence of micropores and mesopores in our sample leads to high BET surface area.

Table 3. Elemental composition measured by ICP-OES and NMR $^{31}$P and textural properties of the samples

| Catalyst | % wt | | | | P/Zn Ratio (ICP)[a] | P/Zn Ratio (NMR)[b] | $S_{BET}$ $(m^2*g^{-1})$ | $S_{micro}$ $(m^2*g^{-1})^c$ |
| | % Al | % P | % Zn | % Si | | | | |
|---|---|---|---|---|---|---|---|---|
| S5-1 | 16.2 | 23.7 | 1.4 | 2.4 | 34.3 | - | 268.6 | 264.4 |
| S5-2 | 7.7 | 18.9 | 3.3 | 2.7 | 11.9 | 11.4 | 148.2 | 55.6 |
| S5-3 | 21.6 | 19.2 | 2.5 | 0.4 | 16.3 | 8.3 | 176.5 | 114.5 |
| S5-4 | 17.7 | 22.4 | 2.2 | 0.5 | 21.9 | 10.2 | 198.4 | 104.8 |
| S5 | 19.4 | 18.3 | - | 4.7 | - | - | 300.5 | 174.6 |
| Z5 | 12.3 | 27.2 | 5.1 | - | 11.1 | 11.6 | 140.9 | 71.8 |
| Z36 | 14.3 | 26.8 | 6.9 | - | 8.1 | 6.8 | 124.2 | 110.5 |
| S36-1 | 11.6 | 21.1 | 2.9 | 3.6 | 15.4 | 11.3 | 326.5 | 249.4 |
| S36-2 | 13.9 | 20.8 | 6.5 | 2.8 | 6.7 | 6.5 | 74.7 | 13.8 |
| S36-3 | 12.4 | 21.4 | 6.4 | 1.2 | 7.1 | 6.4 | 164.2 | 139.7 |
| S36-4 | 17.1 | 22.2 | 7.3 | 0.7 | 6.4 | 4.6 | 153.7 | 120.2 |
| S36-5 | 12.8 | 26.9 | 6.9 | 2.8 | 8.2 | 8.0 | 175.6 | 129.6 |

[a] P/Mg ration derived from chemical analysis.
[b] P/Mg ration of original samples derived from 31P-MAS NMR using dmfit program for convolution process
[c] Using t-plot method

### 3.3. Scanning Electron Microscopy (SEM)

Figure S2 and S3 (material supplementary) show SEM selected images of MeAPSO-36 and MeAPSO-5, respectively. The amount of Si and Zn had influences in a considerate way distribution of crystals sizes and shapes of MeAPSO materials. All MeAPSO-36 materials selected (samples Z36, S36-1, S36-2 and S36-5 in Table 1) presented crystals particles with irregular spheres larger of size 16-22 µm range (Figure S2) formed in turn by small crystals in the form of thin needles [3]. In this study, the crystal size decreased in the order Z36> S36-1 >S36-2 >S36-5 which is also in agreement with the observed relative stability. The intercrystalline space of these crystals is the cause of the formation of an H4 hysteresis cycle visualized in the $N_2$ isotherms.

Figure S3 shows SEM pictures for the MeAPSO-5 materials selected. Solid only silicon content (S5) presented homogeneous distribution of spherical particles, which have a diameter of ca. 1.5 µm. Sample Z5 (only zinc content) consists of homogeneously distributed large porous spherical particles with an approximate diameter of ca. 15 µm [23]. S5.1 presented the same size of particles. However, the S5-2

material presented a different morphology, particles in the form of 3D hexagons with approximately 10 m sizes are observed, this can be attributed to a higher content of Zn (0.15 mol) incorporated in the material. In this study, the crystal size increased in the order S5> Z5 >S5-1 >S5-2.

### 3.4. TGA y DTG analysis

Thermogravimetric analyses (TGA) were performed aiming to verify the incorporation of the SDA molecules in the structure of the as-made samples and their subsequent complete elimination after and before calcination. The ATG/DTG curves of selected material MeAPSO-36 y MeAPSO-5 not calcined selected are shown in Figure 2a and 2b, respectively. TGA profiles are strongly influenced by the Zn and Si incorporation. In both figures, three weight losses are observed. The first weight loss, at temperatures below 150 °C (step I), can be attributed to desorption of adsorbed water. The second weight loss, between 400 and 550 °C (step II) is due to the decomposition of the template in each case (TPA and MCHA) and, finally, the third weight loss at temperatures higher than 600 K (step III) has been associated with the further removal of organic residues occluded in the channels and cages of the MeAPSO materials caused by combustion [27].
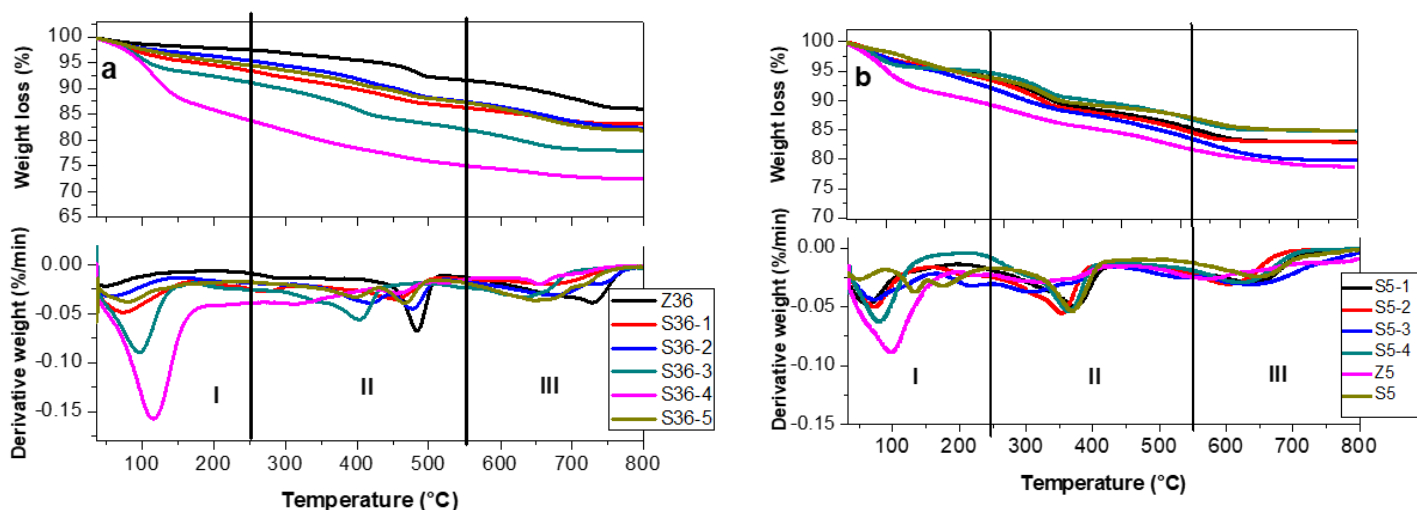


Figure 2. Thermal analysis of the MeAPSO uncalcined materials selected TGA (top) and DTG (bottom) (a) MeAPSO-36 and (b) MeAPSO-5

It can be observed that the decomposition of the template occurs in a different way for sample S36-3. The fact that the template decomposition began at lower temperature in this sample could be possibly attributed to its smaller particle size and the lesser diffusional problems derived from it. On the other hand, in Figures S4 (supplementary material S4) presented the curves ATG and DTG, of some MeAPSO-36 and MeAPSO-5 selected after calcining. In all cases, a single loss of mass less than 100 °C is observed, which corresponds to the physisorption of water retained in the samples. No other significant weight losses are observed at higher temperature which indicates that the SDA was eliminated.

### 3.5. ICP-OES Chemical Composition Analysis

The elemental compositions of the molecular sieves are presented in Table 3. The content of Al, P, Si and Zn was determined, the correct incorporation of zinc and silicon is verified, as already mentioned above, zinc is incorporated according to the substitution mechanism SM1 (occupying an aluminum position), while silicon can be incorporated isolated occupying a phosphorus position or in pairs replacing a pair Al + P (mechanisms SM2 and SM3 respectively). With these values, the P/Zn molar ratio was determined and compared with that calculated by $^{31}$P NMR spectrum using equation 1 reported by Barrie and Klinowski [28].

$$\text{P/Zn} = \sum_{n=0}^{4} I_P(nAl) / \sum_{n=0}^{4} 0.25(4-n)I_{P(nAl)} \tag{1}$$

Where Ip(nAl) being the area of the peak due to the P (n Al, 4-n Zn) structural units calculated by $^{31}$P MAS NMR shows later. The value of Ip was calculated using the spectrum convolution process using the dmfit program created by D.Massiot and coworkers [29].

### 3.6. Solid state NMR spectroscopy of $^{31}$P MAS

The incorporation of Zn to the MeAPSO framework was studied by $^{31}$P MAS NMR. The $^{31}$P spectrum of MeAPSO-5 and MeAPSO-36 materials are showed in Figure 3a and 3b, respectably. The $^{31}$P resonance peak is asymmetrically broadened, which points out a wide distribution of phosphorous sites with different chemical environment [30]. It has been described that when the amount of zinc incorporated to the MeAPSO-5 framework (figure 3a) is low, P atoms are located in a unique P(4Al) environment resulting from the substitution of phosphorous by silicon in the aluminophosphate framework (in their second coordination sphere) [31,32] as case of S5 (SAPO-5). However, if the zinc content is higher (S5-2), multiple

phosphorous environments can occur. The ^{31}P spectrum has a peak at 28 ppm (attributed to P(4A1) sites [29]) and a broad shoulder at 23 ppm indicative of phosphorus having a neighbor other than aluminum, i.e. P(3A1, 1Zn) site in the ATS framework [17,28].

Similarly, the ^{31}P spectrum of MeAPSO-36 materials (Figure 3b) presented the signal at 28 ppm attributed to the P (4Al) sites, followed by a shoulder at 23 ppm (3 Al, 1 Zn) and another signal in the case of material S36-2 (higher content of Zn) at 18 ppm corresponding to 2 Zn as neighbors of the phosphorous denoted as P(2 Al, 2 Zn) [17].

The P/Zn ratio of the materials determined by chemical analysis and ^{31}P NMR spectrum are showed in table 3. The difference observed between both values indicates that a significant amount of Zn is not occupying the framework sites [33]. This technique is a useful tool to demonstrate the correct incorporation of Zn, because the coordination of P is sensitive to the incorporation in the second sphere of coordination by Zn measured by NMR. However, in materials with low zinc content, such as S5-1, only the signal belonging to P (4Al) is observed, so Equation 1 cannot be applied
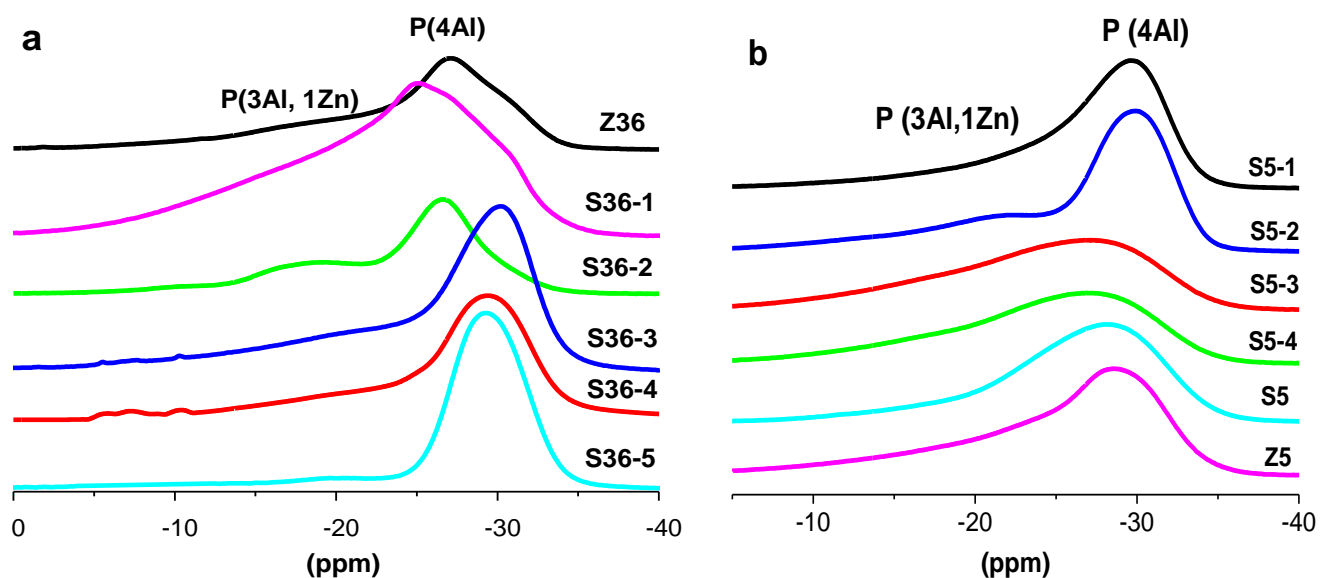


Figure 3. ^{31}P MAS NMR spectra of double modified AlPO$_4$ materials (a) MeAPSO-36 and (b) MeAPSO-5

### 3.7. Temperature-programmed desorption (NH₃-TPD)

The acidity of the calcined samples has been evaluated by $NH_3$-TPD. TPD profiles of the MeAPSO-36 and MeAPSO-5 samples are showed in figure 4a and 4b, respectably. In principle, the increase in the molar ratio of zinc and silicon in gels implies a greater incorporation of both metals in solids, which causes a greater density of weak acid sites. It can be observed that all samples show a maximum at around 270 °C, indicating that these acid sites are relatively weak characteristic of this type of materials. This band can be tentatively assigned to desorption of ammonia on Brønsted acid sites originated by isomorphic substitution of $Al^{3+}$ by $Zn^{2+}$ and $P^{4+}$ by $Si^{3+}$ in the MAPSO structures [34]. However, it is well known that this technique does not allow distinguishing between Brönsted and Lewis acid sites. Therefore, it cannot be excluded that some Lewis acid centres able to adsorb ammonia at moderate temperature are present in the MeAPSO material, probably formed during the calcination treatment [35]. MeAPSO samples with different zinc and silica content show slightly different TPD profiles. The incorporation of zinc species in MeAPSO materials exhibits a significant influence on the distribution of acid sites, when the amount of Zn is increased and if the density of acidic sites increases, it is intuited that the substitution of both metals in the structure provides certain acidic character to the materials, especially for samples S5-2 and S36-2, which have high amounts of substituted Si. The acid property of MeAPSO materials is strongly dependent on the Si content, sitting and ordering in the lattice. SM2 substitution leads to more acid centers while SM2+SM3 combination lead to less acid centers but higher strength than the one arising from only the SM2 substitution [36].
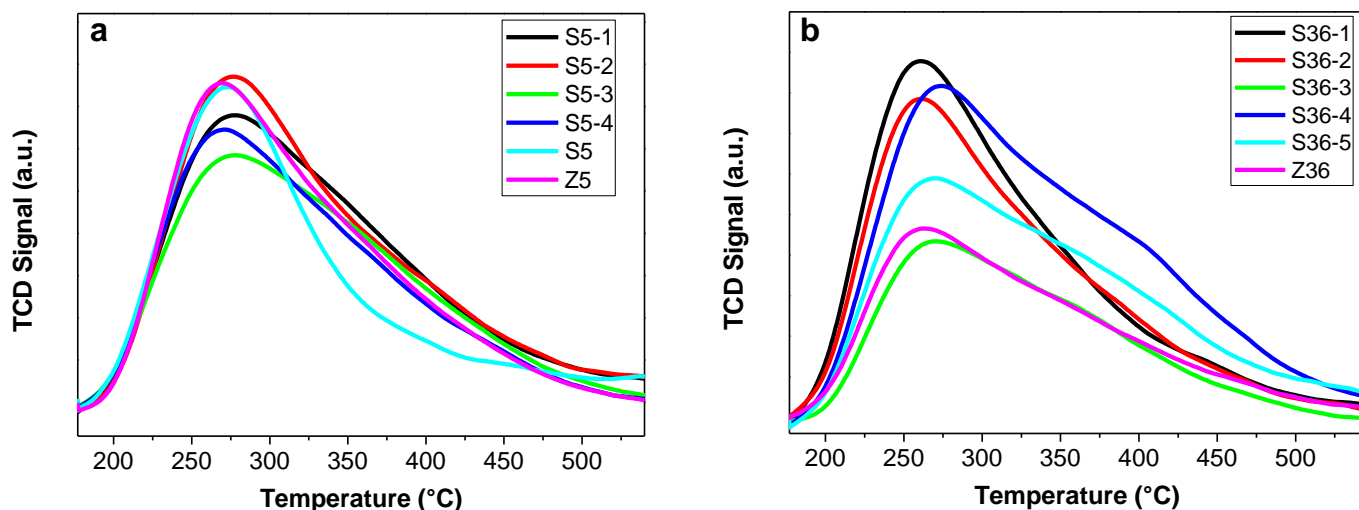
Figure 4. $NH_3$-TPD profiles of double modified $AlPO_4$ materials (a) MeAPSO-36 and (b) MeAPSO-5

The specific peak area is proportional to the number of acid sites in the sample and can be determined by integration by convolution of the area under the curve of the spectra. The amounts of strong and weak acid sites of the samples are listed in Table 4. The acids sites density total is higher in MeAPSO-5 samples indicating that MeAPSO-36 possesses weaker acid sites. These results indicate that the proportion of acid sites increases in the order S5 < Z5 < S5-3 < S5-1 < S5-4 < S5-2 for MeAPSO-5 materials and S36-3 < Z36 < S36-1 < S36-2 < S36-5 < S36-4 for MeAPSO-36 materials. These results indicate that catalytic behavior of all samples is not determined mainly by acidity as presented below.

Table 4. Acidity properties of materials

| Catalyst | Temperature (°C) | Acidity (µmol $NH_3$/g) |
|---|---|---|
| | | Weak acid (LT) |
| S5-1 | 280 | 273.45 |
| S5-2 | 273 | 337.18 |
| S5-3 | 277 | 261.85 |
| S5-4 | 272 | 325.41 |
| S5 | 274 | 144.83 |
| Z5 | 277 | 191.93 |
| Z36 | 271 | 151.63 |
| S36-1 | 263 | 230.93 |
| S36-2 | 261 | 259.78 |
| S36-3 | 275 | 149.56 |
| S36-4 | 272 | 312.91 |
| S36-5 | 268 | 291.12 |

### 3.8. Catalytic Evaluation

#### 3.8.1. Catalytic Evaluation of MeAPSO-5

Figure 5 shows the methanol conversion of MeAPSO-5 materials under conditions of a space velocity (WHSV) 4.24 h$^{-1}$, 400 °C and 0.5 g of catalyst. Among the different parameters that influence the stability of these catalysts, especially the particle size and the acid strength of the active centres have been considered the most important factors affecting the deactivation during the reaction. The S5 material (only silicon, aluminum and phosphorus) showed higher conversion levels during the 9 h reaction due presented a smaller particle size (1.5 µm) and by the generation of Bronsted type acid sites due to the combination of SM2 + SM3 mechanisms. The Z5 material (constituted of zinc, aluminum and phosphorus) showed very minor methanol conversions compared to the other catalysts, due it had a larger particle size (20 µm diameter), which causes rapid deactivation. Some authors mentioned [37,38] that particle size and acid properties of the catalyst have influence on catalyst lifetime in MTH reaction. In general, a smaller particle size improves the diffusion efficiency and accessibility of acid sites for high catalytic activity obtaining higher methanol conversion values [39].
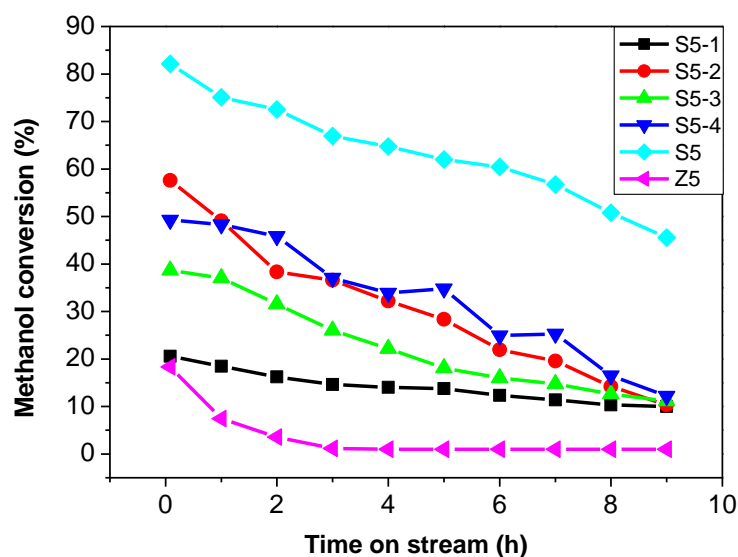


Figure 5. Results of methanol conversion in MTH reaction over MeAPSO-5 catalyst
Conditions reaction: WHSV of 4.24 h$^{-1}$, 400 °C, 0.5 g of catalyst

Table 5 shows distribution of reaction products of MeAPSO-5 materials at short reaction times (TOS 5 min) and 400 °C with similar conversion values It is observed that as the amount of Zn increases, the selectivity increases to total aromatics and therefore the BTX faction, stating the flavoring effect of Zn when it is incorporated by isomorphic substitution. In particular, the S5-1 material presented a low aromatic selectivity (26.9 %) due a low zinc amount, however, the selectivity to olefins was high (49.6 %). These results were with a low methanol conversion value (18 %) at 5 min of reaction, this can be associated with a large particle size measured by SEM. these materials have a selectivity to light olefins (ethylene and propylene) around 50% in all cases, which may indicate that Si can provide acidity necessary to form olefins as mentioned by some authors. SAPO-5 catalyst used above has the 12-ring pores with 0.73 nm straight channels and more alkane molecules can be adsorbed and react with acid centers in SAPO-5 channels due to its large channels and more pore-mouth exposed [40].

Table 5. Distribution of reaction products of MeAPSO-5 catalysts in the same conversion of methanol level

Conditions: TOS 5 min, WHSV 4.24 h$^{-1}$, 400 °C. 0.5 g catalyst

| Sample | % Methanol conversion | Selectivity (%mol) | | | Particule size SEM (μm) |
|---|---|---|---|---|---|
| | | Olefins | Total aromatics | BTX Fraction | |
| S5-1 | 18.3 | 49.6 | 26.9 | 2.2 | 20 |
| S5-2 | 20.2 | 50.2 | 32.4 | 2.7 | 18 |
| S5-3 | 38.6 | 53.6 | 16.0 | 2.1 | 10 |
| Z5 | 18.3 | 33.9 | 41.0 | 2.0 | 20 |

The Z5 material composed of Zn, Al and P had the highest selectivity to total aromatics and therefore to BTX selectivity, due to the high content of the flavoring agent. The total aromatic selectivity increased in the following order, with respect to the table shown: Z5 > S5-2 > S5-1 > S5-3. As mentioned above, these types of materials have not been studied in the MTH reaction, however, materials of the SAPO-5 type have been studied by some authors. Terasaka and coworkers [14] synthesized SAPO-5 samples with different morphologies and sizes and they demonstrated the high catalytic activity of the SAPO-5 exclusively in the MTO process. They demonstrated the high catalytic activity of the SAPO-5 exclusively in the MTO process with complete methanol conversions and selectivity to light olefins (=C2=C4) c.a. 60%.

### 3.8.2. Catalytic Evaluation of MeAPSO-36

Figure 6 shows the methanol conversion of MeAPSO-36 materials with a spatial velocity (WHSV) 2.12 h$^{-1}$, 400 °C and 1 g of catalyst. The deactivation process of the MeAPSO-36 catalysts is slower than the MeAPSO-5 catalysts, resulting in conversion curves vs reaction time up to 25 min due to smaller channels and acidity. The deactivation of the catalyst was thus ascribed to the formation of the bulky aromatic coke in the structure [41]. The fast deactivation could be explained by the shorter size ring in AlPO$_4$-36 materials (7.4 Å x 6.5 Å) that favor of the formation of bulkier organic compounds that cause deactivation. Additionally, it is observed that again the particle size (measured by SEM) had a significant influence on the conversion of methanol. The material S36-4 has higher conversion levels, generating a complete conversion of methanol at 5 min of reaction reaching deactivation after 25 min of reaction. On the contrary, the sample S36-5 showed the lowest conversion level at 5 min (40% mol) reaching deactivation at 10 min, should be attributed to the larger particle size of this catalyst (20 µm). Additionally, the lower methanol conversion over this material is because of the partial transformation of the active catalyst (ATS) phase to less active phase (tridymite).
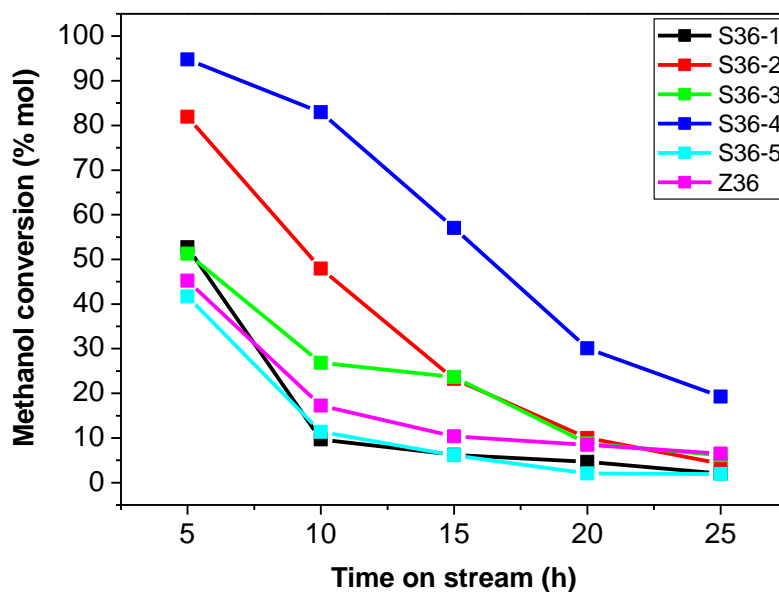


Figure 6. Results of methanol conversion in MTH reaction over MeAPSO-36 catalyst
Conditions reaction: WHSV of 2.12 h$^{-1}$, 400 °C, 1 g of catalyst

Regarding the distribution of reaction products, Table 6 shows the catalytic activity of MeAPSO-36 materials. Similarly, selectivity to total aromatics is related to the amount of Zn incorporated into the structure and to the particle size, a higher molar concentration of Zn, greater selectivity to aromatics and therefore greater selectivity to the BTX fraction. Specifically, the material Z36 (MeAPO-36) presented a high selectivity to aromatics due to aromatizing effect of Zn. On the other hand, S36-3 material presented a total aromatic selectivity of 46.3 %, this is due to the fact that it has the high amount of Zn and 0.05 moles of Si, providing both an acidic (Si) effect and a Zn aromatizing effect isomorphic substitution. Otherwise, the material S36-1, obtained the lowest conversion and total aromatic selectivity (28.1 %) due to the low amount of zinc (0.05 Zn mol) a large particle size (20 µm).

Table 6. Distribution of reaction products of MeAPSO-36 catalysts in the same conversion of methanol level
Conditions: TOS 5 min, WHSV 2.12 h$^{-1}$, 400 °C, 1 g catalyst

| Sample | % Methanol conversion | Selectivity (% mol) | | | Particule size SEM (µm) |
|---|---|---|---|---|---|
| | | Olefins | Total aromatics | BTX Fraction | |
| Z36 | 40.4 | 36.2 | 57.2 | 4.25 | 20 |
| S36-1 | 52.7 | 52.2 | 28.1 | 4.54 | 15 |
| S36-3 | 51.8 | 42.9 | 46.3 | 2.07 | 15 |
| S36-5 | 41.7 | 46.6 | 44.0 | 3.65 | 20 |

*3.8.3. Distribution of reaction products for MeAPSO-5 materials*

Selectivities to the different type of products detected in the effluent stream as a function of time are showed in Figure 7 for MeAPSO-5 materials tests carried out at WHSV = 4.24 h$^{-1}$ and 400 °C. The formation of aromatics (top) and light olefins (bottom) increases with time on stream in most cases. Sample S5-2 presented selectivities greater than total aromatics (red line) with a value of approximately 60 % at 9 h of reaction, which could be attributed to the presence of high amounts of Zn and Si and the high acidity generated for both metals.

The selectivity to light olefins remains constant during the 9 h of reaction even at low conversion rates, this could be ascribed to the growing blockage of the pores in the materials at low conversion rates, hindering the diffusion of the heavier reaction products and enhancing the release of less bulky hydrocarbons [41]. For example, material S5-4 was selective for light olefins (blue line), due to low amounts of the flavoring

metal, followed by SAPO-5 material, which is highly selective for olefins until 9 h reaction, as some authors report it [42]. These results could be attributed to the wider channels of MeAPSO-5 or might be also caused by a higher ratio of external acid sites, considering the higher microporous surface area of this material.
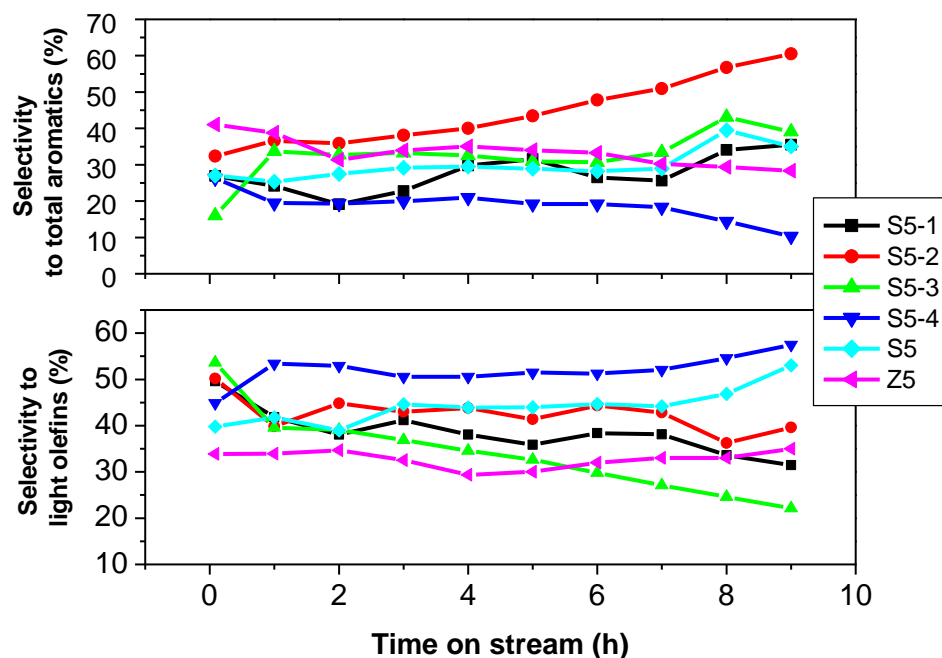


Figure 7. % Selectivity to total aromatics (top) and % selectivity to light olefins (bottom) of MeAPSO-5 materials. Test conditions: T = 400 °C, WHSV = 4.24 $h^{-1}$, 0.5 g of catalyst.

### 3.8.4. Distribution of reaction products for MeAPSO-36 materials

Finally, selectivities to the different type of products of MeAPSO-36 are showed in Figure 8 at WHSV = 2.12 $h^{-1}$ and 400 °C. It is notorious that the Z36 material is selective to the formation of aromatics (black line), because it is only composed of Zn, Al and P. Similar to MeAPSO-5 materials, it can be observed for all catalysts that the production of olefins and aromatics compounds is favored at low conversion rates. As discussed in the $NH_3$-TPD analysis (Figure 7b), the incorporation of Zn into the framework increases the density and strength of the acid sites. Thus, the increased density of active centers is more likely to influence the promotion of selectivity to aromatics compounds.

Regarding olefin selectivity, it is observed that the production of olefins remained constant during the reaction period except for sample S36-3 where olefin selectivity increased up to 60% after 15 min of

reaction. The high activity of MeAPO-36 materials ($Me^{2+}$, Al and P) for obtaining aromatics has been previously studied by some authors [43]. However, doubly substituted materials have not been evaluated in this type of reaction.
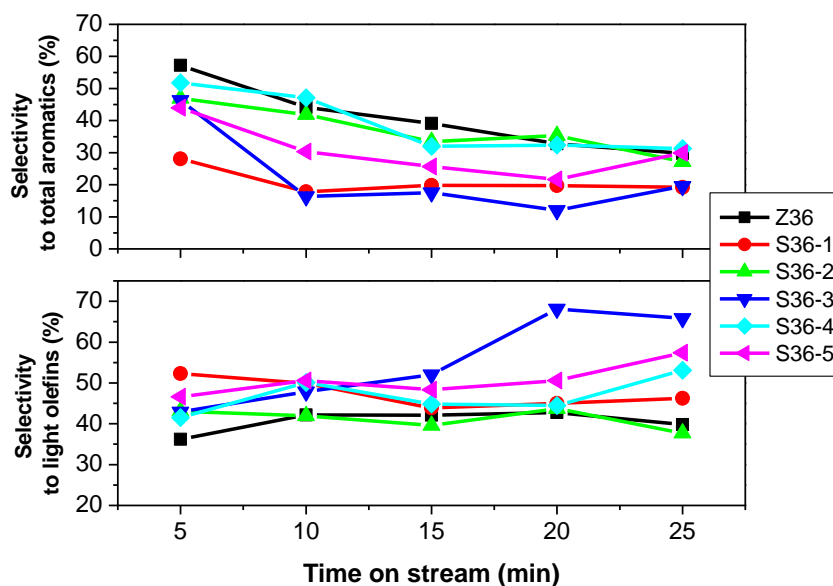


Figure 8. % Selectivity to total aromatics (top) and % selectivity to light olefins (bottom) of MeAPSO-36 materials. Test conditions: T = 400 °C, WHSV = 1.12 h$^{-1}$, 1 g of catalyst.

## 4. Conclusions

Double-substituted AlPO$_4$-5 and AlPO$_4$-36 materials were synthesized with Si as an acid function and Zn as a aromatizing function. The incorporation of Si and Zn by isomorphic substitution influenced the textural, as well as the morphology and catalytic performance of the zeotypes. The incorporation of Zn in MeAPSO-36 materials facilitated the formation of the ATS structure, since this structure is related to the incorporation of divalent metals such as Zn. NH$_3$-TPD results further proved the incorporation of Si and Zn in the framework resulting in improved acidity and therefore had an influence on the catalytic activity for the formation of olefins and aromatic compounds.

The total aromatic selectivity increased as the amount of Zn in the MeAPSO materials increased, stating the aromatizing function of the divalent metal. The particle size had an important effect on the catalytic activity, as the particle size decreases, the methanol conversion increases causing the catalyst to deactivate in a shorter time. Specifically, the S5 material showed high conversions during the 9 h reaction when

presenting a small particle size, however, the aromatic selectivity was lower because the material is only composed of Si, Al and P. Contrarily, the material represented a high selectivity to total aromatics at 5 min (41%) with low methanol conversions. Regarding the MeAPSO-36, the material S36-2 presented a high selectivity to aromatics due to the same amount of Zn and Si (0.15 mol). Both metals provided a certain acidic character to the materials. MeAPSO-36 suffered from fast deactivation because of the formation of coke favored by its shorter channels compared to MeAPSO-5 materials.

In summary, it is demonstrated that the particle size and Zn and Si amount have influence in the stability and in the selectivity of MeAPSO catalysts in the MTH process.

**Acknowledgment**

**Ethical statement**

All authors contributed to the study conception and design. Material preparation, data collection and analysis were performed by Dora A. Solís Casados (supervision), Julia Aguilar Pliego (writing—review and editing), Carlos Márquez Álvarez (methodology), Enrique Sastre de Andrés (supervision), Diana Sanjurjo Tartalo (investigation), Manuel Sanchez-Sanchez and Marisol Grande Casas (methodology). The first draft of the manuscript was written by PhD student, Misael Garcia Ruiz and all authors commented on previous versions of the manuscript. All authors read and approved the final manuscript.

We considerate the submitted is original and unique work and it has not been submitted to another journal simultaneity.

The work is single study and it's not up into several parts and results are presented clearly, honestly, and without, falsification or inappropriate the data manipulation, the study submitted is part of my doctoral thesis.

The authors declare no conflict of interest. The funders had no role in the design of the study; in the collection, analyses, or interpretation of data; in the writing of the manuscript, or in the decision to publish the results.

This work does not contain any studies with human participants or animals performed by any of the authors.

Finally, additional informed consent was obtained from all individual participants for whom identifying information is included in this chapter

# References

[1] Wilson ST, Lok BM. Messina CA, Cannan TR, Flanigen EM (1982) Aluminophosphate molecular sieves: a new class of microporous crystalline inorganic solids. JACS 104: 1146-1147.

[2] Manjón-Sanz A, Sánchez-Sánchez M, Muñoz-Gómez P, García R, Sastre E (2010) Non-templated intercrystalline mesoporosity in heteroatom-doped $AlPO_4$-5 using N-methyldicyclohexylamine as structure-directing agent. Micropor. Mesopor. Mater. 131: 331–341.

[3] Xu J, Zhou D, Song X, Chen L, Yu J, Ye C, Deng F (2008) Crystallization of magnesium substituted aluminophosphate of type-36 as studied by solid-state NMR spectroscopy. Micropor Mesopor Mater. 115: 576–584.

[4] Kumar-Saha S, Waghmode SB, Maekawa H, Kawase R, Komura K, Kubota Y, Sugi Y (2005) Magnesioaluminophosphate molecular sieves with ATS topology: Synthesis by dry-gel conversion method and catalytic properties in the isopropylation of biphenyl. Micropor. Mesopor. Mater. 81: 277–287.

[5] O'Brien MG, Sanchez-Sanchez M, Beale AM, Lewis DW, Sankar G, Catlow CR (2007) Effect of Organic Templates on the Kinetics and Crystallization of Microporous Metal-Substituted Aluminophosphates. J. Phys. Chem. C 111: 16951-16961.

[6] Makarova M, Ojo A, Al-Ghefaili K, Dwyer J (1992) In: Proceedings of the IX International Zeolite Conference. Montreal, Canada 2: 259.

[7] Gómez-Hortigüela L, Márquez-Álvarez C, Grande-Casas M, García R, Pérez-Pariente J (2009) Tailoring the acid strength of microporous silicoaluminophosphates through the use of mixtures of templates: Control of the silicon incorporation mechanism. Micropor. Mesopor. Mater. 121: 129-137.

[8] Chang, CD, Silvestri JA (1977) The conversion of methanol and other O-compounds to hydrocarbons over zeolite catalysts. J. Catal. 47: 249-259.

[9] Zhang J, Qian W, Kong C, Wei F (2015) Increasing para-Xylene Selectivity in Making Aromatics from Methanol with a Surface-Modified Zn/P/ZSM-5 Catalyst. ACS Catal. 5(5): 2982–2988.

[10] Niu X, Gao J, Miao Q, Dong M, Wang G, Weibin F, Qin Z. Wang, J (2014) Influence of preparation method on the performance of Zn-containing HZSM-5 catalysts in methanol-to-aromatics. Micropor. Mesopor. Mater. 197: 252–261.

[11] Choudhary VR, Akocekar DB, Sansare SD (1987) Crystallization of AlPO-5 from a system- 1.5 $(C_3H_7)_3N$-1.0$Al_3O_2$-1.0$P_2O_5$- 40.0 $H_2O$: Characterization of the products of crystallization. Mater. Chem. Phys. 18: 245-254.

[12] Zhao X, Zhao J, Wen J, Li A, Li G, Wang X (2015) Microwave synthesis of AFI-type aluminophosphate molecular sieve under solvent-free conditions. Micropor. Mesopor. Mater. 213: 192-196.

[13] Sanchez-Sanchez M, Sankar G, Simperler A, Bell RG, Catlow CR. Thomas JM (2003) The extremely high specificity of N-methyldicyclohexylamine for the production of the large-pore microporous AFI material. Catal. Lett. 88 (3–4): 163-167.

[14] Terasaka K, Imai H, Li X (2015) Control of Morphology and Acidity of SAPO-5 for the methanol-to-olefins (MTO) reaction. J. Adv. Chem. Eng. 5(4): 1000138.

[15] Akolekar DB (1996) Silicon-containing magnesium aluminophosphate of type 36 (MAPSO-36): Characterization, surface, acidic, and catalytic properties. Zeolites 17: 283-290.

[16] Akolekar DB, Russell F, Howe RF (1997) Metal Substituted ATS Aluminophosphate Molecular Sieves. Stud Surf Sci Catal. 105: 755-762.

[17] Prasad S, Dewey HB, Haw JF (1996) Probing acid sites in MAPO-36 by solid state NMR. Catal Lett. 39: 141-146.

[18] Graetsch HA (2002) Monoclinic AlPO$_4$ tridymite at 473 and 463 K from X-ray powder data. Acta Crystallogr. C. 58: 18-20.

[19] Chen CM, Jehng JM (2004) Structure control of metal aluminum phosphate (MeAlPO-5) molecular sieves and applications in polyethylene glycol amination. Catal Lett. 93(3–4): 213-223.

[20] Du H, Fang M, Xu W, Meng X, Pang W (1997) Preparation by microwave irradiation of nanometre-sized AlPO4-5 molecular sieve J. Mater. Chem. 7: 551.

[21] Thommes M, Kaneko K, Neimark A, Olivier J, Rodriguez-Reinoso F, Rouquerol J, Sing K (2015) Physisorption of gases, with special reference to the evaluation of surface area and pore size distribution (IUPAC Technical Report). Pure Appl. Chem. 87: 1051–1069.

[22] Wang Q, Chen G, Xu S (2009) Hierarchical architecture observed in microspheres comprising microporous AlPO$_4$-11 nanocrystals. Micropor. Mesopor. Mater. 119: 315–321.

[23] Basina G, Shamia DA, Polychronopoulou K, Tzitzios V, Balasubramanian VV, Dawaymeh F, Karanikolosa GN, Wahedi YA (2018) Hierarchical AlPO$_4$-5 and SAPO-5 microporous molecular sieves with mesoporous connectivity for water sorption applications. Surf. Coat. Tech. 353: 1-29.

[24] Gao B, Tian P, Li M, Yang M, Qiao Y, Wang L, Xu S, Liu Z (2015) In situ growth and assembly of microporous aluminophosphate nanosheets into ordered architectures at low temperature and their enhanced catalytic performance. J. Mater. Chem. A. 3: 7741-7749.

[25] Utchariyajit K, Wongkasemjit S (2008) Structural aspects of mesoporous AlPO$_4$-5 (AFI) zeotype using microwave radiation and alumatrane precursor. Micropor. Mesopor. Mater. 114: 175-184.

[26] Lin Y, Wei Y, Zhang L, Guo K, Wang M, Huang P, Meng X, Zhang R (2019) Facile ionothermal synthesis of SAPO-LTA zeotypes with high structural stability and their catalytic performance in MTO reaction. Micropor. Mesopor. Mater. 288: 109611.

[27] Álvaro-Muñoz T, Márquez-Álvarez C, Sastre E (2012) Use of different templates on SAPO-34 synthesis: Effect on the acidity and catalytic activity in the MTO reaction. Catal. Today 179: 27-34.

[28] Barrie PJ, Klinowski J (1989) Ordering in the framework of a magnesium aluminophosphate molecular sieve. J. Phys. Chem. 93(16): 5972-5974.

[29] Massiot D, Fayon F, Capron M, King I, Le Calvé S, Alonso B, Durand JO, Bujoli B, Gan Z, Hoatson G (2002) Modelling one- and two-dimensional Solid State NMR spectra. Magn. Reson. Chem. 40: 70-76.

[30] Blackwell CS, Patton RL (1984) Aluminum-27 and Phosphorus-31 Nuclear Magnetic Resonance Studies of Aluminophosphate Molecular Sieves. J. Phys. Chem. 88: 6135-6139.

[31] Naydenov V, Tosheva L, Antzutkin ON, Sterte J (2005) Meso/macroporous AlPO-5 spherical macrostructures tailored by resin templating. Micropor. Mesopor. Mater. 78: 181–188.

[32] Zhao X, Wang H, Kang C, Sun Z, Li G, Wang X (2012) Ionothermal synthesis of mesoporous SAPO-5 molecular sieves by microwave heating and using eutectic solvent as structure-directing agent. Micropor. Mesopor. Mater. 151: 501-505.

[33] Blasco T, Fernandez L, Martinez-Arias A, Sanchez-Sanchez M, Concepcion P, Lopez-Nieto JM (2000) Magnetic resonance studies on V-containing, and V,Mg-containing AFI aluminophosphates. Micropor. Mesopor. Mater. 39: 219-228.

[34] Machado MS, Perez-Pariente J, Sastre, E, Cardoso ED, Giotto MV, García-Fierro J, Fornes V (2002) Characterization and Catalytic Properties of MAPO-36 and MAPO-5: Effect of Magnesium Content. J. Catal. 205: 299–308.

[35] Álvaro-Muñoz T, Márquez-Álvarez C, Sastre E (2013) Effect of silicon content on the catalytic behavior of chabazite type silicoaluminophosphate in the transformation of methanol to short chain olefins. Catal. Today 213: 219– 225.

[36] Wang L, Guo Ch, Yan S, Huang X, Li Q (2003) High-silica SAPO-5 with preferred orientation: synthesis, characterization and catalytic applications. Micropor. Mesopor. Mater. 64: 63–68.

[37] Zhao YH, Gao TY, Wang YJ, Zhou YJ, Huang GQ (2018) Zinc supported on alkaline activated HZSM-5 for aromatization reaction. React Kinet Mechanisms Catal. 125 (2): 1085–1098.

[38] Schulz H (2010) "Coking" of zeolites during methanol conversion: Basic reactions of the MTO-, MTP- and MTG processes Catal. Today 154: 183–194.

[39] Ji Y, Yang H, Yan W (2017) Strategies to Enhance the Catalytic Performance of ZSM-5 Zeolite in Hydrocarbon Cracking: A Review. Catalysts 7 (367): 1-31.

[40] Sinha AK, Sainkar S, Sivasanker S (1999) An improved method for the synthesis of the silicoaluminophosphate molecular sieves, SAPO-5, SAPO-11 and SAPO-31. Micropor. Mesopor. Mater. 31: 321-331.

[41] Pinilla-Herrero I, Olsbye U, Márquez-Álvarez C, Sastre E (2017) Effect of framework topology of SAPO catalysts on selectivity and deactivation profile in the methanol-to-olefins reaction. J. Catal. 352: 191-207.

[42] Westgård-Erichsen M, Svelle S, Olsbye U (2013) H-SAPO-5 as methanol-to-olefins (MTO) model catalyst: Towards elucidating the effects of acid strength. J.Catal. 298: 94-101.

[43] Akolekar DB, Bhargava S (1997) Investigations on the aqueous solution and solid-state cation exchanged MAPO-ATS type molecular sieve. J. Mol. Catal. A-Chem. 122(1): 81-90.

## 9. Resultados importantes obtenidos

Se realizó la síntesis de diferentes estructuras zeolíticas modificadas con Zn y se evaluaron en la conversión de metanol a hidrocarburos (MTH).

Las zeolitas ZSM-5, TNU-9, MCM-22 y MCM-68 son activas en la conversión de metanol a diferentes temperaturas, sin embargo, la distribución de los productos de reacción fue diferente para cada una. La incorporación de Zn influyó en las propiedades texturales, morfológicas, ácidas y por lo tanto en la actividad catalítica de las zeolitas. La selectividad BTX se mejoró efectivamente, mediante la introducción de especies de Zn por intercambio iónico para todas las zeolitas, debido a la generación de sitios ácidos fuertes, activos para la conversión de metanol a compuestos aromáticos.

Mediante intercambio iónico se forman sitios aislados $ZnOH^+$, los cuales actúan como sitios ácidos responsables de catalizar la reacción. El Zn mediante gel de síntesis forma clústers de ZnO que impiden la difusión de reactivos en los canales de la zeolita y pueden acelerar la desactivación del catalizador debido a la deposición de coque que bloquea los sitios ácidos de la zeolita. Por lo que la técnica de incorporación influyo en gran medida por la actividad catalítica siendo más eficiente el intercambio iónico de Zn.

La generación de nanocristales de aproximadamente 60-80 nm en la zeolita ZSM-5 mejoró drásticamente la actividad catalítica en términos de conversión de metanol, así como en la selectividad. La nano zeolita aumentó la eficiencia de difusión de las moléculas y la accesibilidad de los centros activos, mejorando la selectividad BTX y la vida útil del catalizador. Existe una clara influencia entre el tamaño cristalino y el tiempo de vida media de los catalizadores. Conforme disminuye el tamaño de cristal aumenta la vida útil de la zeolita en términos de conversión de metanol.

En condiciones de 450 °C, WHSV 4.74 $h^{-1}$, 0.5 g de catalizador y 50 µm/min de metanol, se obtuvo una completa conversión de metanol y 32.5% de selectividad BTX (con 9 h de vida útil) con la zeolita nanocristalina ZSM-5.

La selectividad a los aromáticos totales de zeolitas T9-15 (Si /Al 15), siguió el orden: T9-15 0.5 Zn > ZT9-15 > T9-15 > T9-15 0.2 Zn. El catalizador T9-15 0.5 Zn a condiciones de 400°C y WHSV de 4.74 $h^{-1}$ presentó una selectividad a aromáticos totales de 32% a 1 h de reacción.

La zeolita MCM-22, independientemente de la morfología, fueron selectivas para obtener olefinas ligeras (etileno y propileno), debido a su estructura formada por supercajas y canales sinuosidales de 10 anillos, así como su acidez moderada.

Por otro lado, la zeolita MCM-68 modificada con Zn presentó altas conversiones de metanol a 400 °C, sin embargo, presentó alta selectividad a compuestos aromáticos pesados de C9 a C12 (37.6 %), debido a los grandes canales de la zeolita (supercajas de 12 y 18 anillos). Grandes canales provocan la generación de moléculas de mayor tamaño como consecuencia del espacio vacío existente en los canales.

Se sintetizaron materiales AlPO-5 y AlPO-36 doblemente sustituidos con Si como función ácida y Zn como función aromatizante (materiales MeAPSO) con diferentes concentraciones de Zn y Si. Así como materiales SAPO-5 (Si, Al y P), ZnAPO-5 y ZnAPO-36 (constituidos por Zn, Al y P). La selectividad en cada material fue distinta, así como la densidad de sitios ácidos débiles y la morfología.

La selectividad a aromáticos totales aumentó conforme aumentaba la cantidad de Zn en los materiales MeAPSO, comprobando la función aromatizante que presenta el metal divalente. Específicamente el material SAPO-5 (S5) presentó conversiones altas durante las 9 h de reacción al presentar un tamaño pequeño de partícula (1.5 μm), sin embargo, la selectividad a aromáticos fue menor debido a que el material solo se compone de Si, Al y P. Contrariamente, el material ZnAPO-5 (Z5) presentó una selectividad alta a aromáticos totales a los 5 min (41 %) con conversiones bajas de metanol debido a un gran tamaño de partícula del material (20 μm).

Respecto a los MeAPSO-36, el material A36-0.15 Zn-0.15 Si (S36-2) presentó una alta selectividad a aromáticos totales debido a la alta cantidad de Zn y Si. Ambos metales proporcionaron carácter ácido a los materiales comparado por TPD de amoniaco al presentar parecida densidad de sitios ácidos (145 µmol $NH_3$/g para el material Z5 y 192 µmol $NH_3$/g para el S5).

## 10. Conclusiones generales

- El método de incorporación de Zn en las zeolitas tuvo influencias importantes en las propiedades texturales, morfologícas, así como en las propiedades ácidas y por lo tanto en la actividad catalítica.

- La incorporación de Zn en todas las zeolitas mediante intercambio iónico mejoró la actividad catalítica en comparación con Zn en el gel de síntesis, debido a que por intercambio iónico se forman sitios aislados $ZnOH^+$, los cuales actúan como sitios activos responsables de catalizar la reacción.

- La selectividad a aromáticos totales y la fracción BTX mejoraron efectivamente mediante la introducción de especies de Zn por intercambio iónico, debido a una mayor distribución de sitios ácidos fuertes y estos sitios ácidos son los sitios responsables de la conversión de metanol a aromáticos.

- La temperatura de reacción es una variable importante en el proceso de MTA. A 450 ° C se logra una mejor activación de los sitios ácidos en la zeolita ZSM-5 y TNU-9 con Zn y, por lo tanto, se obtiene un alto porcentaje de selectividad BTX.

- La combinación de características físicas como un tamaño de cristal muy pequeño, un área de superficie externa alta y una acidez fuerte hacen que la zeolita nano cristalina ZSM-5 sea un catalizador potencialmente interesante en los procesos de MTA.

- La incorporación de Si y Zn por sustitución isomórfica en los zeotipos influyó en las propiedades texturales, ácidas, en la morfología y en la actividad catalítica.

- La incorporación de Zn en los materiales MeAPSO-36 facilitó la formación de la estructura ATS, ya que esta estructura es afín a la incorporación de metales divalentes como el Zn.

- El tamaño de partícula de los materiales MeAPSO tuvo un efecto importante en la conversión de metanol, conforme disminuye el tamaño de partícula, la conversión aumenta haciendo que el catalizador se desactive a menor tiempo.

- Finalmente, se mejoró la selectividad BTX, así como la estabilidad y resistencia a la desactivación mediante el control y diseño de propiedades químicas y estructurales, como el control de la morfología, la acidez y el tamaño de cristal de diferentes tipos de zeolitas de canales de 10 y 12 miembros.